

UNIVERSIDADE DE LISBOA  
FACULDADE DE CIÊNCIAS  
DEPARTAMENTO DE FÍSICA



## **Constraints from muon related observables in BSM physics**

Gabriel de Sousa Lourenço

**Mestrado em Física**  
Especialização em Física Nuclear e Partículas

Dissertação orientada por:  
Doutor Rui Alberto Serra Ribeiro dos Santos



# Acknowledgements

I would like to thank my advisor Professor Dr Rui Santos for all the invaluable guidance and advice. His insight proved numerous times pivotal in advancing this project. I deeply appreciate his patience and willingness to answer my many, sometimes repeated questions. It has been a pleasure to work with him.

This work was done in collaboration with André Santos, without whom it would have taken twice as long and been certainly more frustrating. I would like to thank him for all his contributions, substantial support and thoughtful discussions. I must also thank Professor Dr João Paulo Silva, who accompanied this work from the very beginning, providing valuable input and guidance.

I would also like to thank my friends, whose support has been truly extraordinary and at times instrumental in keeping my sanity. In particular, I would like to thank Rodrigo Capucha for the assistance he provided with the code `micrOMEGAS` and for all the advice he gave over the past year.

Finally, I would like to thank my family for their unconditional and unwavering support. They have provided me with a loving home and numerous opportunities that have profoundly influenced my personal and academic life, ultimately leading to this moment. They are in great measure responsible for what success I may have. To them I will be forever grateful.



# Abstract

The Standard Model is an achievement of modern physics, but is still not without flaws. One of its most important shortcomings is the lack of a dark matter candidate. Some experimental results are also not consistent with the theory either, chief among them the measurements of the anomalous magnetic moment of the muon. In the past few years, beyond the Standard Model scenarios have been proposed to address these issues in tandem.

In this work, we present a method to use precision muon-related observables for constraining new physics. The two key quantities are the muon asymmetry parameter,  $\mathcal{A}_\mu$ , and the ratio of hadronic decay rates,  $R_{e\mu} = R_e/R_\mu$ . We use Hollik's on-shell renormalisation scheme to get the one loop electroweak radiative corrections to  $Z \rightarrow \mu^+\mu^-$  and  $e^+e^- \rightarrow \mu^+\mu^-$ . We conclude that if new physics does not alter the theory's tree-level structure, the one loop matrix elements have Born-like expressions, with redefined left- and right-handed chiral couplings, QED and weak neutral couplings and Weinberg angle. We test our constraint on a model that introduces a vector-like fermion and two scalar singlets of  $SU(2)_L$ , one of them with a colour charge. We calculate the contributions to the chiral couplings and see that they can lead to a significant deviation to the observables, mainly through the left-handed coupling. This model impacts several flavour-related processes at one loop order. We take advantage of experimental bounds on these processes and on dark matter observables to restrict the parameter space of the model by performing a multiparameter scan where we also impose the constraint derived from  $\mathcal{A}_\mu$  and  $R_{e\mu}$ . The results are in line with previous studies, with only minor alterations from the precision observables. Finally, we employ the same approach to a different decay channel,  $Z \rightarrow \tau^+\tau^-$ , and compare it with the case of the muon.

**Keywords:** Electroweak corrections, renormalisation,  $Z$ -pole physics, dark matter,  $g - 2$ .



# Resumo

O Modelo Padrão da Física de partículas é uma das mais bem sucedidas teorias físicas, tendo ultrapassado inúmeros testes experimentais e guiado a comunidade à descoberta de novas partículas e a um conhecimento mais profundo da constituição do universo. Apesar do seu êxito, o Modelo Padrão tem algumas limitações, sendo uma das mais relevantes a ausência de um candidato a matéria escura. Do ponto de vista experimental, existem resultados que não estão de acordo com a teoria, em particular medições do momento magnético anômalo do muão. Vários modelos com extensões ao Modelo Padrão têm sido propostos para resolver estes problemas. Em particular, alguns destes modelos que pretendem solucionar a anomalia do muão e simultaneamente apresentar um candidato a matéria escura necessitam de um acoplamento forte entre as novas partículas e o muão.

Neste trabalho, apresentamos um método para constrangir o espaço de parâmetros de extensões do Modelo Padrão com recurso a observáveis de precisão relacionados com muões. A ideia central do nosso procedimento é calcular o impacto da nova física a um *loop* em observáveis experimentalmente bem determinados e verificar se a previsão teórica é aceite pelo intervalo experimental. Para isso, recorremos a dois observáveis que medem a assimetria *forward-backward* e as taxas de decaimento hadrónicas no pólo do  $Z$ , o parâmetro de assimetria do muão,  $\mathcal{A}_\mu$ , e  $R_{e\mu} = R_e/R_\mu$ , respectivamente. Escolhemos trabalhar com este rácio em vez das taxas de decaimento por si só, porque estas são definidas com correcções aos estados finais que em primeira ordem são independentes do leptão e como tal cancelam-se em  $R_{e\mu}$ .  $\mathcal{A}_f$  é extraído do processo  $e^+e^- \rightarrow f^+f^-$  e  $R_f$  de  $Z \rightarrow f^+f^-$ .

Antes de proceder à análise das correcções radiativas, deduzimos as expressões a nível-árvore dos elementos de matriz de  $Z \rightarrow f^+f^-$  e  $e^+e^- \rightarrow f^+f^-$ , juntamente com as dos observáveis e demonstrámos como estes podem ser escritos de forma aproximada exclusivamente em termos dos acoplamentos quirais esquerdo e direito,  $g_{L,R}$ . Para calcular as correcções radiativas aos processos, seguimos o esquema de renormalização *on-shell* de Hollik. Este esquema permite separar as correcções em duas classes invariantes de gauge, correcções de QED e correcções fracas, o que se revela útil por permitir determinar as contribuições da física da interacção fraca independentemente dos pormenores experimentais que têm de ser tidos em conta para cancelar as divergências IR fotónicas com a emissão de fótons reais sob a forma de *bremsstrahlung*. As correcções QED são, então, tratadas à parte e consideram-se apenas as correcções fracas. Estas dividem-se em três grupos, correcções ao vértice, correcções aos propagadores e correcções de diagramas tipo *box*. Neste texto, nós identificamos quais os diagramas que contribuem para cada correcção e explicamos como alteram os elementos de matriz dos processos. As correcções aos vértices e as provenientes dos diagramas tipo *box* resultam em termos aditivos às constantes de acoplamento quirais, enquanto que as correcções aos propagadores levam a redefinições das constantes de acoplamento da QED

e da corrente fraca e do ângulo de Weinberg. A correcção a um *loop* ao propagador do  $Z$  é insuficiente, visto que se cancela na secção eficaz de  $e^+e^- \rightarrow f^+f^-$ . Por isso, consideramos o propagador completo e com os termos de mistura  $\gamma Z$ . Desta revisão, concluímos que caso o novo modelo em estudo não altere as relações a nível-árvore do Modelo Padrão, os efeitos da nova física podem ser introduzidos de forma simples, somando os diagramas a um *loop* para o vértice ou auto-energias que contribuem para as correcções aos propagadores. Neste caso, como as correcções aos propagadores estão constrangidas pelos parâmetros oblíquos de Peskin-Takeuchi, pode-se contabilizar o efeito da nova física unicamente no vértice, redefinindo os acoplamentos quirais como  $g_{L,R} \rightarrow g_{L,R}^{\text{SM}} + \delta g_{L,R}^{\text{NP}}$ , onde o primeiro termo contém todos os efeitos do Modelo Padrão e o segundo aquele que deve ser um pequeno desvio causado pelos efeitos quânticos das novas partículas. Finalmente, quantificamos o impacto das contribuições de nova física em  $\mathcal{A}_\mu$ , e  $R_{e\mu}$  partindo das expressões dos observáveis em termos de  $g_{L,R}$  e fazendo uma expansão em primeira ordem para  $\delta g_{L,R}^{\text{NP}}$ . Daqui resulta uma fórmula para os desvios  $\delta \mathcal{A}_\mu$  e  $\delta R_{e\mu}$  que vêm da nova física a um *loop*. Estes desvios têm de ser tais que, quando somados à melhor previsão do Modelo Padrão para os observáveis, o resultado esteja contido no intervalo de incerteza experimental a  $1\sigma$ . Definimos assim o constrangimento.

Para testar o nosso constrangimento, usamos um modelo designado por Modelo 5 que introduz um fermião vectorial,  $\chi$ , e dois escalares,  $\Phi_l$  e  $\Phi_q$ , que são singletos de  $SU(2)_L$ .  $\Phi_q$  é um triplete de  $SU(3)_c$  e tem uma carga de cor. Impomos uma simetria  $\mathbb{Z}_2$  para a qual os campos do Modelo Padrão são pares e os campos do Modelo 5 ímpares. Isto impossibilita o decaimento da partícula nova mais leve, que, portanto, é estável. A partícula neutra mais leve é assim o candidato a matéria escura. Escolhemos a componente real de  $\Phi_l = (S + iA)/\sqrt{2}$  como o candidato a matéria escura, embora a fenomenologia fosse a mesma para  $A$ . A componente neutra de  $\chi$  também podia ser considerada, mas esta escolha impossibilita a solução do problema do momento anómalo do muão. O Modelo 5 leva a contribuições a um *loop* para vários processos de física do sabor. Para além do momento anómalo, os processos  $B \rightarrow K^{(*)}\mu^+\mu^-$ ,  $B_s \rightarrow \mu^+\mu^-$ ,  $b \rightarrow s\gamma$  e  $B_s - \bar{B}_s$  são influenciados pelas novas partículas. Para além destes, também observáveis relacionados com matéria escura, a densidade de relíquia, a secção eficaz de detecção directa e o decaimento invisível do Higgs, são afectados pelos campos do Modelo 5. Nós indicamos qual a contribuição de nova física para cada processo e observável de matéria escura e os valores experimentais mais recentes para de seguida os conjugar e limitar o espaço de parâmetros da teoria.

Usando os pacotes de Mathematica FeynRules, FeynArts, FeynCalc e LoopTools calculamos os diagramas que contribuem para as correcções ao vértice  $Z\mu^+\mu^-$  no Modelo 5. Ao variar os parâmetros do modelo que entram nas correcções, as massas das partículas  $M_S$ ,  $M_A$  e  $m_\chi$  e o acoplamento entre os campos novos e o muão,  $y_\mu$ , vimos que a correcção a  $g_L$  é dominante, sendo sempre pelo menos duas ordens de grandeza superior às restantes, que são por comparação negligenciáveis. Tendo isto em conta, e como  $\delta g_{L,R}^{\text{NP}} < 0$ ,  $\delta \mathcal{A}_\mu > 0$  e  $\delta R_{e\mu} > 0$ . De seguida, estudamos o impacto do constrangimento muónico no plano  $M_S - M_A$  para diferentes valores de  $m_\chi$  e  $y_\mu$  e verificamos que quanto mais forte o acoplamento para uma massa de  $\chi$  fixa, mais forte é o constrangimento. Por outro lado, para  $y_\mu$  fixo o constrangimento é tão mais forte quanto menor for  $m_\chi$ .

Finalmente, realizamos um *scan* multiparámetro e aplicamos os constrangimentos do sabor, matéria escura e dos observáveis relacionados com muões. A equação de Boltzmann foi resolvida numericamente com o programa micrOMEGAS. Os resultados do *scan* são consistentes com os estudos realizados anteri-



ormente para este modelo. No nosso caso, aumentamos o limite superior de  $y_\mu$  de  $\sqrt{4\pi}$  para  $4\pi$ . Isto leva a um novo limite superior para  $M_S$  de 389 GeV e um limite inferior de  $|y_b|$  de 0.07. Fora estas pequenas mudanças,  $\mathcal{A}_\mu$ , e  $R_{e\mu}$  não restringem substancialmente o espaço de parâmetros para além daquilo que resultava da aplicação do constrangimento do  $g - 2$ . Concluimos o nosso estudo comparando a região de aceitação a  $2\sigma$  no plano  $M_S - M_A$  do múon com os observáveis equivalentes para o decaimento  $Z \rightarrow \tau^+\tau^-$ . As expressões teóricas são como esperávamos iguais à parte da massa do fermião. Como tal, o comportamento qualitativo é semelhante, embora uma comparação directa da aplicação dos constrangimentos para múons e taus neste método seja delicada, uma vez que os valores teóricos de  $\mathcal{A}_\tau$  e  $R_{e\tau}$  não estão contidos no seu intervalo experimental.

**Palavras chave:** Correções electrofracas, renormalização, física no pólo do Z, matéria escura,  $g - 2$ .



# Contents

Acknowledgements	iii
Abstract	v
Resumo	vii
List of Tables	xiii
List of Figures	xv
List of Abbreviations	xvii
<b>1 Introduction</b>	<b>1</b>
<b>2 The Standard Model</b>	<b>5</b>
2.1 Mathematical description of elementary particles . . . . .	5
2.2 The electroweak sector . . . . .	7
2.3 The Higgs mechanism . . . . .	8
2.4 The Yukawa sector . . . . .	12
2.5 Problems of the SM . . . . .	14
2.5.1 Dark Matter . . . . .	14
2.5.2 The anomalous magnetic moment of the muon . . . . .	15
<b>3 Experimental observables</b>	<b>17</b>
3.1 Precision electroweak observables . . . . .	17
3.2 $R_f$ and $\mathcal{A}_f$ at tree-level . . . . .	19
3.2.1 $Z \rightarrow f^+ f^-$ and $R_f$ . . . . .	20
3.2.2 $e^+ e^- \rightarrow f^+ f^-$ and $\mathcal{A}_\mu$ . . . . .	23
<b>4 Radiative corrections</b>	<b>29</b>
4.1 Regularisation and renormalisation . . . . .	29
4.1.1 Renormalisation transformations for the electroweak sector of the SM . . . . .	31
4.1.2 Renormalisation of the vector boson propagators . . . . .	33
4.1.3 Renormalisation of the fermion propagator . . . . .	36

4.1.4	Renormalisation of the neutral vertices . . . . .	36
4.1.5	On-shell conditions . . . . .	37
4.2	Radiative corrections to $Z \rightarrow f^+ f^-$ and $e^+ e^- \rightarrow f^+ f^-$ . . . . .	40
4.2.1	QED corrections . . . . .	40
4.2.1.1	Final state corrections . . . . .	41
4.2.1.2	Initial state corrections . . . . .	43
4.2.2	Weak corrections . . . . .	44
4.2.2.1	Vertex corrections . . . . .	44
4.2.2.2	Propagator corrections . . . . .	46
4.2.2.3	Box corrections . . . . .	48
4.3	$A_\mu$ and $R_{e\mu}$ at one loop level and new physics . . . . .	49
<b>5</b>	<b>New model</b>	<b>53</b>
5.1	General description . . . . .	53
5.2	Model 5 . . . . .	54
5.2.1	Flavour and dark matter constraints . . . . .	56
5.2.1.1	Muon $g - 2$ . . . . .	57
5.2.1.2	Dark matter . . . . .	57
5.2.1.3	$B \rightarrow K^{(*)} \mu^+ \mu^-$ . . . . .	58
5.2.1.4	$B_s \rightarrow \mu^+ \mu^-$ . . . . .	60
5.2.1.5	$b \rightarrow s \gamma$ . . . . .	60
5.2.1.6	$B_s - \bar{B}_s$ mixing . . . . .	62
<b>6</b>	<b>Results</b>	<b>63</b>
6.1	One loop radiative corrections in Model 5 . . . . .	63
6.1.1	New diagrams . . . . .	63
6.1.1.1	Vertex diagrams . . . . .	64
6.1.1.2	Muon self-energy diagrams . . . . .	65
6.1.1.3	$\gamma Z$ self-energy diagrams . . . . .	65
6.1.2	Impact on $\hat{R}_{e\mu}$ and $\hat{\mathcal{A}}_\mu$ . . . . .	66
6.2	Parameter space scans . . . . .	68
<b>7</b>	<b>Conclusion</b>	<b>73</b>
	<b>Bibliography</b>	<b>75</b>

# List of Tables

2.1	Fermion fields of the SM. Left-handed fermions are doublets of $SU(2)_L$ and right-handed fermions are in a singlet representation of the same group. For each field we indicate the family, gauge group representation and weak hypercharge. The electric charge $Q$ is obtained from the third component of the weak isospin and the hypercharge. There are no right-handed neutrinos in the SM. . . . .	7
3.1	Experimental (Exp) values and SM predictions of the main $Z$ pole observables [47]. The hadronic, electron and muon partial decay widths are derived from the previous quantities without assuming lepton universality. $R_{e\mu}$ and $R_{e\tau}$ were computed from the hadronic decay rates. . . . .	20
3.2	Experimental (Exp) values and SM predictions for the left- and right-handed chiral couplings of the electron, muon and tau [122]. . . . .	20
5.1	$SU(3)_c$ , $SU(2)_L$ and $U(1)_Y$ charge assignments for the new fields of Model 5. . . . .	54



# List of Figures

3.1	SM tree-level diagram for $Z \rightarrow f^+ f^-$ . . . . .	21
3.2	SM tree-level diagram for $e^+ e^- \rightarrow f^+ f^-$ . . . . .	23
4.1	Diagrams that contribute to one 1PI self energy function. . . . .	33
4.2	Resummed photon, Z boson and $\gamma Z$ propagators. . . . .	35
4.3	QED diagrams that contribute to the $e^+ e^- \rightarrow f^+ f^-$ initial-final state interference corrections. . . . .	41
4.4	QED diagrams that contribute to the $Z \rightarrow f^+ f^-$ final state corrections. . . . .	42
4.5	QED diagrams that contribute to the $e^+ e^- \rightarrow f^+ f^-$ final state corrections. . . . .	42
4.6	QED diagrams that contribute to the $e^+ e^- \rightarrow f^+ f^-$ initial state corrections. . . . .	43
4.7	Weak diagrams that contribute to the $Z \rightarrow f^+ f^-$ vertex corrections. . . . .	45
4.8	Weak diagrams that contribute to the $e^+ e^- \rightarrow f^+ f^-$ vertex corrections. . . . .	45
4.9	Weak diagrams that contribute to the $e^+ e^- \rightarrow f^+ f^-$ propagator corrections. . . . .	46
4.10	Weak diagrams that contribute to the $Z \rightarrow f^+ f^-$ propagator corrections. . . . .	46
4.11	Weak diagrams that contribute to the $e^+ e^- \rightarrow f^+ f^-$ box corrections. . . . .	49
5.1	Feynman diagrams for the anomalous magnetic moment of the muon. . . . .	57
5.2	Feynman diagrams for the dark matter annihilation channels with Higgs mediation (left) and $\chi$ mediation (right). "SM" represents all massive SM particles. . . . .	57
5.3	Feynman diagrams for $SN \rightarrow SN$ and $h \rightarrow SS$ . . . . .	58
5.4	Feynman diagrams for $B \rightarrow K^{(*)} \mu^+ \mu^-$ . . . . .	59
5.5	Feynman diagrams for $B_s \rightarrow \mu^+ \mu^-$ . . . . .	60
5.6	Feynman diagrams for $b \rightarrow s \gamma$ . . . . .	61
5.7	Feynman diagrams for $B_s - \bar{B}_s$ mixing. . . . .	62
6.1	Scatter plot of $\delta g_{L,R}^{\text{NP}}$ in terms of $M_S$ , $m_\chi$ and $y_\mu$ for $10^4$ random points where the free parameters are varied in 6.14. $ \delta g_L^{\text{NP}} $ is always at least 100 times larger than $ \delta g_R^{\text{NP}} $ , with the largest deviations corresponding to $\delta g_L^{\text{NP}} = -0.022$ and $\delta g_L^{\text{NP}} = -8.043 \times 10^{-8}$ . . . . .	67
6.2	Plot of $\hat{R}_{e\mu} - \hat{\mathcal{A}}_\mu$ for $10^4$ random points shown in red. The central SM value is show in blue and the experimental value in green. The green box represents the $1\sigma$ uncertainty interval around the experimental point. $\delta R_{e\mu}$ and $\delta \mathcal{A}_\mu$ are always positive. Most of the points lie outside the experimental uncertainty range. . . . .	68

- 6.3  $M_S - M_A$  parameter space regions for which  $\hat{R}_{e\mu}$  and  $\hat{\mathcal{A}}_\mu$  are within their  $1\sigma$  uncertainty range for fixed values of  $m_\chi$  and  $y_\mu$ . For fixed  $m_\chi$ , darker shades of orange correspond to higher values of the coupling. The grey zone is excluded because  $M_A > M_S + 10$  GeV and  $m_\chi > M_S + 10$  GeV. Higher values of  $y_\mu$  lead to more stringent constraints for fixed  $m_\chi$ . If  $y_\mu$  is fixed, the constraint becomes less stringent for larger  $m_\chi$ . . . . . 69
- 6.4 Allowed parameter space projected in the planes  $M_S - M_A$  (top left),  $m_\chi - y_\mu$  (top right),  $M_S - m_\chi$  (bottom left) and  $M_S - y_\mu$  (bottom right). The cyan points agree with the flavour constraints (6.15). In addition the blue points verify the dark matter relic density results and the green points also the direct detection and invisible decay results. The red points agree with all previous constraints as well as the muon  $g - 2$  limits. The yellow points satisfy all constraints including the one from the muon-related observables. . . . . 70
- 6.5 Allowed parameter space projected in the planes  $|y_b| - y_\mu$  (left) and  $\lambda_{H\Phi_l} + \lambda'_{H\Phi_l}$  (right). The cyan points agree with the flavour constraints (6.15). In addition the blue points verify the dark matter relic density results and the green points also the direct detection and invisible decay results. The red points agree with all previous constraints as well as the muon  $g - 2$  limits. The yellow points satisfy all constraints including the one from the muon-related observables. The clean separation of the green points is due to the experimental bound from [178]. . . . . 71
- 6.6  $M_S - M_A$  parameter space regions for which  $\hat{R}_{e\mu}$ ,  $\hat{\mathcal{A}}_\mu$ ,  $\hat{R}_{e\tau}$  and  $\hat{\mathcal{A}}_\mu$  are within their  $2\sigma$  uncertainty range for  $m_\chi = 200$  GeV and fixed  $y_\mu$  or  $y_\tau$ . Darker shades of orange correspond to higher values of the coupling. The grey zone is excluded because  $M_A > M_S + 10$  GeV and  $m_\chi > M_S + 10$  GeV. Higher values of  $y_\mu$  or  $y_\tau$  lead to more stringent constraints for fixed  $m_\chi$ . . . . . 72



# List of Abbreviations

<b><math>\overline{\text{MS}}</math></b>	Modified Minimal Subtraction.
<b>ALPs</b>	Axion-Like Particles.
<b>BAO</b>	Baryonic Acoustic Oscillations.
<b>BSM</b>	Beyond the Standard Model.
<b>CDM</b>	Cold Dark Matter.
<b>CERN</b>	European Organization for Nuclear Research.
<b>CKM</b>	Cabibbo–Kobayashi–Maskawa.
<b>CM</b>	Center-of-Mass.
<b>CMB</b>	Cosmic Microwave Background.
<b>DM</b>	Dark Matter.
<b>EM</b>	Electromagnetic.
<b>LEP</b>	Large Electron–Positron Collider.
<b>MACHOs</b>	Massive Compact Halo Objects.
<b>MS</b>	Minimal Subtraction.
<b>NP</b>	New Physics.
<b>PMNS</b>	Pontecorvo–Maki–Nakagawa–Sakata.
<b>QCD</b>	Quantum Chromodynamics.
<b>QED</b>	Quantum Electrodynamics.
<b>SLAC</b>	Stanford Linear Accelerator Center.
<b>SLC</b>	Stanford Linear Collider.
<b>SLD</b>	Stanford Large Detector.
<b>SM</b>	Standard Model.
<b>UV</b>	Ultraviolet.
<b>vev</b>	Vacuum Expectation Value.
<b>WIMPS</b>	Weakly Interactive Massive Particles.



# Chapter 1

## Introduction

It is only human to ponder on the nature of the world, on what it is made of and on what binds it together, weaving such complex patterns as if to amaze us. And the study of these patterns in the most fundamental elements of reality is what particle physics is about.

The twentieth century was the century of modern physics, triggered by the development and subsequent establishment of both the theory of relativity and quantum theory in its first two decades. By the end of 1933, the electron, the proton, neutron, photon and Dirac's anti-electron had been detected experimentally [1–5]. The muon was discovered in 1936 [6] and Pauli's beta-decay missing energy particle, later named neutrino by Fermi, was first observed in 1956 [7]. Around this time, increasingly better detectors and more powerful accelerators lead to Oppenheimer's "sub-nuclear zoo" [8], whose elementary animals were categorised by physicist according to intrinsic quantum proprieties. Once again, repeating patterns emerged and in the 1960s Gell-Mann and Ne'man explained them with the Eight-fold Way [9, 10], which later lead to the quark model [11, 12], which describes most of the new particles as combinations of elementary quarks. The up and down quarks were first observed in the SLAC experiments of 1968 as constituents of the proton and the neutron [13, 14].

At the same time, there were attempts to create mathematically consistent, renormalisable quantum theories for fields. The theoretical description of particle physics was made in terms of quantised fields in a Lagrangian formalism, but there were numerous technical difficulties. Towering above all else were divergences which plagued the calculations whenever the effect of virtual particles had to be included. Dyson, Feynman, Schwinger and Tomonaga successfully develop Quantum Electrodynamics (QED) and the renormalisation techniques needed to deal with the divergences in the theory in the late 1940s [15–17]. Similar efforts were then undertaken for the weak and strong interactions. In 1967, Glashow, Salam and Weinberg devised the electroweak theory, successfully unifying the weak and electromagnetic interactions [18–20] and incorporating Higgs's spontaneous symmetry breaking mechanism [21–23], which gives mass to the particles. The theory is later proven renormalisable by 't Hooft and Veltman [24, 25]. In the 1970s, the concepts of asymptotic freedom and confinement became cornerstones of Quantum Chromodynamics (QCD), the theory of the strong interaction of quarks and the force carriers, the gluons. At the end of the decade, the sum of all the knowledge of particle physics at the time is codified in the Standard Model of particle physics.

The Standard Model (SM) is one of the most successful physical theories. Many, if not most, theo-

retical predictions seem to be in agreement with experimental results and with great accuracy. More than that, all particles that make up the SM have been detected. With the discovery of the tau neutrino in 2000 [26], only the Higgs boson remained exclusively in the realm of theory. In 2012, the ATLAS and CMS Collaborations at the LHC finally observed the Higgs boson, the last piece of the electroweak puzzle [27]. For all its merits, however, the SM has several shortcomings. One major component of what aims to be a theory of everything is gravity, which is not explained in this context. Among others, the abundance of matter over antimatter [28], the mass of the neutrinos [29], the hierarchy problem [30] and the nature of dark-matter are not explained by the SM. There are also some experimental observations that are not in agreement with the best theoretical results, like the most recent measurements of the anomalous magnetic moment of the muon [31].

Beyond the Standard Model (BSM) scenarios have been developed by adding new hypothetical fields with the required properties to solve some of the issues that face the SM. Depending on the structure of the new theory, the new particles can contribute to physical processes in quantum loop corrections at higher orders. This means that extending the SM can change the expected values of already experimentally well known observables. Hence, experimental results can be used to constrain free parameters of the new model such as masses and couplings. Even if a particular model seems to solve one of the aforementioned problems, if there is no region of the parameter space which is compatible with experimental results for some observable, then that model is excluded. The smaller the uncertainty on a certain measurement, the tighter the bounds it will impose on the new parameters.

Several models have been proposed in recent years that attempt to explain the observed discrepancies of the muon  $g - 2$  experiments while also introducing viable dark matter candidates [32–34]. These models require a strong coupling to the muon and it is important to know whether this is compatible with precision tests of the electroweak theory. In particular, measurements at the  $Z$  pole provide excellent probes of fermionic couplings.

In this work, we present a method to constrain extended sectors of the SM based on two precision muon-related observables. Our procedure is similar to the studies of a possible anomalous right-handed  $Zb^+b^-$  coupling [35–37], but has the advantage of dealing only with leptonic final states. We make use of the hadronic decay rate,  $R_\mu$ , and the fermionic asymmetry parameter,  $\mathcal{A}_\mu$ , the latter extracted from the forward-backward asymmetries. To avoid dealing with the final state corrections to  $R_\mu$ , we define the quantity  $R_{e\mu} = R_e/R_\mu$ , which gives the ratio between the partial decay widths of the  $Z$  to muons and to electrons and use this instead of  $R_\mu$ . We discuss the general structure of the radiative corrections to  $Z \rightarrow \mu^+\mu^-$  and  $e^+e^- \rightarrow \mu^+\mu^-$  at one loop level and argue that the most significant new physics contributions come from  $Z\mu^+\mu^-$  vertex corrections. These are accounted for as additive corrections to the left- and right-handed chiral couplings. Because the observables can on approximation be written exclusively in terms of these couplings, it is possible to get the deviation to the SM prediction caused by new physics writing the coupling as the sum of the SM part with the new physics term. We use as a test case a model from [33] which introduces two scalar fields, one with a colour charge, and a vector-like fermion. The scalars are singlets of  $SU(2)_L$ , while the fermion is a doublet of the same group. Finally, we perform a random scan over the parameter space and apply flavour and dark matter related constraints, followed by the condition that the new physics contribution to  $\mathcal{A}_\mu$  and  $R_{e\mu}$  must keep the final result in agreement with the experimental values of the observables to  $1\sigma$ .

This thesis is structured as follows. In Chapter 2, the SM is briefly reviewed with emphasis given to some topics relevant for the rest of the work. Two challenges to the SM are presented, dark matter and the anomalous magnetic moment of the muon, with a brief discussion of the current theoretical and experimental situation. In Chapter 3, we introduce the observables on which we base our study. First, some experimental context is provided and after that the tree-level expressions are deduced. In Chapter 4, we discuss the radiative corrections to  $Z \rightarrow f^+ f^-$  and  $e^+ e^- \rightarrow f^+ f^-$ . After introducing the renormalisation procedure and the different types of corrections, we explain why the new physics effects can be considered to be mostly contained in the vertex corrections and how this allows to parameterise the effects of physics beyond the SM in the observables. In Chapter 5, the new model and the flavour and dark matter related constraints used in the scan are introduced. For each constraint, we show how the new particles contribute to the physical process that defines it. In Chapter 6, we present our results. We begin by showing the diagrams that contribute to the vertex corrections and computing the corresponding analytical expressions. We then study the importance of the corrections and their dependence on the free parameters. Finally, we perform a random scan over the parameter space and discuss how the flavour, dark matter and muon-related constraints restrict the masses and couplings of the model. Chapter 7 contains a summary of our results and offers a few concluding remarks.



## Chapter 2

# The Standard Model

The SM is the theory that describes particle physics in the context of quantum field theory. It is a gauge theory based on the symmetry group  $SU(3)_c \times SU(2)_L \times U(1)_Y$ , which explains the strong, weak and electromagnetic interactions. The particle content of the theory is given by the fermions, charged leptons, neutrinos and quarks, and the bosons, the gluons of the strong interactions, the photon of electromagnetism and the  $Z$  and  $W^\pm$  bosons of the weak interaction. Electromagnetism and the weak force are described in a unified manner. Despite all its successes, the SM fails to explain some important experimental observations. In this chapter, we review the structure and components of the SM, beginning by giving a primer on quantum field theory and gauge theories and then introducing the parts of the SM which will be relevant for this work. We finish by introducing the two main challenges to the SM that the model we test tries to answer, dark matter and the anomalous magnetic moment of the muon.

### 2.1 Mathematical description of elementary particles

The mathematical framework used to describe elementary particles and their interactions is that of quantum field theory, which combines relativistic quantum mechanics with classical field theory [38–41]. Unlike classical quantum mechanics or even its relativistic counterpart, it is able to account for states with any possible number of particles together with the creation and annihilation of particles while respecting the causality principle. After quantisation, fields are operator-valued distributions that act on a Fock state and which obey some commutation or anti-commutation relation. Bosonic fields have integer spin and commute, meaning that multiple bosons can occupy the same quantum state, whereas fermionic fields, which have half-integer spin, follow an anti-commutation relation and are forbidden from occupying the same state. This leads to the statistical behaviour of bosons and fermions, the particles associated with the homonymous fields, being described by Bose-Einstein statistics and Fermi-Dirac statistics. The statement that fermions are not allowed to occupy the same quantum state is the well known Pauli exclusion principle.

The dynamics of the fields  $\phi_i = \phi_i(x)$  is described in a manner analogous to classical field theory.

One begins by introducing a dimensionless quantity called action,

$$S = \int d^4x \mathcal{L}(\phi_i, \partial_\mu \phi_i), \quad (2.1)$$

which is a functional which operates on field configurations over space-time.  $x$  is the four-vector that represents the position in space-time.  $\mathcal{L}$  is the Lagrangian density, which is a function of the fields and their derivatives. It depends on a number of parameters like masses and couplings. The Lagrangian density, from now on Lagrangian for short, contains all the information about the fields and their interactions. The principle of stationary action applied to (2.1) gives the equations of motion for the fields.

The action, hence the Lagrangian, is invariant under Poincaré transformations. The Poincaré group includes Lorentz transformations and space-time translations. According to Noether's first theorem [42], to every continuous global symmetry of the action corresponds a conservation law. Linear and angular momentum conservation as well as energy conservation are a result of space translation, space rotation and time translation symmetries, which are all Poincaré symmetries. A different type of symmetry, an internal symmetry, comes from a redundancy in the definition of the fields. The so called gauge symmetries correspond to local transformations of the fields under which the Lagrangian is invariant. There is a freedom to redefine the fields without altering the Lagrangian. Gauge invariance under a particular symmetry transformation is achieved by the application of the gauge principle, through the introduction of interaction terms with gauge fields encoded in the kinetic part of the Lagrangian. This defines a covariant derivative that when acting on the field transforms the same way as the field. The form of this derivative depends on the symmetry group, as does the number of interacting gauge fields, which is equal to the number of generators of the group. A theory whose Lagrangian is invariant under gauge transformations is called a gauge theory. The Standard Model of particle physics is one such theory.

The SM [19, 20, 43–46] is a gauge theory based on the symmetry group  $SU(3)_c \times SU(2)_L \times U(1)_Y$  which provides a unified description for three fundamental forces of nature, the strong and weak nuclear forces and electromagnetism, via the exchange of spin-1 gauge bosons. The fermionic matter content is given by spin- $\frac{1}{2}$  leptons and quarks. The mediators of the strong interaction are the eight gluons, the mediator of the electromagnetic interaction is the photon and the mediators of the weak interaction are the neutral  $Z$  and the charged  $W^+$  and  $W^-$  bosons. The gluons and the photon are massless and the weak bosons are massive. There is also a neutral, massive, spin-0 boson called the Higgs boson. The fermions are organised in three families or generations with identical proprieties distinguished only by their mass and flavour quantum number. There are six quarks which interact via all forces and six leptons which do not interact via the strong force. Each fermion has a corresponding anti-particle. The masses of the weak bosons and the fermions are generated through the spontaneous symmetry breaking of the electroweak group to the electromagnetic subgroup,  $SU(2)_L \times U(1)_Y \rightarrow U(1)_{EM}$ . This happens when the Higgs doublet gets a non-zero vacuum expectation value, giving rise to the Higgs boson in the process. The strong  $SU(3)_c$  part of the model concerns the particles with a colour charge, the gluons and the quarks. The name given to this part of the theory is Quantum Chromodynamics. Table 2.1 shows fermions of the SM and some selected proprieties that are relevant for this work.



**Table 2.1:** Fermion fields of the SM. Left-handed fermions are doublets of  $SU(2)_L$  and right-handed fermions are in a singlet representation of the same group. For each field we indicate the family, gauge group representation and weak hypercharge. The electric charge  $Q$  is obtained from the third component of the weak isospin and the hypercharge. There are no right-handed neutrinos in the SM.

Multiplet	Family			$SU(3)_c$	$SU(2)_L$	$U(1)_Y$	$Q = I_3 + Y$
	I	II	III				
Leptons	$\begin{pmatrix} \nu_{eL} \\ e_L \end{pmatrix}$	$\begin{pmatrix} \nu_{\mu L} \\ \mu_L \end{pmatrix}$	$\begin{pmatrix} \nu_{\tau L} \\ \tau_L \end{pmatrix}$	<b>1</b>	<b>2</b>	$-\frac{1}{2}$	$0 = \frac{1}{2} - \frac{1}{2}$ $-1 = -\frac{1}{2} - \frac{1}{2}$
	$e_R$	$\mu_R$	$\tau_R$	<b>1</b>	<b>1</b>	$-1$	$-1 = 0 - 1$
Quarks	$\begin{pmatrix} u_L \\ d_L \end{pmatrix}$	$\begin{pmatrix} c_L \\ s_L \end{pmatrix}$	$\begin{pmatrix} t_L \\ b_L \end{pmatrix}$	<b>3</b>	<b>2</b>	$\frac{1}{6}$	$\frac{2}{3} = \frac{1}{2} + \frac{1}{6}$ $-\frac{1}{3} = -\frac{1}{2} + \frac{1}{6}$
	$u_R$	$c_R$	$t_R$	<b>3</b>	<b>1</b>	$\frac{2}{3}$	$\frac{2}{3} = 0 + \frac{2}{3}$
	$d_R$	$s_R$	$b_R$	<b>3</b>	<b>1</b>	$-\frac{1}{3}$	$-\frac{1}{3} = 0 - \frac{1}{3}$

The Lagrangian of the SM can be divided in the following manner

$$\mathcal{L}_{SM} = \mathcal{L}_{QCD} + \mathcal{L}_{EW} + \mathcal{L}_H + \mathcal{L}_Y + \mathcal{L}_{GF} + \mathcal{L}_{Ghost}, \quad (2.2)$$

where  $\mathcal{L}_{QCD}$  is the QCD Lagrangian,  $\mathcal{L}_{EW}$  is the electroweak Lagrangian,  $\mathcal{L}_H$  is the scalar (Higgs) Lagrangian,  $\mathcal{L}_Y$  is the Yukawa Lagrangian,  $\mathcal{L}_{GF}$  is the gauge fixing Lagrangian and  $\mathcal{L}_{Ghost}$  is the ghost Lagrangian. Because the specificities of QCD are not relevant for this work,  $\mathcal{L}_{QCD}$  is left out of the following discussion. A review of QCD related topics can be seen in [47]. A proper definition of the field propagators in a gauge theory requires gauge fixing terms and the ghost fields are needed to cancel virtual degrees of freedom of gauge bosons in loops. Their precise form is, however, irrelevant for this work. As such,  $\mathcal{L}_{GF}$  and  $\mathcal{L}_{Ghost}$  will also not be shown, but are discussed in [41].

## 2.2 The electroweak sector

The electroweak group  $SU(2)_L \times U(1)_Y$  is a non-Abelian group, with three isospin operators  $I_i = \frac{\sigma_i}{2}$ ,  $i = 1, 2, 3$ , with  $\sigma_i$  the Pauli matrices. [48], and the weak hypercharge  $Y$  acting as generators of  $SU(2)_L$  and  $U(1)_Y$ , respectively. Each generator is associated with a spin-1 field. To the isospin operators corresponds a triplet of fields  $W_\mu^i$ , and to the hypercharge a singlet  $B_\mu$ . Before defining the covariant derivative through the application of the gauge principle, it is important to mention that the SM is also a chiral theory, meaning that the left- and right-handed components of the fermions lay in different representations of the  $SU(2)_L$  group. Left-handed fermions,  $\Psi^L$ , are isospin doublets and right-handed fermions,  $\psi^R$ , are isospin singlets,

$$\Psi_j^L = \begin{pmatrix} \psi_{j+}^L \\ \psi_{j-}^L \end{pmatrix}, \quad \psi_{j+}^R, \quad \psi_{j-}^R, \quad (2.3)$$

where  $j$  is the family index and the  $\omega$  index denotes the up-type fermions,  $\omega = +$ , and the down-type fermions,  $\omega = -$ . Each left- and right-handed fermion is an eigenstate of  $Y$  with an eigenvalue such

that the Gell-Mann-Nishijima relation  $Q = I_3 + Y$  [49, 50] for the electric charge,  $Q$ , and isospin and hypercharge quantum numbers is fulfilled. A fermion is decomposed into its chiral components by the application of the chirality projection operators

$$P_L = \frac{1}{2}(1 - \gamma_5), \quad P_R = \frac{1}{2}(1 + \gamma_5), \quad (2.4)$$

with  $\gamma_5 = i\gamma_0\gamma_1\gamma_2\gamma_3$ , where  $\gamma_i$ ,  $i = 0, 1, 2, 3$ , are the Dirac matrices,

$$\psi = (P_L + P_R)\psi = \psi_L + \psi_R. \quad (2.5)$$

The covariant derivative acting on left- and right-handed fermions is

$$D_\mu \Psi_j^L = [\partial_\mu - ig I_a W_\mu^a + ig' Y B_\mu] \Psi_j^L, \quad (2.6)$$

$$D_\mu \psi_{j\omega}^R = [\partial_\mu + ig' Y B_\mu] \psi_{j\omega}^R \quad (2.7)$$

where  $g$  and  $g'$  are the  $SU(2)_L$  and  $U(1)_Y$  gauge couplings. To get the kinetic term for the gauge bosons themselves, first one defines the field strength tensors

$$\begin{aligned} W_{\mu\nu}^a &= \partial_\mu W_\nu^a - \partial_\nu W_\mu^a + g\epsilon_{abc} W_\mu^b W_\nu^c, \\ B_{\mu\nu} &= \partial_\mu B_\nu - \partial_\nu B_\mu. \end{aligned} \quad (2.8)$$

where the Levi-Civita tensor  $\epsilon_{abc}$  plays the role of the structure constant for  $SU(2)_L$ .

The Lagrangian for the electroweak sector can now be written in full as

$$\mathcal{L}_{EW} = -\frac{1}{4}W_{\mu\nu}^a W^{a,\mu\nu} - \frac{1}{4}B_{\mu\nu} B^{\mu\nu} + \sum_j \bar{\Psi}_j^L i\gamma^\mu D_\mu \Psi_j^L + \sum_{j,\omega} \bar{\psi}_{j,\omega}^R i\gamma^\mu D_\mu \psi_{j,\omega}^R, \quad (2.9)$$

with  $\bar{\psi} = \psi^\dagger \gamma_0$  the adjoint spinor in the Dirac representation. The first two terms are sometimes referred to as the Yang-Mills Lagrangian [51] and contain cubic and quartic interactions between the gauge fields.

$\mathcal{L}_{EW}$  is missing mass terms for both gauge fields and fermions. In fact, adding a mass term for the bosons would break the gauge symmetry. A Dirac mass term for the fermions,  $m\bar{\psi}\psi = m(\bar{\psi}^L \psi^R + \bar{\psi}^R \psi^L)$ , would explicitly break the symmetry, because its chiral components transform differently under  $SU(2)_L$ . At this moment, even the relation between the gauge fields  $W_\mu^a$  and  $B_\mu$  and the physical fields  $A_\mu$ ,  $Z_\mu$  and  $W_\mu^\pm$ , the last three of which are massive, is not clear. The Higgs mechanism and spontaneous symmetry breaking will resolve these issues.

## 2.3 The Higgs mechanism

To generate masses for the gauge bosons in a way that does not explicitly break the symmetry one must make use of the Higgs mechanism [21–23], which allows to spontaneously break the electroweak symmetry down to the local electromagnetic group,  $SU(2)_L \times U(1)_Y \rightarrow U(1)_{EM}$ . In the process, three out of four electroweak generators are broken, keeping the combination  $Q = I_3 + Y$  unbroken and as a

consequence the photon massless. The minimal theory that gives the intended result is with a complex scalar doublet of  $SU(2)_L$  with hypercharge  $1/2$  and a non-vanishing vacuum expectation value (vev)  $v$ ,

$$H = \begin{pmatrix} \phi^+ \\ \phi^0 \end{pmatrix}, \quad \langle 0 | H | 0 \rangle = \langle 0 | \phi^0 | 0 \rangle = \frac{1}{\sqrt{2}} \begin{pmatrix} 0 \\ v \end{pmatrix}, \quad (2.10)$$

which is called the Higgs scalar. The vev is the minimum of the potential of the Lagrangian. The Lagrangian that describes the Higgs field is given by

$$\mathcal{L}_H = (D_\mu H)^\dagger (D^\mu H) - V(H), \quad V(H) = \mu^2 H^\dagger H + \lambda (H^\dagger H)^2, \quad (2.11)$$

with  $\mu^2 < 0$ . To ensure the potential is bounded from below, we define  $\lambda > 0$ . From here, the vev is determined to be  $v = \sqrt{-\mu^2/\lambda}$ . The covariant derivative is defined in (2.6). There is, in fact, an infinite number of degenerate states with the minimum energy defined in (2.10). The act of choosing a particular minimum is what leads to symmetry breaking. Although  $\mathcal{L}_H$  remains invariant under transformations of the full electroweak group  $SU(2)_L \times U(1)_Y$ , the vacuum is only invariant under  $U(1)_{\text{EM}}$ . This is what is meant by spontaneous symmetry breaking.

For the vacuum of the theory, only one combination of the weak generators remains unbroken, corresponding to the electric charge

$$Q \langle 0 | \phi^0 | 0 \rangle = (I_3 + Y) \begin{pmatrix} 0 \\ v \end{pmatrix} = 0, \quad I_1, I_2, (I_3 - Y) \langle 0 | \phi^0 | 0 \rangle \neq 0. \quad (2.12)$$

The Goldstone theorem [52, 53] states that a massless boson is generated for each broken generator of the symmetry. For the case of the electroweak symmetry, there are three broken generators, hence three Goldstone bosons. These Goldstone bosons,  $\pi_i$ ,  $i = 1, 2, 3$ , can be parameterised as complex phases writing the Higgs scalar as

$$H = \begin{bmatrix} 0 \\ \frac{1}{\sqrt{2}}(v + h) \end{bmatrix} e^{i \frac{\sigma_i}{2v} \pi^i}, \quad (2.13)$$

where  $h$  and  $\pi_i$  are real fields with vev=0. The  $SU(2)_L$  invariance of the Lagrangian allows to eliminate the dependence on the Goldstone bosons by choosing the unitary gauge [41] in which the Higgs field becomes

$$H = \begin{bmatrix} 0 \\ \frac{1}{\sqrt{2}}(v + h) \end{bmatrix} \quad (2.14)$$

and the three massless degrees of freedom  $\pi_i$  are "absorbed" into the definitions of the  $Z$  and  $W^\pm$  bosons' longitudinal polarisations. The remaining degree of freedom, an excitation around the vacuum, corresponds to a physical field that gets a mass term  $m_h = \sqrt{-2\mu^2}$  from the kinetic term of  $\mathcal{L}_H$ . This is the Higgs boson.

The Higgs boson has triple and quartic couplings coming from the terms in the scalar potential  $V(H)$ . Expanding the kinetic term reveals the mass terms for  $W_\mu^1, W_\mu^2, W_\mu^3$  and  $B_\mu$  in the form of a non-diagonal mass matrix,

$$\frac{gv^2}{8} (W_1^2 + W_2^2) + \frac{v^2}{4} \begin{pmatrix} W_\mu^3 & B_\mu \end{pmatrix} \begin{pmatrix} g^2 & gg' \\ gg' & g'^2 \end{pmatrix} \begin{pmatrix} W_\mu^3 \\ B_\mu \end{pmatrix}. \quad (2.15)$$

The symmetries of the theory are more apparent when the Lagrangian is written in terms of the gauge fields  $W_\mu^a$  and  $B_\mu$ . However, for practical purposes it is much more useful to write the Lagrangian in terms of the physical fields  $A_\mu, Z$  and  $W^\pm$ , which are the ones that are observed experimentally. To do this, the following transformations are applied to the Lagrangian,

$$W_\mu^\pm = \frac{W_\mu^1 \mp iW_\mu^2}{\sqrt{2}}, \quad (2.16)$$

and

$$\begin{pmatrix} Z_\mu \\ A_\mu \end{pmatrix} = \begin{pmatrix} c_W & s_W \\ -s_W & c_W \end{pmatrix} \begin{pmatrix} W_\mu^3 \\ B_\mu \end{pmatrix}, \quad (2.17)$$

where  $s_W = \sin \theta_W$  and  $c_W = \cos \theta_W$  are the sine and cosine of the Weinberg angle,  $\theta_W$ . In terms of the couplings,

$$s_W = \frac{g'}{\sqrt{g'^2 + g^2}} \quad c_W = \frac{g}{\sqrt{g'^2 + g^2}}. \quad (2.18)$$

In terms of the physical fields, (2.15) is

$$M_W^2 W_\mu^+ W^{-\mu} + \frac{1}{2} \begin{pmatrix} A_\mu & Z_\mu \end{pmatrix} \begin{pmatrix} 0 & 0 \\ 0 & M_Z^2 \end{pmatrix} \begin{pmatrix} A_\mu \\ Z_\mu \end{pmatrix}, \quad (2.19)$$

where the mass matrices are now in a diagonal form and the  $W^\pm$  and  $Z$  bosons have masses given by

$$M_W = \frac{1}{2}gv, \quad (2.20)$$

$$M_Z = \frac{1}{2}\sqrt{g'^2 + g^2}v = \frac{1}{2}\frac{gv}{c_W} = \frac{1}{c_W}M_W,$$

while the photon remains massless.

The covariant derivatives (2.6) and (2.7) are written in terms of the physical fields as

$$D_\mu \Psi^L = \left[ \partial_\mu - i\frac{g}{\sqrt{2}} (\sigma^+ W_\mu^+ + \sigma^- W_\mu^-) + ieQA_\mu - i\frac{g}{c_W} (I_3 - Qs_W^2) Z_\mu \right] \Psi^L, \quad (2.21)$$

$$D_\mu \psi_{j\omega}^R = \left[ \partial_\mu + ieQA_\mu + i\frac{g}{c_W} Qs_W^2 Z_\mu \right] \psi_{j\omega}^R, \quad (2.22)$$

with  $\sigma^\pm = (\sigma^1 \pm i\sigma^2)/2$  and the charge operator is

$$Q = \begin{pmatrix} \frac{1}{2} + Y & 0 \\ 0 & -\frac{1}{2} + Y \end{pmatrix}. \quad (2.23)$$

The electric charge of QED can now be identified as

$$e = g s_W = g' c_W = \frac{g g'}{\sqrt{g'^2 + g^2}}, \quad (2.24)$$

unifying the weak and electromagnetic coupling constants.

It is useful to write the weak neutral interaction terms in a way that emphasises the different couplings to the chiral components of the fermions. Doing this also reveals in a clearer way the underlying vector-axial nature of the current and the couplings to the photon and  $Z$ . Considering the relation between the left- and right-handed components of the fermions and the properties of the chiral projectors,

$$\bar{\psi}_{j\omega}^L \gamma^\mu \psi_{j\omega}^L = \bar{P}_L \bar{\psi}_{j\omega} \gamma^\mu P_L \psi_{j\omega} = \bar{\psi}_{j\omega} P_R \gamma^\mu P_L \psi_{j\omega} = \bar{\psi}_{j\omega} \gamma^\mu P_L^2 \psi_{j\omega} = \bar{\psi}_{j\omega} \gamma^\mu P_L \psi_{j\omega}, \quad (2.25)$$

where  $\bar{P}_L \bar{\psi}_{j\omega} = \psi_{j\omega}^\dagger \frac{1}{2}(1 - \gamma^5)^\dagger \gamma^0 = \psi_{j\omega}^\dagger \frac{1}{2}\gamma^0(1 + \gamma^5) = \bar{\psi}_{j\omega} P_R$ . Proceeding in a similar way for the term with the right-handed components,

$$\bar{\psi}_{j\omega}^R \gamma^\mu \psi_{j\omega}^R = \bar{\psi}_{j\omega} \gamma^\mu P_R \psi_{j\omega}. \quad (2.26)$$

The weak neutral interaction in (2.9) can then be written as

$$\frac{e}{s_W c_W} \bar{\psi}_{j\omega} \gamma^\mu (g_L P_L + g_R P_R) \psi_{j\omega} Z_\mu = \frac{e}{s_W c_W} \bar{\psi}_{j\omega} \gamma^\mu (g_V - g_A \gamma^5) \psi_{j\omega} Z_\mu \quad (2.27)$$

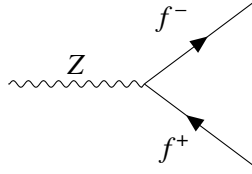
where the left- and right-handed coupling constants,  $g_{L,R}$ , and the equivalent vector and axial coupling constants,  $g_{V,A}$ , are defined as

$$\begin{aligned} g_L &= I_3^f - Q_f s_W^2, & g_V &= \frac{1}{2} I_3^f - Q_f s_W^2, \\ g_R &= -Q_f s_W^2, & g_A &= \frac{1}{2} I_3^f, \\ g_L &= g_V + g_A, & g_V &= \frac{1}{2} (g_L + g_R), \\ g_R &= g_V - g_A, & g_A &= \frac{1}{2} (g_L - g_R). \end{aligned} \quad (2.28)$$

$I_3^f$  corresponds to the eigenvalue of  $I_3$  and  $Q_f$  is the electric charge of the fermion  $f$ . Similarly for the interaction terms with the photon,

$$-e Q_f \bar{\psi}_{j\omega} \gamma^\mu \psi_{j\omega} A_\mu \quad (2.29)$$

which is identical to the QED interaction. From these terms, the Feynman rules for the  $Zf^+f^-$  and  $\gamma f^+f^-$  vertices can be extracted as usual [38],



$$= -i \frac{e}{s_W c_W} \gamma^\mu (g_L P_L + g_R P_R) = -i \frac{e}{s_W c_W} \gamma^\mu (g_V - g_A \gamma^5), \quad (2.30)$$



$$= -ie Q_f \gamma^\mu. \quad (2.31)$$

## 2.4 The Yukawa sector

A Dirac mass term for the fermions would violate the  $SU(2)_L \times U(1)_Y$  symmetry. In order to provide masses to the fermions, an interaction between the fermions and the Higgs is introduced in a manner that the Higgs mechanism can generate mass for the fermions while preserving the symmetry. The Lagrangian for this interaction is called Yukawa Lagrangian and can be written in a general form as

$$\begin{aligned} \mathcal{L}_Y &= -y_{ij-} \bar{\Psi}_i^L H \psi_{j-}^R - y_{ij+} \bar{\Psi}_i^L \tilde{H} \psi_{j+}^R + \text{h.c.} \\ &= -y_{ij-} \bar{\psi}_{i+}^L \phi^+ \psi_{j-}^R - y_{ij-} \bar{\psi}_{i-}^L \phi^0 \psi_{j-}^R - y_{ij+} \bar{\psi}_{i+}^L \phi^{0*} \psi_{j+}^R + y_{ij+} \bar{\psi}_{i-}^L \phi^- \psi_{j+}^R + \text{h.c.} \end{aligned} \quad (2.32)$$

with  $y_{ij\omega}$  the Yukawa matrices, which are  $3 \times 3$  complex matrices.  $i$  and  $j$  are the family indices.  $\tilde{H}$  is the charge-conjugate of the Higgs doublet,

$$\tilde{H} = i\sigma_2 H^* = \begin{pmatrix} \phi^{0*} \\ -\phi^- \end{pmatrix}, \quad (2.33)$$

which transforms the same way as  $H$  under  $SU(2)_L$ , but has hypercharge  $-1/2$ . This term is required to give masses to the up type quarks. After symmetry breaking,  $\phi^0 = (v + h)/\sqrt{2} = \phi^{0*}$ , resulting in interaction terms with the Higgs boson and mass matrices

$$Y_{ij\omega} = \frac{v}{\sqrt{2}} y_{ij\omega} \quad (2.34)$$

for the fermions. The matrices  $Y_{ij\omega}$  are not necessarily diagonal because of the gauge interactions. Following [41, 54], by rotating the fermions to the mass basis from the flavour basis in which the Lagrangian was originally written, it happens that different flavours of quarks interact via exchange of the charged  $W^\pm$  bosons. The matrix that connects the flavour states to the mass states is called the Cabibbo-Kobayashi-Maskawa (CKM) matrix. This mixing of states is no longer true for the leptons, due to the absence of right-handed neutrinos in the SM.

In order to make the previous remarks clearer, a less general notation closer to that of Table 2.1 is

introduced, with the Lagrangian (2.32) now written as

$$\begin{aligned}\mathcal{L}_Y &= -y_{ij}^l \bar{L}^i H l_R^j - y_{ij}^d \bar{Q}^i H d_R^j - y_{ij}^u \bar{Q}^i \tilde{H} u_R^j + \text{h.c.} \\ &= -y_{ij}^l \frac{v}{\sqrt{2}} \bar{l}_L^i l_R^j - y_{ij}^d \frac{v}{\sqrt{2}} \bar{d}_L^i d_R^j - y_{ij}^u \frac{v}{\sqrt{2}} \bar{u}_L^i u_R^j + \cdots + \text{h.c.},\end{aligned}\quad (2.35)$$

with  $\bar{L}^i = (\nu_L \ l_L)^i$  the left-handed lepton doublet,  $l_R$  the right handed (charged) lepton singlets,  $\bar{Q}^i = (u_L \ d_L)^i$  the left-handed quark doublets and  $d_R$  and  $u_R$  the down and up type right-handed quark singlets. In the second line only the mass terms obtained after symmetry breaking were kept. The matrices  $Y^a = -y^a(v/\sqrt{2})$ ,  $a = l, d, u$ , can be diagonalised through bi-unitary transformations. For each matrix  $Y^a$ , two unitary matrices  $U_a$  and  $K_a$  can be found such that

$$U_a^\dagger Y^a K_a = M^a, \quad (2.36)$$

where  $M^a$  is diagonal and has positive eigenvalues. Thus, one needs to rotate the fermion states to a new basis according to the transformations

$$\begin{aligned}l_L &\rightarrow U_l l_L, & d_L &\rightarrow U_d d_L, & u_L &\rightarrow U_u u_L, \\ l_R &\rightarrow K_l l_R, & d_R &\rightarrow K_d d_R, & u_R &\rightarrow K_u u_R.\end{aligned}\quad (2.37)$$

After these transformations, the Lagrangian becomes

$$\mathcal{L}_Y = -m_i^l \bar{l}_L^i l_R^i - m_i^d \bar{d}_L^i d_R^i - m_i^u \bar{u}_L^i u_R^i + \cdots + \text{h.c.} \quad (2.38)$$

where  $m_i^a$  are the diagonal elements of  $M^a$  which correspond to the physical masses of the fermions. Applying the same transformations in the interaction terms of the fermions with the charged weak bosons in (2.21), gives

$$\bar{d}_L U_d^\dagger \gamma^\mu \frac{g}{\sqrt{2}} W_\mu^- U_u u_L + \bar{u}_L U_u^\dagger \gamma^\mu \frac{g}{\sqrt{2}} W_\mu^+ U_d d_L = \frac{g}{\sqrt{2}} \left[ W_\mu^- \bar{d}_L \gamma^\mu (V^\dagger)_{ij} u_L^j + W_\mu^+ \bar{u}_L \gamma^\mu V_{ij} d_L^j \right], \quad (2.39)$$

where the matrix  $V = U_u^\dagger U_d$  is the CKM matrix [55, 56]. Because the right-handed quarks are  $SU(2)_L$  singlets, they do not couple to  $W^\pm$ , hence there is no mixing in the interaction terms with the neutral bosons. There are no flavour changing neutral currents in the SM. The procedure is formally equivalent for the leptons, but because the neutrinos are massless in the SM they are degenerate and any transformation by a unitary matrix must lead to the same state. Hence, we can use the same unitary matrix to transform both the neutrinos and the charged leptons, which leads to the absence of mixing in the leptonic sector.

Although neutrinos are massless in the SM, they are experimentally known to have a small mass due to the observation of neutrino oscillations [47]. This implies the existence of a  $3 \times 3$  matrix that mixes the flavour states like the CKM matrix does for the quarks - the Pontecorvo-Maki-Nakagawa-Sakata (PMNS) matrix [57–59].

## 2.5 Problems of the SM

The two problems of the SM that serve as the main motivation for the class of models we study are dark matter and the anomalous magnetic moment of the muon. Understanding the nature of dark matter is currently one of physics greatest challenges and the SM is unable to provide an answer. No particle in the SM is a good dark matter candidate. The anomalous magnetic moment of the muon, also designated as the muon  $g - 2$ , is a problem of a slightly different nature. At present, there is a large discrepancy between the experimental results and the best (perturbative) theoretical predictions which could indicate the presence of new physics. However, even on the theory side there are conflicting results from different groups, not all in agreement with the FermiLab result [31].

### 2.5.1 Dark Matter

The first evidences of the existence of dark matter hail from astronomical observations. After some early attempts at measuring the non-luminous matter in the galaxy [60–62], the first major indication of a missing mass came from Zwicky’s study of the Coma cluster that showed that in order to remain stable, the mass density of this galaxy cluster had to be much higher than it would be considering only visible matter [63]. Other impactful results like the rotation curves of galaxies [64, 65], measurements of gravitational lensing and X-ray emission from galaxy clusters [66], the bullet cluster [67, 68] and from a number of other sources like the CMB or BAO [69] all point to the existence of invisible matter which we call dark matter. Moreover, experimental observations show that only about 15% of the matter content of the universe corresponds to the fermions and bosons of the SM. Explanations for structure formation in particular rely heavily on dark matter, since in the radiation-dominated era its density perturbations can be large enough to gravitationally attract ordinary matter that later collapses [70]. Dark matter has been detected in collapsed structures of different scales [66, 71, 72]. In spite of overwhelming experimental evidence pointing to its existence, the exact nature of dark matter is unknown and currently one of physic’s greatest open questions. No particle in the SM is a suitable dark matter candidate. Some effects observed to be caused by dark matter can be explained in the context of modified gravity theories [73], but unlike in models with particle dark matter these often fail at reproducing some larger scale observations like the bullet cluster [74, 75].

The  $\Lambda$ CDM model of cosmology, the current standard of that field, considers that 84.4% of the total matter density is due to a non-baryonic matter species which must be electromagnetically close-to-neutral, have negligible velocity at the time of structure formation and interact weakly with baryonic matter - Cold Dark Matter (CDM) [47]. Some possible components of cold dark matter are Weakly Interactive Massive Particles (WIMPS) or Axion-Like Particles (ALPs) [76, 77]. Other models propose astronomical bodies like Massive Compact Halo Objects (MACHOs) as cold dark matter candidates [78]. A discussion on particle dark matter candidates, cold and non-cold, can be seen in [79].

Dark matter production mechanisms are an essential part of this subject, with several thermal and non-thermal scenarios being proposed, like freeze-out or freeze-in [47] and production via decays [80, 81], respectively. All possibilities must reproduce the observed dark matter relic density. The most recent value, measured by the Planck Collaboration, is  $\Omega_{DM}h^2 = 0.1200 \pm 0.0012$  [69].

Constraining the parameter space associated to dark matter is a subject of intense research and searches



for dark matter are ongoing. There are three main types of dark matter searches, direct detection, indirect detection and production at colliders. Direct detection experiments intend to observe scattering processes of dark matter particles with atomic nuclei. Indirect detection searches look for SM particles produced in processes that involve dark matter that would occur in regions of high dark matter density like the galactic center. Collider searches look for dark matter particles that are produced in the machine but escape without interacting with the detectors, leading to a large missing energy associated with a particle.

So far, astrophysical and cosmological data as well as constraints from direct detection and collider searches establish limits on mass [82–86], charge [87] and self-interactions [88]. Because of its role in structure formation, dark matter must be stable, with an estimated lifetime of at least 160 Gyr [89].

### 2.5.2 The anomalous magnetic moment of the muon

Consider a spin- $\frac{1}{2}$  particle of mass  $m$  and charge  $q$  in an external electromagnetic field described by the four-potential  $A^\mu = (\phi, \vec{A})$ . With a minimal coupling to the field, which means taking the momentum operator in position space as  $\hat{\vec{p}} = -i\vec{\nabla} - q\vec{A}$ , the non-relativistic limit of the Dirac equation leads to the Schrödinger-Pauli equation [90]

$$\mathcal{H}\psi = i\frac{\partial\psi}{\partial t} \Leftrightarrow \left\{ \frac{1}{2m} \left[ (-i\vec{\nabla} - q\vec{A})^2 + q\vec{\sigma} \cdot \vec{B} \right] + q\phi \right\} \psi = i\frac{\partial\psi}{\partial t}. \quad (2.40)$$

$\psi = \psi(t, \vec{r})$  is the wavefunction that describes the fermion,  $\vec{B} = \vec{\nabla} \times \vec{A}$  is the magnetic field and  $\vec{\sigma} = (\sigma_1, \sigma_2, \sigma_3)$  the Pauli matrices. For a weak uniform magnetic field  $\vec{A} = \frac{1}{2}\vec{B} \times \vec{r}$  and keeping only first order terms in the interaction, the Hamiltonian becomes [48]

$$\mathcal{H} \approx \frac{-i\vec{\nabla}^2}{2m} - \frac{q}{2m} \left( \hat{\vec{L}} + 2\hat{\vec{S}} \right) \cdot \vec{B}, \quad (2.41)$$

with

$$\hat{\vec{L}} = \hat{\vec{r}} \times \hat{\vec{p}}, \quad \hat{\vec{S}} = \frac{1}{2}\vec{\sigma}, \quad (2.42)$$

the orbital angular momentum operator and the spin operator. Comparing this expression with the classical result for a charged particle in an external uniform magnetic field [91], the magnetic moment of the fermion is defined as [92]

$$\hat{\vec{\mu}} = \frac{q}{2m} \left( \hat{\vec{L}} + 2\hat{\vec{S}} \right), \quad (2.43)$$

where the second term corresponds to an intrinsic magnetic moment. The coefficient of the interaction between the spin and magnetic field  $gq/2m$  is called the gyromagnetic ratio. The adimensional constant  $g$  is called the  $g$ -factor and for fermions  $g = 2$ . This result is exact in the context of the Dirac theory, accounting for two Bohr magnetons  $q/2m$ , but quantum field theoretical corrections in the context of the SM will alter this value.

The most general amplitude for the interaction between a photon and a charged particle in the SM can

be written as

$$\bar{u}(p_1)\hat{\Gamma}u(p_2) = \bar{u}(p_1) \left[ e\gamma_\mu F_E(k^2) + \frac{ie\sigma_{\mu\nu}k^\nu}{2m} F_M(k^2) \right] u(p_2), \quad (2.44)$$

where  $\bar{u}(p_1)$  and  $u(p_2)$  are the spinor functions for the charged particle with momenta  $p_1$  and  $p_2$ .  $k = p_1 + p_2$  is the momentum of the photon.  $F_E$  and  $F_M$  are the electric and magnetic form factors, which include higher order contributions from the perturbation expansion.

By taking once again the non-relativistic limit, a comparison can be drawn between the classical expression and the Dirac result, but now also with the quantum corrections from quantum field theory. Doing this shows that  $F_E(0) = 1$  and that the coefficient that multiplies the spin operator in (2.43) becomes

$$\frac{q}{2m}2 + \frac{q}{2m}2F_M(0). \quad (2.45)$$

Defining the corrected gyromagnetic factor as  $g = 2 + 2F_M(0)$ , where the first factor of 2 corresponds to the Dirac result, allows to parametrise the difference as

$$a = F_M(0) = \frac{1}{2}(g - 2), \quad (2.46)$$

which we call the anomalous magnetic moment. An extensive review of the fundamental theoretical aspects of the anomalous moment of the muon can be found in [92].

At the moment, the best SM theoretical prediction for the anomalous magnetic moment of the muon from the Muon g-2 Theory Initiative is  $a_\mu = 116591810(43) \times 10^{-11}$  [93]. This value contains QED corrections up to order five, QCD corrections up to third order and two loop weak corrections. Most of the uncertainty comes from the hadronic contributions.

The first experiments aimed at measuring the anomalous moment at CERN were in agreement with the SM [94], but a 2006 measurement from the Brookhaven National Laboratory [95], validated by the Fermilab National Accelerator Laboratory in 2021 [96], showed some tension with the expected value, the latter with a significant  $4.2\sigma$  deviation. The most recent results from Fermilab based on data collected for the first three years published in 2023 show an even starker departure from the SM prediction, with  $a_\mu^{\text{Exp}} = 116592059(22) \times 10^{-11}$ , which in relation to the 2020 theoretical prediction corresponds to a  $5\sigma$  discrepancy [31]. Such a striking deviation could point to new physics. This could be considered a fully fledged discovery were it not for its disagreement with results from lattice calculations of the hadronic vacuum polarisation [97] and with measurements of the  $e^+e^- \rightarrow \pi^+\pi^-$  cross-section [98].

## Chapter 3

# Experimental observables

Our end goal is to use results from  $Z$  pole experiments to constrain the parameter space of extended sectors of the SM. For this, we require physically motivated experimental observables to test the new models. In this chapter, we introduce two  $Z$  pole quantities,  $\mathcal{A}_\mu$  and  $R_{e\mu}$ , used to formulate our new constraints. We begin by defining the relevant electroweak observables at the  $Z$  resonance and then derive the tree-level expressions for  $\mathcal{A}_f$  and  $R_{el}$ , highlighting results which are important later on.

### 3.1 Precision electroweak observables

With the advent of electron-positron colliders like LEP at CERN [99, 100] or SLC at SLAC [101], precision measurements of many electroweak quantities became possible to the point of detecting small deviations from tree-level predictions. Between 1989 and 2000, seventeen million  $Z$  boson events were recorded by the four LEP experiments ALEPH [102, 103], DELPHI [104, 105], L3 [106–109] and OPAL [110–113] and 0.55 million at the SLC [114–119] between 1992 and 1998.

High precision measurements of several observables around the  $Z$  resonance, that is at a center-of-mass (CM) energy  $s \approx M_Z^2$ , at LEP [120, 121] and SLC [122–126] allowed for accurate determinations of the cross-section "lineshape" parameters, the position and height of the peak and the width of the distribution. These determine the mass of the  $Z$ , the partial decay widths  $\Gamma_f = \Gamma(Z \rightarrow f^+ f^-)$ , for all fermions  $f$  except the top quark, and the total  $Z$  width,  $\Gamma_Z = \sum_f \Gamma_f$ . Other observables, namely  $Z$  pole asymmetries, provide constraints to initial and final state couplings, the Weinberg angle and to the left- and right-handed chiral couplings, thus probing the quantum structure of the theory.

The principal set of fitting parameters chosen by the LEP Collaboration was  $M_Z$ ,  $\Gamma_Z$ , the hadronic decay rate for leptons,  $R_l^0$  and the hadronic pole cross-section,  $\sigma_{\text{had}}^0$ , and the leptonic forward-backward asymmetry,  $A_{\text{FB}}^{0,l}$ , with the latter three defined as [122, 127]

$$R_l^0 = \frac{\Gamma_{\text{had}}}{\Gamma_l}, \quad \sigma_{\text{had}}^0 = \frac{12\pi}{m_Z^2} \frac{\Gamma_e \Gamma_{\text{had}}}{\Gamma_Z^2}, \quad A_{\text{FB}}^{0,l} = \frac{3}{4} \mathcal{A}_l \frac{\mathcal{A}_e + P_e}{1 + P_e \mathcal{A}_e}, \quad (3.1)$$

where  $\Gamma_{\text{had}} = \Gamma_u + \Gamma_d + \Gamma_c + \Gamma_s + \Gamma_b$  is the partial decay width of the  $Z$  to light quarks.  $P_e$  is the polarisation

of the initial state electrons, which is zero at LEP giving  $A_{\text{FB}}^{0,l} = \frac{3}{4}\mathcal{A}_e\mathcal{A}_f$  with

$$\mathcal{A}_f = \frac{g_{L_f}^2 - g_{R_f}^2}{g_{L_f}^2 + g_{R_f}^2} = \frac{2g_{V_f}g_{A_f}}{g_{V_f}^2 + g_{A_f}^2} \quad (3.2)$$

the fermionic asymmetry parameter.  $\mathcal{A}_f$  gives information on the final state couplings for leptons,  $f = l$ , or quarks,  $f = q$ . For leptons, this is a set of nine parameters:  $M_Z$ ,  $\Gamma_Z$ ,  $\sigma_{\text{had}}^0$ , three hadronic decay rates and three asymmetry parameters. Assuming lepton flavour universality, this reduces to five parameters, with only one hadronic decay rate and one asymmetry parameter for the leptons. These parameters are weakly correlated experimentally and for this reason are chosen instead of the more natural set of  $m_Z$ ,  $\Gamma_Z$ ,  $\Gamma_f$  and  $\mathcal{A}_f$  which are strongly correlated [47, 121].

These quantities are affected by QED and QCD initial and final state corrections [122], as well as electroweak radiative corrections at one loop order. A discussion on these contributions and their relative importance will be given in section 4.2.1. It is, however, necessary to mention that the initial and final state corrections are independent of the underlying structure of the theory and treated separately from the electroweak corrections. An index "0" will be used to indicate when a certain quantity has been deconvoluted from these corrections and is therefore only dependent on the details of the model.  $\sigma_{\text{had}}^0$ , for example, is the cross section of annihilation of  $e^+e^-$  into hadrons after removing the final state QED corrections included by definition in  $\Gamma_e$ .

A distinction must be made at this point between an observable and a pseudo-observable. Strictly speaking, only quantities measured directly should be considered observables proper like cross-sections and asymmetries. Any other quantity derived from these is of a secondary nature and called a pseudo-observable. From now on, the designation of observable will be used indiscriminately.

Of central importance to this work are two observables, the hadronic decay rate,  $R_f$ , and  $\mathcal{A}_f$ . The latter is determined from more than one  $Z$  pole asymmetry [114–119]. Considering only  $Z$  boson exchange at  $s = M_Z^2$  and deconvoluting the QED corrections, the relevant asymmetries can be written in terms of the fermionic asymmetry parameters (3.2). These are the unpolarised forward-backward asymmetry,  $A_{\text{FB}}^{0,f} = \frac{3}{4}\mathcal{A}_e\mathcal{A}_f$ , and the average polarisation of the final state tau,  $\langle\mathcal{P}_\tau\rangle = -\mathcal{A}_\tau$ , measured at LEP and the polarisation asymmetries, the left-right forward-backward asymmetry,  $A_{\text{LRFB}}^{0,f} = \frac{3}{4}\mathcal{A}_f$ , and the left-right asymmetry,  $A_{\text{LR}}^0 = \mathcal{A}_e$ , measured at SLC. Unlike LEP, the SLC functioned with longitudinally polarised electrons. This allowed to measure polarised asymmetries and then compute the unpolarised results by taking into account the luminosity-weighted polarisation [122]. The measurements of these observables at LEP and SLC form a complementary set of asymmetry parameter results. For the sake of simplicity, in section 3.2,  $\mathcal{A}_f$  will be derived from  $A_{\text{FB}}^{0,f}$ .  $A_{\text{FB}}^{0,f}$  measures an asymmetry in the angular distribution of the final state particles produced in the forward direction, meaning they are scattered in the hemisphere defined by the polar angle  $\theta < \frac{\pi}{2}$  they make with the initial electron beam, versus the ones that are produced backwards,  $\theta > \frac{\pi}{2}$ . In terms of the cross-sections,

$$A_{\text{FB}}^{0,f} = A_{\text{FB}}(e^+e^- \rightarrow f^+f^-) = \frac{\sigma_F^0 - \sigma_B^0}{\sigma_F^0 + \sigma_B^0}, \quad (3.3)$$

with the forward and backward cross-sections

$$\sigma_F^0 = \int_{\theta < \frac{\pi}{2}} \frac{d\sigma^0}{d\Omega}(s, \theta) d\Omega, \quad \sigma_B^0 = \int_{\theta > \frac{\pi}{2}} \frac{d\sigma^0}{d\Omega}(s, \theta) d\Omega, \quad (3.4)$$

where  $d\sigma^0/d\Omega$  is the deconvoluted differential cross-section for unpolarised beams and  $\Omega$  the solid angle. The fact that the left- and right-handed couplings of the fermions to the  $Z$  are different means that even when the colliding beams are unpolarised the  $Z$  exhibits a polarisation. As such, because of parity non-conservation the final state fermions will have a non-symmetric angular distribution. The hadronic decay rate for leptons and quarks is defined as

$$R_l = \frac{\Gamma_{\text{had}}}{\Gamma_l}, \quad R_q = \frac{\Gamma_q}{\Gamma_{\text{had}}}. \quad (3.5)$$

$R_f$  is typically defined inclusively, meaning that the partial widths include the final state QED and QCD corrections [122]. In this way, the sum of the partial widths corresponds to the total width of the  $Z$ . Not wanting to deal with the hadronic part of the observable which leads to the QCD contributions, we define the quantity

$$R_{el} = \frac{R_e}{R_l} = \frac{\Gamma_l}{\Gamma_e}, \quad (3.6)$$

which is "hadronically clean", depending only on decays to leptonic final states and on the QED corrections.

The most up-to-date values for the main  $Z$  pole observables can be seen in Table 3.1. We use these results to compute an approximate SM prediction and experimental value for  $R_{e\mu}$ .

From the definition (3.6), for the muon we get

$$R_{e\mu}^{\text{Exp}} \approx 1.0009 \pm 0.0029, \quad R_{e\mu}^{\text{SM}} \approx 1.0000 \pm 0.0007. \quad (3.7)$$

To compute  $R_{e\mu}^{\text{Exp}}$ , we used the hadronic decay rate values of Table 3.1, since these are the primary experimental measurements. For consistency, we use the associated theoretical values to get  $R_{e\mu}^{\text{SM}}$ . The uncertainty was determined by propagation.  $R_{e\mu}^{\text{Exp}}$  and  $R_{e\mu}^{\text{SM}}$  are in fairly good agreement and with uncertainties of the order of  $10^{-3}$  and  $10^{-4}$ , respectively, meaning any deviation from the SM values coming from new physics is tightly constrained.

## 3.2 $R_f$ and $\mathcal{A}_f$ at tree-level

We now derive the tree-level expressions for the decay rate of  $Z \rightarrow f^+ f^-$  and the cross section of  $e^+ e^- \rightarrow f^+ f^-$ , from which we get the lowest order expressions for the observables  $R_{el}$  and  $\mathcal{A}_f$ . With these somewhat extensive calculations we aim also to set some notation and discuss physical concepts and definitions that here arise naturally and that will be useful in other chapters.

**Table 3.1:** Experimental (Exp) values and SM predictions of the main Z pole observables [47]. The hadronic, electron and muon partial decay widths are derived from the previous quantities without assuming lepton universality.  $R_{e\mu}$  and  $R_{e\tau}$  were computed from the hadronic decay rates.

Observable	Exp	SM
$M_Z$ (GeV)	$91.1876 \pm 0.0021$	$91.1882 \pm 0.0020$
$\Gamma_Z$ (GeV)	$2.4955 \pm 0.0023$	$2.4941 \pm 0.0009$
$R_e$	$20.804 \pm 0.050$	$20.736 \pm 0.010$
$R_\mu$	$20.784 \pm 0.034$	$20.736 \pm 0.010$
$R_\tau$	$20.764 \pm 0.045$	$20.781 \pm 0.010$
$\mathcal{A}_e$	$0.15138 \pm 0.00216$	$0.1468 \pm 0.0003$
$\mathcal{A}_\mu$	$0.142 \pm 0.015$	$0.1468 \pm 0.0003$
$\mathcal{A}_\tau$	$0.136 \pm 0.015$	$0.1468 \pm 0.0003$
$\sigma_{\text{had}}$ (nb)	$41.481 \pm 0.033$	$41.482 \pm 0.008$
$\Gamma_{\text{had}}$ (MeV)	$1744.8 \pm 2.6$	$1740.97 \pm 0.85$
$\Gamma_e$ (MeV)	$83.87 \pm 0.12$	$83.942 \pm 0.085$
$\Gamma_\mu$ (MeV)	$83.95 \pm 0.18$	$83.941 \pm 0.085$
$\Gamma_\tau$ (MeV)	$84.03 \pm 0.21$	$83.759 \pm 0.085$
$R_{e\mu}$	$1.0009 \pm 0.0029$	$1.0000 \pm 0.0007$
$R_{e\tau}$	$1.0019 \pm 0.0032$	$0.9978 \pm 0.0007$

**Table 3.2:** Experimental (Exp) values and SM predictions for the left- and right-handed chiral couplings of the electron, muon and tau [122].

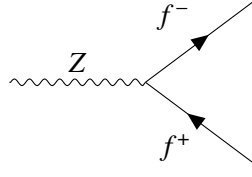
Coupling	Exp	SM
$gL_e$	$-0.26963 \pm 0.00030$	$0.26919 \pm 0.00020$
$gR_e$	$+0.23148 \pm 0.00029$	$0.23208 \pm_{0.00018}^{0.00016}$
$gL_\mu$	$-0.2689 \pm 0.0011$	$0.26919 \pm 0.00020$
$gR_\mu$	$+0.2323 \pm 0.0013$	$0.23208 \pm_{0.00018}^{0.00016}$
$gL_\tau$	$-0.26930 \pm 0.00058$	$0.26919 \pm 0.00020$
$gR_\tau$	$+0.23274 \pm 0.00062$	$0.077345 \pm_{0.000061}^{0.000053}$

### 3.2.1 $Z \rightarrow f^+ f^-$ and $R_f$

Consider the process of Z decay into a fermion anti-fermion pair  $Z \rightarrow f^+ f^-$  in Fig. 3.1, with  $f$  any fermion but the top quark, since  $m_t > M_Z$ . Using the Feynman rules in (2.30), the matrix element for the process is

$$-i\mathcal{M}(Z \rightarrow f^+ f^-) = -i\mathcal{M} = -i \frac{e}{s_W c_W} \epsilon^\mu(k, \lambda) \bar{u}_f(q_1) \gamma_\mu (g_{V_f} - g_{A_f} \gamma_5) v_f(q_2), \quad (3.8)$$

where  $q_1$  and  $q_2$  are the momenta of the fermion and anti-fermion, respectively, and  $k = q_1 + q_2$  is the momentum of the Z boson. The  $Z f^+ f^-$  coupling is written in terms of the vector and axial components to simplify the trace calculations and also to use a notation closer to that of [128, 129].  $\epsilon^\mu(k, \lambda)$  is the Z polarisation vector for the state  $\lambda$ ,  $u_f(q_1)$  and  $v_f(q_2)$  are the particle and anti-particle spinors. The

**Figure 3.1:** SM tree-level diagram for  $Z \rightarrow f^+ f^-$ .

squared matrix element is

$$|\mathcal{M}|^2 = \left( \frac{e}{s_W c_W} \right)^2 \epsilon^\mu(k, \lambda) \epsilon^{*\nu}(k, \lambda) \left[ \bar{u}_f(q_1) \gamma_\mu (g_{V_f} - g_{A_f} \gamma_5) v_f(q_2) \right] \quad (3.9)$$

$$\cdot \left[ \bar{v}_f(q_2) \gamma_\nu (g_{V_f} - g_{A_f} \gamma_5) u_f(q_1) \right]. \quad (3.10)$$

Summing over the spin and polarisation states gives

$$\begin{aligned} \langle |\mathcal{M}|^2 \rangle &= \left( \frac{e}{s_W c_W} \right)^2 \frac{1}{3} \sum_\lambda \epsilon^\mu(k, \lambda) \epsilon^{*\nu}(k, \lambda) \\ &\quad \sum_{s,r} \left[ \bar{u}_f^s(q_1) \gamma_\mu (g_V - g_A \gamma_5) v_f^r(q_2) \right] \left[ \bar{v}_f^r(q_2) \gamma_\nu (g_{V_f} - g_{A_f} \gamma_5) u_f^s(q_1) \right]. \end{aligned} \quad (3.11)$$

where  $s$  and  $r$  label the possible spin states of the fermion and anti-fermion and the  $\frac{1}{3}$  factor comes from averaging over the three possible initial state polarisations. The sum over the spins can be calculated by applying the trace formalism [130], which results in

$$\sum_{s,r} (...) = \text{Tr} \left[ (\gamma_\rho q_1^\rho + m_f) \gamma_\mu (g_{V_f} - g_{A_f} \gamma_5) (\gamma_\sigma q_2^\sigma + m_f) \gamma_\nu (g_{V_f} - g_{A_f} \gamma_5) \right]. \quad (3.12)$$

By applying the proprieties of the Dirac gamma matrices [38], we get

$$\sum_{s,r} (...) = 4 \left( g_{V_f}^2 + g_{A_f}^2 \right) (q_{1\mu} q_{2\nu} + q_{1\nu} q_{2\mu} - g_{\mu\nu} (q_1 \cdot q_2)) + 4 \left( g_{V_f}^2 - g_{A_f}^2 \right) m_f^2 g_{\mu\nu} \quad (3.13)$$

$$- 8 g_{V_f} g_{A_f} q_1^\rho q_2^\sigma i \epsilon_{\rho\mu\sigma\nu}. \quad (3.14)$$

The completeness relation for the sum over the polarisation states of a massive vector boson  $V$  is

$$\sum_\lambda \epsilon^\mu(k, \lambda) \epsilon^{*\nu}(k, \lambda) = -g^{\mu\nu} + \frac{k^\mu k^\nu}{M_V^2}. \quad (3.15)$$

Inserting these results in (3.11) and performing some simple algebraic manipulations gives

$$\langle |\mathcal{M}|^2 \rangle = \left( \frac{e}{s_W c_W} \right)^2 \frac{1}{3} \left\{ (g_{V_f}^2 + g_{A_f}^2) \left[ (q_1 \cdot q_2) + \frac{2}{M_Z^2} (k \cdot q_1)(k \cdot q_2) \right] + 3(g_{V_f}^2 - g_{A_f}^2) \frac{k^2 m_f^2}{M_Z^2} \right\}. \quad (3.16)$$

At the  $Z$  pole,  $k^2 = s = M_Z^2$  and considering that the  $Z$  boson momentum is defined as  $k = q_1 + q_2$ , the last expression can be further simplified by using the following relations

$$q_1 \cdot q_2 = \frac{1}{2} (M_Z^2 - 2m_f^2), \quad (3.17)$$

$$k \cdot q_1 = k \cdot q_2 = \frac{1}{2} M_Z^2, \quad (3.18)$$

to give

$$\langle |\mathcal{M}|^2 \rangle = N_c^f \frac{4}{3} \left( \frac{e}{s_W c_W} \right)^2 M_Z^2 \left[ g_{V_f}^2 + g_{A_f}^2 + 2 (g_{V_f}^2 - 2g_{A_f}^2) \left( \frac{m_f}{M_Z} \right)^2 \right], \quad (3.19)$$

where the colour factor  $N_c^f$  is added to distinguish the final state fermions.  $N_c^f = 3$  for quarks and  $N_c^f = 1$  for leptons.

The general expression for the decay rate for a two-body decay  $a \rightarrow b + c$  is [130]

$$\Gamma(a \rightarrow b + c) = \frac{p^*}{32\pi^2 m_a^2} \int |\mathcal{M}|^2 d\Omega, \quad (3.20)$$

with  $p^* = \sqrt{[m_a^2 - (m_b + m_c)^2][m_a^2 - (m_b - m_c)^2]}/2m_a$  the momentum of the final-state particles in the centre-of-mass frame. For the  $Z$  decay to fermions, this is equal to

$$\Gamma_f = N_c^f \left( \frac{e}{s_W c_W} \right)^2 \frac{M_Z}{12\pi} \sqrt{1 - 4 \left( \frac{m_f}{M_Z} \right)^2} \left[ g_{V_f}^2 + g_{A_f}^2 + 2 (g_{V_f}^2 - 2g_{A_f}^2) \left( \frac{m_f}{M_Z} \right)^2 \right]. \quad (3.21)$$

Defining  $\mu_f = m_f^2/M_Z^2$  and the standard width  $\Gamma_0 = (\frac{e}{s_W c_W})^2 \frac{M_Z}{36\pi}$ , the previous result can be rewritten as

$$\Gamma_f = 3N_c^f \Gamma_0 \sqrt{1 - 4\mu_f} \left[ g_{V_f}^2 + g_{A_f}^2 + 2 (g_{V_f}^2 - 2g_{A_f}^2) \mu_f \right] \quad (3.22)$$

$$= \frac{3}{2} N_c^f \Gamma_0 \sqrt{1 - 4\mu_f} \left[ g_{L_f}^2 + g_{R_f}^2 - (g_{L_f}^2 + g_{R_f}^2 - 6g_{L_f}g_{R_f}) \mu_f \right]. \quad (3.23)$$

Considering that for all SM fermions with the exception of the top quark  $\mu_f \ll 1$ , we can safely neglect the terms proportional to  $\mu_f$  and get the following approximate expression for the decay rate

$$\Gamma_f \approx 3N_c^f \Gamma_0 (g_{V_f}^2 + g_{A_f}^2) = \frac{3}{2} N_c^f \Gamma_0 (g_{L_f}^2 + g_{R_f}^2). \quad (3.24)$$

It is now possible to write an approximate SM expression for  $R_{el}$  using this final result. In terms of  $g_{L_l}$  and  $g_{R_l}$ ,

$$R_{el} = \frac{g_{L_l}^2 + g_{R_l}^2}{g_{L_e}^2 + g_{R_e}^2}. \quad (3.25)$$

which depends only on the left- and right-handed couplings of the final state fermion and electrons.



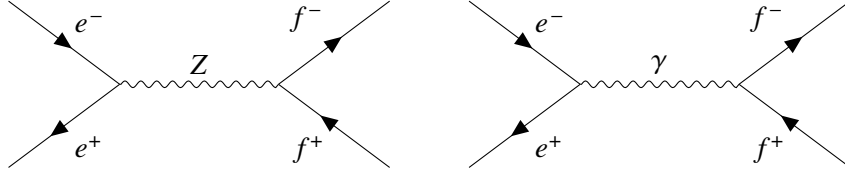


**Figure 3.2:** SM tree-level diagram for  $e^+e^- \rightarrow f^+f^-$ .

### 3.2.2 $e^+e^- \rightarrow f^+f^-$ and $\mathcal{A}_\mu$

Consider the process of fermion pair production from electron-positron annihilation in the context of the electroweak interaction,  $e^+e^- \rightarrow f^+f^-$ . The lowest order Feynman diagrams for the process can be seen in Fig. 3.2. The Higgs exchange contribution is neglected [128], since the Yukawa couplings are much weaker than the couplings to the Z. In this case,  $f$  can be any fermion other than the electron and its neutrino. For those final states there are also t-channel photon and Z exchanges related to the scattering process that occurs when the initial and final state fermions are a part of the same fermion doublet [131]. Using the Feynman rules in (2.30), the matrix element for the process is given by the sum of the two diagrams,

$$\begin{aligned}
 -i\mathcal{M} = & \bar{v}_e(p_2) (-ieQ_e\gamma_\mu) u_e(p_1) \frac{-ig^{\mu\nu}}{k^2} \bar{u}_f(q_1) (-ieQ_f\gamma_\nu) v_f(q_2) \\
 & + \bar{v}_e(p_2) \left( \frac{-ie}{s_W c_W} \right) \Gamma_{e\rho} u_e(p_1) \frac{-i \left( g^{\rho\sigma} - \frac{k^\rho k^\sigma}{M_Z^2} \right)}{k^2 - M_Z^2 + iM_Z\Gamma_Z^0} \bar{u}_f(q_1) \left( \frac{-ie}{s_W c_W} \right) \Gamma_{f\sigma} v_f(q_2),
 \end{aligned} \tag{3.26}$$

where  $p_1, p_2, q_1$  and  $q_2$  are the momenta of the electron, positron, fermion and anti-fermion, respectively, and  $k = p_1 + p_2 = q_1 + q_2$  is the exchanged boson's momentum.  $\Gamma_{e\rho} = \gamma_\rho (g_{V_e} - g_{A_e}\gamma_5)$  and  $\Gamma_{f\sigma} = \gamma_\sigma (g_{V_f} - g_{A_f}\gamma_5)$  represent the vector-axial  $Ze^+e^-$  and  $Zf^+f^-$  couplings. The Z propagator is written in the lowest order Breit-Wigner approximation [132], which takes into account the fact that the Z is an unstable particle. More than that, it removes the divergence at the Z pole of the ordinary tree-level propagator by displacing the pole from the real axis.

The terms proportional to  $k^\rho k^\sigma / M_Z^2$  cancel in the approximation that  $m_e \approx 0$ ,

$$\begin{aligned}
 \bar{v}_e(p_2) \Gamma_{e\rho} u_e(p_1) k^\rho &= \bar{v}_e(p_2) (g_{V_e} + g_{A_e}\gamma_5) \not{k} u_e(p_1) + \bar{v}_e(p_2) \not{k} (g_{V_e} - g_{A_e}\gamma_5) u_e(p_1) \\
 &= \bar{v}_e(p_2) (g_{V_e} + g_{A_e}\gamma_5) u_e(p_1) m_e + m_e \bar{v}_e(p_2) (g_{V_e} - g_{A_e}\gamma_5) u_e(p_1) \\
 &\approx 0,
 \end{aligned} \tag{3.27}$$

where we used the Dirac equation for spinors,

$$\not{k} u_e(p_1) = m_e u_e(p_1), \tag{3.28}$$

$$\bar{v}_e(p_2) \not{k} = m_e \bar{v}_e(p_2). \tag{3.29}$$

The matrix element can now be written in the form  $\mathcal{M} = \mathcal{M}_\gamma + \mathcal{M}_Z$ ,

$$\begin{aligned} \mathcal{M} \approx & -e^2 Q_e Q_f \bar{v}_e(p_2) \gamma_\mu u_e(p_1) \frac{g^{\mu\nu}}{k^2} \bar{u}_f(q_1) \gamma_\nu v_f(q_2) \\ & - \left( \frac{e^2}{s_W c_W} \right) \bar{v}_e(p_2) \Gamma_{e\rho} u_e(p_1) \frac{g^{\rho\sigma}}{k^2 - M_Z^2 + iM_Z \Gamma_Z^0} \bar{u}_f(q_1) \Gamma_{f\sigma} v_f(q_2). \end{aligned} \quad (3.30)$$

The squared matrix element averaged over the initial state spin states is

$$\langle |\mathcal{M}|^2 \rangle = \langle |\mathcal{M}_\gamma|^2 \rangle + 2 \langle \text{Re} \{ \mathcal{M}_Z \mathcal{M}_\gamma^\dagger \} \rangle + \langle |\mathcal{M}_Z|^2 \rangle, \quad (3.31)$$

where we consider that both the electron and positron beams are unpolarised. By applying the same techniques as in the previous section, we arrive at

$$\langle |\mathcal{M}_\gamma|^2 \rangle = \frac{8e^4}{s^2} Q_e^2 Q_f^2 \left[ (p_1 \cdot q_2)(p_2 \cdot q_1) + (p_1 \cdot q_1)(p_2 \cdot q_2) + (p_1 \cdot p_2)m_f^2 \right], \quad (3.32)$$

$$\begin{aligned} \langle \text{Re} \{ \mathcal{M}_Z \mathcal{M}_\gamma^\dagger \} \rangle = & \frac{8e^4}{s^2} Q_e Q_f \text{Re} \{ |\chi(s)| \} \left\{ g_{V_f} g_{V_e} [(p_2 \cdot q_1)(p_1 \cdot q_2) + (p_1 \cdot q_1)(p_2 \cdot q_2)] \right. \\ & + g_{A_f} g_{A_e} [(p_2 \cdot q_1)(p_1 \cdot q_2) - (p_1 \cdot q_1)(p_2 \cdot q_2)] \\ & \left. - g_{V_f} g_{V_e} (p_1 \cdot p_2)m_f^2 \right\}, \end{aligned} \quad (3.33)$$

$$\begin{aligned} \langle |\mathcal{M}_Z|^2 \rangle = & \frac{8e^4}{s^2} |\chi(s)|^2 \left\{ (g_{V_f}^2 + g_{A_f}^2)(g_{V_e}^2 + g_{A_e}^2) [(p_2 \cdot q_1)(p_1 \cdot q_2) + (p_1 \cdot q_1)(p_2 \cdot q_2)] \right. \\ & - (g_{V_f}^2 - g_{A_f}^2)(g_{V_e}^2 + g_{A_e}^2) (p_1 \cdot p_2)m_f^2 \\ & \left. - 4g_{V_f} g_{A_f} g_{V_e} g_{A_e} [(p_1 \cdot q_1)(p_2 \cdot q_2) - (p_2 \cdot q_1)(p_1 \cdot q_2)] \right\}, \end{aligned} \quad (3.34)$$

where we define

$$\chi(s) = \left( \frac{1}{s_W c_W} \right)^2 \frac{s}{s - M_Z^2 + iM_Z \Gamma_Z^0} \quad (3.35)$$

$$\text{Re} \{ \chi(s) \} = \left( \frac{1}{s_W c_W} \right)^2 \frac{s(s - M_Z^2)}{(s - M_Z^2)^2 + M_Z^2 \Gamma_Z^{02}} \quad (3.36)$$

At tree-level the electroweak axial-vector or left- and right-handed couplings are real. This is no longer the case at higher orders [128, 129].

In the centre-of-mass reference frame, defining  $\theta$  as the angle between the forward scattered fermion

and the electron-positron beam and defining the  $xz$  plane as the scattering plane, the four-momenta are

$$\begin{aligned} p_1 &= \frac{\sqrt{s}}{2}(1, 0, 0, 1), & q_1 &= \frac{\sqrt{s}}{2}(1, \beta \sin \theta, 0, \beta \cos \theta), \\ p_2 &= \frac{\sqrt{s}}{2}(1, 0, 0, -1), & q_2 &= \frac{\sqrt{s}}{2}(1, -\beta \sin \theta, 0, -\beta \cos \theta), \end{aligned} \quad (3.37)$$

with  $\beta = \sqrt{1 - 4m_f^2/s}$  the velocity of the final state fermion. Replacing the momenta,

$$\langle |\mathcal{M}_\gamma|^2 \rangle = e^4 Q_f^2 [1 + \cos^2 \theta + (1 - \beta^2) \sin^2 \theta] \quad (3.38)$$

$$\begin{aligned} \langle \text{Re} \{ \mathcal{M}_Z \mathcal{M}_\gamma^\dagger \} \rangle &= \frac{8e^4}{s^2} Q_e Q_f \text{Re} \{ |\chi(s)| \} \{ g_{V_f} g_{V_e} \frac{s^2}{8} [(1 + \beta^2) \cos^2 \theta + \sin^2 \theta] \\ &\quad + g_{A_f} g_{A_e} \frac{s^2}{8} 2\beta \cos \theta - g_{V_f} g_{V_e} \frac{s}{2} m_f^2 \}, \end{aligned} \quad (3.39)$$

$$\begin{aligned} \langle |\mathcal{M}_Z|^2 \rangle &= \frac{8e^4}{s^2} |\chi(s)|^2 \{ (g_{V_f}^2 + g_{A_f}^2) (g_{V_e}^2 + g_{A_e}^2) \frac{s^2}{8} [(1 + \beta^2) \cos^2 \theta + \sin^2 \theta] \\ &\quad - (g_{V_f}^2 - g_{A_f}^2) (g_{V_e}^2 + g_{A_e}^2) \frac{s}{2} m_f^2 + 4g_{V_f} g_{A_f} g_{V_e} g_{A_e} s^2 \beta \cos \theta \}, \end{aligned} \quad (3.40)$$

where the last two can also be expressed in terms of the left- and right-handed couplings as

$$\begin{aligned} \langle \text{Re} \{ \mathcal{M}_Z \mathcal{M}_\gamma^\dagger \} \rangle &= \frac{2e^4}{s^2} Q_e Q_f \text{Re} \{ |\chi(s)| \} \{ (g_{L_f} + g_{R_f})(g_{L_e} + g_{R_e}) \frac{s^2}{8} [(1 + \beta^2) \cos^2 \theta + \sin^2 \theta] \\ &\quad + (g_{L_f} - g_{R_f})(g_{L_e} - g_{R_e}) \frac{s^2}{8} 2\beta \cos \theta \\ &\quad - (g_{L_f} + g_{R_f})(g_{L_e} + g_{R_e}) \frac{s}{2} m_f^2 \}, \end{aligned} \quad (3.41)$$

$$\begin{aligned} \langle |\mathcal{M}_Z|^2 \rangle &= \frac{2e^4}{s^2} |\chi(s)|^2 \{ (g_{L_f}^2 + g_{R_f}^2) (g_{L_e}^2 + g_{R_e}^2) \frac{s^2}{8} [(1 + \beta^2) \cos^2 \theta + \sin^2 \theta] \\ &\quad - g_{L_f} g_{R_f} (g_{L_e}^2 + g_{R_e}^2) s m_f^2 + (g_{L_f}^2 - g_{R_f}^2) (g_{L_e}^2 - g_{R_e}^2) s^2 \beta \cos \theta \}. \end{aligned} \quad (3.42)$$

The total squared matrix element can be written in a way that organises the components by their dependence on the scattering angle  $\theta$ . Grouping the terms in this way gives

$$\langle |\mathcal{M}|^2 \rangle = e^4 N_c^f \left[ G_1(s) (1 + \cos^2 \theta) + 4\mu_f G_2(s) \sin^2 \theta + 2\sqrt{1 - \frac{4m_f^2}{s}} G_3(s) \cos \theta \right], \quad (3.43)$$

where we define the functions

$$G_1(s) = Q_e^2 Q_f^2 + 2g_{V_e} g_{V_f} Q_e Q_f \operatorname{Re} \{ \chi(s) \} + \left( g_{V_e}^2 + g_{A_e}^2 \right) \left( g_{V_f}^2 + g_{A_f}^2 - 4g_{A_f}^2 \mu_f \right) |\chi(s)|^2, \quad (3.44)$$

$$G_2(s) = Q_e^2 Q_f^2 + 2g_{V_e} g_{V_f} Q_e Q_f \operatorname{Re} \{ \chi(s) \} + \left( g_{V_e}^2 + g_{A_e}^2 \right) g_{V_f}^2 |\chi(s)|^2, \quad (3.45)$$

$$G_3(s) = 2g_{A_e} g_{A_f} Q_e Q_f \operatorname{Re} \{ \chi(s) \} + 4g_{V_e} g_{A_e} g_{V_f} g_{A_f} |\chi(s)|^2, \quad (3.46)$$

and  $N_c^f$  is the colour factor as in (3.19).

Neglecting the mass of the initial state particles, the expression for the differential cross section of a two body process  $a + b \rightarrow c + d$  is [130]

$$\frac{d\sigma^0}{d\Omega} = \frac{1}{64\pi^2 s} \beta \langle |\mathcal{M}|^2 \rangle. \quad (3.47)$$

Replacing (3.43) in (3.47) and integrating in the solid angle gives the total cross section

$$\sigma^0(s) = \frac{e^4}{12\pi s} N_c^f \beta \left[ G_1(s) + 2 \frac{m_f^2}{s} G_2(s) \right]. \quad (3.48)$$

As  $s \rightarrow 0$  or  $s \rightarrow \infty$ , the total cross section approaches a constant. For energies below the  $Z$  resonance, the QED contribution is the most important and the cross section decreases with increasing energy as  $1/s$ . When  $s \approx M_Z^2$ , the pure  $Z$  contribution is dominant and would technically diverge when  $s \rightarrow M_Z^2$  if it were not for the resummed propagator. This behaviour is called the  $Z$  resonance, or Breit-Wigner resonance. At the peak of the resonance, the  $Z$  boson exchange diagram is roughly three orders of magnitude greater than the QED diagram [122]. The interference term (3.41) vanishes at the pole, but becomes important off-peak. Notice also that the terms proportional to  $\cos \theta$  do not contribute to the total cross section.

Integrating the differential cross section in the forward and backward hemispheres as defined in (3.4) gives

$$\sigma_F^0(s) = \int_{\theta < \frac{\pi}{2}} \frac{d\sigma^0}{d\Omega}(s, \theta) d\Omega = \frac{e^4}{96\pi s} N_c^f \beta \left[ 4G_1(s) + 8 \frac{m_f^2}{s} G_2(s) + 3\beta G_3(s) \right], \quad (3.49)$$

$$\sigma_B^0(s) = \int_{\theta > \frac{\pi}{2}} \frac{d\sigma^0}{d\Omega}(s, \theta) d\Omega = \frac{e^4}{96\pi s} N_c^f \beta \left[ 4G_1(s) + 8 \frac{m_f^2}{s} G_2(s) - 3\beta G_3(s) \right]. \quad (3.50)$$

From the definition in (3.3) the tree-level expression for the asymmetry can now be written as

$$A_{FB}^{0,f}(s) = \frac{\sigma_F^0 - \sigma_B^0}{\sigma_F^0 + \sigma_B^0} = \frac{3}{4} \beta \frac{G_3(s)}{G_1(s) + 2 \frac{m_f^2}{s} G_2(s)}. \quad (3.51)$$

Unlike the cross section, this observable allows some insight into the  $\cos \theta$  dependent term in the matrix element (3.43).

At the  $Z$  pole  $A_{FB}^{0,f}$  can on approximation be written as the product of two factors that each depend

exclusively on the initial or final stated fermions. For  $s = M_Z^2$ ,  $\text{Re} \{ \chi(M_Z^2) \} = 0$ ,  $\beta = \beta_Z = \sqrt{1 - 4\mu_f}$  and

$$|\chi(M_Z^2)|^2 = \frac{M_Z^2}{\Gamma_Z^{02}}. \quad (3.52)$$

Taking the narrow width approximation,  $\Gamma_Z^{02} \ll M_Z^2$ , (3.51) becomes

$$A_{FB}^{0,f} \approx \frac{3}{4} \beta_Z \frac{2g_{V_e}g_{A_e}}{g_{V_e}^2 + g_{A_e}^2} \frac{2g_{V_f}g_{A_f}}{g_{V_f}^2(1 - 2\mu_f) + g_{A_f}^2\beta_Z^2} \quad (3.53)$$

$$= \frac{3}{4} \beta_Z \frac{g_{L_e}^2 - g_{R_e}^2}{g_{L_e}^2 + g_{R_e}^2} \frac{2(g_{L_f}^2 - g_{R_f}^2)}{(g_{L_f} + g_{R_f})^2(1 - 2\mu_f) + (g_{L_f} - g_{R_f})^2\beta_Z^2}, \quad (3.54)$$

and in the case where  $m_f \ll M_Z$ ,  $\mu_f \approx 0$ ,  $\beta_Z \approx 1$  and

$$A_{FB}^{0,f} \approx \frac{3}{4} \frac{2g_{V_e}g_{A_e}}{g_{V_e}^2 + g_{A_e}^2} \frac{2g_{V_f}g_{A_f}}{g_{V_f}^2 + g_{A_f}^2} = \frac{3}{4} \frac{g_{L_e}^2 - g_{R_e}^2}{g_{L_e}^2 + g_{R_e}^2} \frac{g_{L_f}^2 - g_{R_f}^2}{g_{L_f}^2 + g_{R_f}^2} = \frac{3}{4} \mathcal{A}_e \mathcal{A}_f \quad (3.55)$$

where we recover the approximate formulas in (3.2).

The fermionic asymmetry parameters quantify the parity violation of the weak interaction. If  $g_{L_f} = g_{R_f} \Leftrightarrow g_{A_f} = 0$ , then  $\mathcal{A}_f = 0$ . This observable, depends only on the square of the couplings, being unable to give information about the relative signs.



## Chapter 4

# Radiative corrections

The amplitudes of the two processes discussed in the previous chapters were only analysed at order zero in perturbation theory. These are the leading terms of the expansion. The contributions from higher orders are called radiative corrections. Diagrammatically they are described by graphs with loops or the emission of particles from the initial or final states and their interference. A thorough understanding of the radiative corrections and their profound relation to renormalisation is needed for a high precision study, where the sensitivity of the detectors makes it possible to discern the effect of these smaller contributions, whether coming from SM physics or beyond.

In this chapter, the one loop radiative corrections to  $e^+e^- \rightarrow f^+f^-$  and  $Z \rightarrow f^+f^-$  are discussed. Starting with a brief introduction to renormalisation, the renormalisation of the weak neutral current vertex is presented following Böhm, Hollik and Spiesberger's multiplicative renormalisation in the on-shell scheme [128, 133, 134]. Then the radiative corrections are explained, making a distinction between the QED and weak corrections, and how they change the two observables  $R_{el}$  and  $\mathcal{A}_f$  at one loop. Finally, the inclusion of physics beyond the SM is discussed.

### 4.1 Regularisation and renormalisation

When resorting to the method of the perturbation expansion in QFT [38], one inevitably finds divergences in the calculations. These divergences, Ultraviolet (UV) divergences, are inescapable and a consequence of large fluctuations of the fields in short distance scales [135]. As a consequence, the momenta of the loops are unbounded and tend to infinity. This mathematical downside of perturbativity leads to nonphysical divergent results. How to address these problems and recover physical meaning, hence the possibility of making testable predictions, is the domain of renormalisation. The main working principle of renormalisation is that it is possible to define the free parameters of the theory in such a way that they cancel the divergences.

The first step in dealing with the divergent integral is to separate the finite and singular parts of the integral in a process called regularisation. There are several methods to regularise the integrals, for example lattice regularisation [136] or Pauli-Villars regularisation [137]. In this work we follow the process of dimensional regularisation [25, 138, 139]. The main advantage of this method is that, because it is based on an analytical continuation of the original four dimensional integral, it preserves Lorentz and

gauge invariance [25]. On the other hand, one is required to work with the Dirac algebra in  $d$  dimensions as well as with  $\gamma_5$ , whose treatment in higher dimensions is complicated due to the possible appearance of axial anomalies [140–142]. The loop momenta in dimensional regularisation have components in all dimensions, but the momenta of the external legs and the  $\gamma_5$  matrix are inherently defined in four dimensions. The  $\gamma_5$  matrix in particular cannot be defined in dimensions higher than four in a way that preserves all its properties, like the anticommutation relation  $\{\gamma_5, \gamma_\mu\} = 0$ . This leads to the non-conservation of the axial current [39]. The general idea of dimensional regularisation is to extend the dimensionality of space-time from 4 to an arbitrary number  $d$  of dimensions,

$$\int \frac{d^4 k}{(2\pi)^4} \rightarrow \mu^{4-d} \int \frac{d^d k}{(2\pi)^d}. \quad (4.1)$$

$d$  is a continuous variable, thus not necessarily an integer. In doing so, the UV divergences are replaced after integration by singularities related to the number of dimensions and the integral is split into a finite and a singular part. This singular part is then to be cancelled by renormalisation so that the final results are finite for  $d \rightarrow 4$ . The integrals are commonly written in terms of a set of functions called Passarino-Veltman integrals [143].

The masses and couplings of the Lagrangian as defined in (2.1) are free parameters of the theory. A general free parameter of the unrenormalised Lagrangian is called "bare" parameter and represented by  $g_0$ . The divergences from the one loop diagrams can be interpreted as shifts in these quantities. As such, because the parameters can be redefined,  $g_0$  can be written as

$$g_0 = Z_g^{\frac{1}{2}} g \approx \left(1 + \frac{1}{2} \delta Z_g\right) g \quad (4.2)$$

where  $Z_g$  is a renormalisation constant and  $g$  is the renormalised parameter.  $g$  is finite after being fixed by a renormalisation condition. There must be as many renormalisation conditions as free parameters.  $\delta g$  is the counter-term which is chosen to cancel the divergences coming from the corrections to the parameter. This procedure assures that the S-matrix elements are finite, but in order to obtain finite propagators and vertices it is necessary to ensure that the residue of the pole of the propagator is equal to one. This is done by introducing a field strength renormalisation constant

$$\phi_0 = Z_\phi^{\frac{1}{2}} \phi \approx \left(1 + \frac{1}{2} \delta Z_\phi\right) \phi, \quad (4.3)$$

where similarly to the parameter  $g_0$ ,  $\phi_0$  is the bare field,  $\phi$  the renormalised physical field and  $\delta Z_\phi$  is the counter-term. Like with the free parameters, renormalisation conditions fix  $\phi$  and there must be as many of them as there are fields.

The expansion in the counter-terms of the renormalisation constant for a field or parameter  $i$ ,  $Z_i$ , is done to the same order as the perturbative expansion. So, for first order calculations as exemplified for a general  $g$  and  $\phi$  above,  $Z_i = 1 + \delta Z_i + O(\delta Z_i^2)$ . Replacing the bare parameters and fields in the Lagrangian



with their renormalised counterparts and respective counter-terms allows to rewrite the Lagrangian as

$$\mathcal{L}_0(\phi_0, g_0) \approx \mathcal{L}(\phi, g) + \mathcal{L}_{\text{ct}}(\phi, g, \delta Z_\phi, \delta g), \quad (4.4)$$

with  $\mathcal{L}$  the Lagrangian from where one builds the tree-level and one loop diagrams and  $\mathcal{L}_{\text{ct}}$  the counter-term Lagrangian. Here lies the distilled essence of renormalisation, where for the renormalisation of a certain diagram one needs to add to it a certain number of counter-term diagrams to cancel the divergence. Not all theories, however, are fully renormalisable, even if they can be renormalised to a certain order [135]. This method of multiplying the parameters by a renormalisation constant is called multiplicative renormalisation. In this work, we follow [128, 133, 134], from where the notation heavily borrows.

#### 4.1.1 Renormalisation transformations for the electroweak sector of the SM

There are several possible renormalisation prescriptions, like the  $\overline{\text{MS}}$  scheme [144, 145], the  $\overline{\text{MS}}$  scheme [146, 147] or the on-shell scheme [143, 148–150]. In this work, we use Böhm, Hollik and Spiesberger's on-shell renormalisation [128, 133, 134]. This could be called a semi on-shell scheme, due to a number of noteworthy caveats that distinguish it from the other on-shell schemes. Renormalisation is done in a way that respects the electroweak symmetry. A single field renormalisation constant,  $\delta Z_2^W$  and  $\delta Z_2^B$ , is introduced for each multiplet. This is the minimum required to get finite self-energies and vertex corrections, as well as to fulfil the on-shell condition for the charge and that the residue of the photon propagator is equal to one like in QED. On the other hand, the  $Z$ ,  $W^\pm$  and  $I_3 = +1/2$  quark propagators do not have residue equal to one [133]. This scheme is a natural extension of the QED on-shell renormalisation, with the renormalised electric charge being defined as the full  $\gamma e^+ e^-$  coupling for on-shell external particles in the Thomson limit ( $k^2 = 0$ ) of Compton scattering.

To renormalise the Lagrangian of the electroweak sector of the SM (2.9) in line with what was discussed in the previous section, the following renormalisation transformations for the fields or symmetry multiplets of fields and free parameters of the model are introduced

$$\begin{aligned} W_{0\mu}^a &\rightarrow (Z_2^W)^{\frac{1}{2}} W_{\mu}^a, & \psi_{i0}^L &\rightarrow (Z_L^i)^{\frac{1}{2}} \psi_i^L, & H_0 &\rightarrow (Z^H)^{\frac{1}{2}} H, \\ B_{0\mu} &\rightarrow (Z_2^B)^{\frac{1}{2}} B_{\mu}, & \psi_{i\omega 0}^R &\rightarrow (Z_R^{i\omega})^{\frac{1}{2}} \psi_{i\omega}^R, \\ g_0 &\rightarrow Z_1^W (Z_2^W)^{-\frac{3}{2}} g, & v_0 &\rightarrow (Z^H)^{\frac{1}{2}} (v - \delta v), \\ g'_0 &\rightarrow Z_1^B (Z_2^B)^{-\frac{3}{2}} g', & y_{i\omega 0} &\rightarrow (Z^H)^{\frac{1}{2}} Z_1^{i\omega} y_{i\omega}. \end{aligned} \quad (4.5)$$

The transformations for the remaining parameters are not written here explicitly, since they are not necessary for the coming calculations. The field renormalisation constants are identified by an index "2". The tadpole diagrams originating from the Higgs potential in one loop order are renormalised independently in a way that the relation between the vev and the parameters of the Higgs potential,  $v = \sqrt{-\mu^2/\lambda}$ , remains valid after renormalisation. This allows to remove the tadpole diagrams from the renormalised Green's functions and amplitudes, but in that case the mass counter-terms are not gauge invariant [133].

The input parameters are chosen to be the fundamental charge  $e$ , the masses of the physical bosons

$M_W$ ,  $M_Z$  and  $M_H$  and of the fermions,  $m_f$ , as well as the fields  $A_\mu$ ,  $Z_\mu$  and  $W_\mu^\pm$  themselves. This choice is not unique, but it configures a set of relevant, experimentally measurable physical quantities. Moreover, it is the most natural choice for the electroweak renormalisation in the on-shell scheme. The renormalised Lagrangian can be written in terms of the fields  $A_\mu$ ,  $Z_\mu$ ,  $W_\mu^\pm$  and  $h$  by following the same steps as in section 2.3 and taking into account the renormalisation transformations. By doing this, equivalent expressions to (4.5) are obtained for the physical fields

$$\begin{aligned} W_{0\mu}^\pm &\rightarrow (Z^W)^\frac{1}{2} W_\mu^\pm, & M_{W_0}^2 &\rightarrow M_W^2 + \delta M_W^2, & m_{f_0}^2 &\rightarrow m_f^2 + \delta m_f^2, \\ \begin{pmatrix} Z_{0\mu} \\ A_{0\mu} \end{pmatrix} &\rightarrow \begin{pmatrix} (Z_2^Z)^\frac{1}{2} & (Z_2^{\gamma Z})^\frac{1}{2} \\ (Z_2^{\gamma Z})^\frac{1}{2} & (Z_2^\gamma)^\frac{1}{2} \end{pmatrix} \begin{pmatrix} Z_\mu \\ A_\mu \end{pmatrix}, & M_{Z_0}^2 &\rightarrow M_Z^2 + \delta M_Z^2, & e_0 &\rightarrow e + \delta e \\ h_0 &\rightarrow (Z^h)^\frac{1}{2} h, & M_{h_0}^2 &\rightarrow M_h^2 + \delta M_h^2, \end{aligned} \quad (4.6)$$

which now include also the masses of the bosons and fermions. The mixing of the photon and the  $Z$  is parameterised by a real  $2 \times 2$  matrix. The counter-terms are obtained by performing the renormalisation transformation in (2.9) and rewriting the result in terms of the physical fields with (2.16) and (2.17). Comparing the following terms in the renormalised Lagrangian,

$$-\frac{1}{4}\delta Z_2^W (\partial_\mu W_\nu^a - \partial_\nu W_\mu^a)^2 - \frac{1}{4}\delta Z_2^B (\partial_\mu B_\nu - \partial_\nu B_\mu)^2 + \dots, \quad (4.7)$$

with the terms obtained after rotation to the physical basis

$$\begin{aligned} &-\frac{1}{4} (c_W^2 \delta Z_2^W + s_W^2 \delta Z_2^B) (\partial_\mu Z_\nu - \partial_\nu Z_\mu)^2 - \frac{1}{4} (s_W^2 \delta Z_2^W + c_W^2 \delta Z_2^B) (\partial_\mu A_\nu - \partial_\nu A_\mu)^2 \\ &-\frac{1}{2} c_W s_W (\delta Z_2^W - \delta Z_2^B) (\partial_\mu Z_\nu - \partial_\nu Z_\mu) (\partial_\mu A_\nu - \partial_\nu A_\mu) + \dots, \end{aligned} \quad (4.8)$$

gives the following relations between the counter-terms of  $W_\mu^3$  and  $B_\mu$  and those of the photon and  $Z$  boson

$$\begin{pmatrix} \delta Z_i^\gamma \\ \delta Z_i^Z \end{pmatrix} \approx \begin{pmatrix} s_W^2 & c_W^2 \\ c_W^2 & s_W^2 \end{pmatrix} \begin{pmatrix} \delta Z_i^W \\ \delta Z_i^B \end{pmatrix} \quad (4.9)$$

and

$$\delta Z_i^{\gamma Z} = c_W s_W (\delta Z_i^W - \delta Z_i^B) = \frac{c_W s_W}{c_W^2 - s_W^2} (\delta Z_i^Z - \delta Z_i^\gamma). \quad (4.10)$$

To find the connection between the counter-terms and the quantum corrections of the theory, first the propagators of the free fields must be written at one loop level so that the renormalisation transformations in (4.6) can be applied. The propagator represents the probability of the particle to move between two points in space-time. It is formally described by the causal Green function of the equations of motion of the field. As an example, consider a generic scalar field  $\phi$  with momentum  $p$ . The full bare propagator is

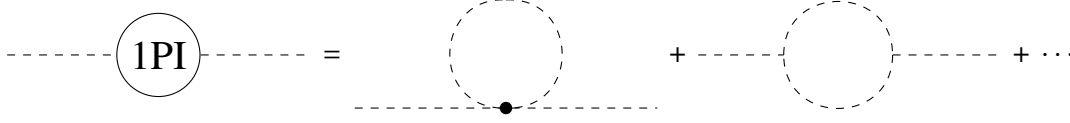


**Figure 4.1:** Diagrams that contribute to one 1PI self energy function.

given by [39]

$$\begin{aligned}
 G_0(p^2) &= \int d^4x e^{ip \cdot x} \langle \Omega | T \phi_0(x) \phi_0^*(x) | \Omega \rangle = \sqrt{Z_\phi}^* \int d^4x e^{ip \cdot x} \langle \Omega | T \phi(x) \phi^*(x) | \Omega \rangle \sqrt{Z_\phi} \\
 &= \sqrt{Z_\phi}^* \hat{G}(p^2) \sqrt{Z_\phi}
 \end{aligned} \tag{4.11}$$

where  $T$  is the time ordering operator,  $Z_\phi$  the field strength renormalisation constant and  $\hat{G}(p^2)$  is the renormalised propagator. The circumflex symbol “ $\hat{\phantom{x}}$ ” is used to denote a renormalised quantity. In the language of perturbation theory, the full or dressed propagator is given by the sum of the tree-level propagator with all one particle irreducible (1PI) self-energy diagrams. 1PI self-energies are all topologies that cannot be split into two distinct graphs by cutting a single internal line.  $-i\Sigma(p^2)$  is defined as the sum of the truncated diagrams of Fig. 4.1.

#### 4.1.2 Renormalisation of the vector boson propagators

The vector boson propagator is written in terms of transverse and longitudinal amplitudes,  $A_V^T$  and  $A_V^L$ , as

$$D_{V_{\mu\nu}}(k) = -ig_{\mu\nu}A_V^T(k^2) + k_\mu k_\nu A_V^L(k^2) \tag{4.12}$$

with  $V = \gamma, Z, W$ .  $A_V^T$  is given by the sum of the transverse components of the tree-level propagator and of the higher-order corrections. In physical amplitudes the longitudinal component of the vector boson propagators is suppressed as a consequence of the Slavnov-Taylor identities [151, 152]. As such, only the transverse component has to be taken into account. From now on, every mention to the propagator is to be understood as meaning the transverse component that multiplies the factor  $g_{\mu\nu}$ , which is omitted for simplicity.

The quantum corrections to the propagators come in the form of the 1PI diagrams of Fig. 4.1. The

full bare propagator for the  $W$  boson is given by the Dyson sum of the 1PI self-energies,

$$\begin{aligned}
 -iD_W &= \text{diagram with a shaded circle} = \text{diagram with a wavy line} + \text{diagram with a wavy line and a 1PI circle} + \text{diagram with a wavy line and two 1PI circles} + \dots \\
 &= \frac{-i}{s - M_{W_0}^2} + \frac{-i}{s - M_{W_0}^2} (-i\Sigma_W(s)) \frac{-i}{s - M_{W_0}^2} + \frac{-i}{s - M_{W_0}^2} (-i\Sigma_W(s)) \frac{-i}{s - M_{W_0}^2} (-i\Sigma_W(s)) \frac{-i}{s - M_{W_0}^2} + \dots \\
 &= \frac{-i}{s - M_{W_0}^2} + \frac{-i}{s - M_{W_0}^2} \left( -i\Sigma_W(s) \frac{-i}{s - M_{W_0}^2} \right) + \frac{-i}{s - M_{W_0}^2} \left( -i\Sigma_W(s) \frac{-i}{s - M_{W_0}^2} \right)^2 + \dots \\
 &= \frac{-i}{s - M_{W_0}^2} \sum_{n=0}^{\infty} \left( -i\Sigma_W(s) \frac{-i}{s - M_{W_0}^2} \right)^n \\
 &= \frac{-i}{s - M_{W_0}^2 + \Sigma_W(s)},
 \end{aligned} \tag{4.13}$$

which is a geometric series. This result leads to interpreting the inverse of the bare propagator as the sum of the 1PI functions

$$D_W^{-1} = s - M_{W_0}^2 + \Sigma_W(s) = \text{diagram with a wavy line and a shaded circle}^{-1}, \tag{4.14}$$

called the 1PI two point function.

Making use of the general expression (4.11) and of the renormalisation transformations (4.6) to first order, that is keeping only terms linear in the counter-terms and neglecting the products of counter-terms and  $\Sigma_W$ , one gets

$$\hat{D}_W^{-1} \approx s - M_W^2 - \delta M_W^2 + \Sigma_W(s) + \delta Z_2^W (s - M_W^2), \tag{4.15}$$

from where the renormalised self-energy is defined as

$$\hat{\Sigma}_W(s) = \Sigma_W(s) - \delta M_W^2 + \delta Z_2^W (s - M_W^2). \tag{4.16}$$

At tree-level the photon and the  $Z$  propagate independently. The fields are mass eigenstates. However, because of the mixing of the fields at higher orders the propagator has to be considered a  $2 \times 2$  matrix, since higher order corrections introduce non-diagonal terms. The simplest way to compute the  $\gamma Z$  propagator is to first consider the corresponding 1PI two point function, the inverse propagator

$$\mathbf{D}^{-1} = \begin{pmatrix} s + \Sigma_{\gamma\gamma}(s) & \Sigma_{\gamma Z}(s) \\ \Sigma_{\gamma Z}(s) & s - M_{Z_0}^2 + \Sigma_{ZZ}(s) \end{pmatrix}. \tag{4.17}$$

Inverting this matrix gives the full bare photon,  $Z$  and mixing  $\gamma Z$  propagators represented in Fig. 4.2

$$\mathbf{D} = \begin{pmatrix} D_\gamma & D_{\gamma Z} \\ D_{\gamma Z} & D_Z \end{pmatrix}, \tag{4.18}$$

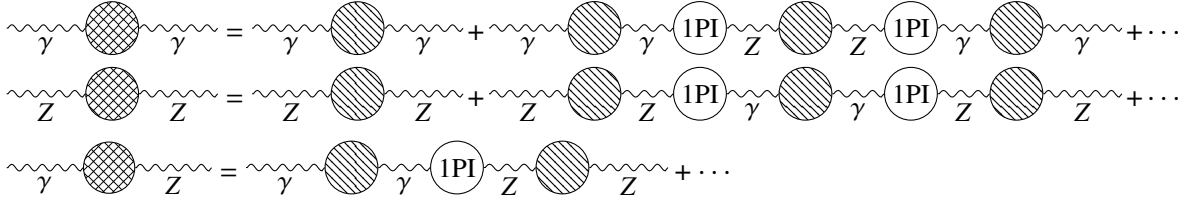


**Figure 4.2:** Resummed photon, Z boson and  $\gamma Z$  propagators.

$$\begin{aligned}
 D_\gamma &= \frac{1}{s + \Sigma_{\gamma\gamma}(s) - \frac{\Sigma_{\gamma Z}^2(s)}{s - M_{Z_0}^2 + \Sigma_Z(s)}}, \\
 D_Z &= \frac{1}{s - M_{Z_0}^2 + \Sigma_Z(s) - \frac{\Sigma_{\gamma Z}^2(s)}{s + \Sigma_\gamma(s)}}, \\
 D_{\gamma Z} &= \frac{-\Sigma_{\gamma Z}(s)}{[s + \Sigma_\gamma(s)] [s - M_{Z_0}^2 + \Sigma_Z(s)] - \Sigma_{\gamma Z}^2(s)}.
 \end{aligned} \tag{4.19}$$

Proceeding in the same manner as for the  $W$  propagator, but taking into consideration the matrix structure of the  $\gamma Z$  propagator, one obtains the one-loop renormalised self-energies

$$\begin{aligned}
 \hat{\Sigma}_\gamma(s) &= \Sigma_\gamma(s) + \delta Z_2^\gamma s, \\
 \hat{\Sigma}_Z(s) &= \Sigma_Z(s) - \delta M_Z^2 + \delta Z_2^Z (s - M_Z^2), \\
 \hat{\Sigma}_{\gamma Z}(s) &= \Sigma_{\gamma Z}(s) - \delta Z_2^{\gamma Z} s + (\delta Z_1^{\gamma Z} - \delta Z_2^{\gamma Z}) M_Z^2.
 \end{aligned} \tag{4.20}$$

The mass counter-terms are related by

$$\frac{\delta M_Z^2}{M_Z^2} - \frac{\delta M_W^2}{M_W^2} = \frac{s_W}{c_W} (\delta Z_2^{\gamma Z} - 2\delta Z_1^{\gamma Z}). \tag{4.21}$$

Keeping only the leading terms resummed to all orders, the propagators in (4.19) are after renormalisation written as

$$\begin{aligned}
 D_\gamma &\approx \frac{1}{s + \hat{\Sigma}_{\gamma\gamma}(s)}, \\
 D_Z &\approx \frac{1}{s - M_Z^2 + \hat{\Sigma}_Z(s)}, \\
 D_{\gamma Z} &\approx \frac{-\hat{\Sigma}_{\gamma Z}(s)}{s(s - M_Z^2)}.
 \end{aligned} \tag{4.22}$$

This expression for the  $Z$  propagator can be identified with the Breit-Wigner form in (3.26) at the  $Z$  pole if  $\text{Re} \{ \hat{\Sigma}_Z(M_Z^2) \} \approx 0$  and  $\text{Im} \{ \hat{\Sigma}_Z(M_Z^2) \} \approx M_Z \Gamma_Z^0$ .

The full bare fermion propagator is obtained in the same way as for the  $W$  boson. Summing all 1PI diagrams gives

where in the third line we consider the self-energy of the fermion  $\Sigma_f$  a function of  $\not{k} = \gamma_\mu k^\mu$  and rewrite the propagator as  $i/(\not{k} - m_{f_0})$  [39]. Here we drop the family indices and write these expressions for any fermion  $f$ .

$$\Sigma_f(k) = k P_L \Sigma_{f_L}(s) + k P_R \Sigma_{f_R}(s) + m_{f_0} \Sigma_{f_S}(s), \quad (4.24)$$

putting into evidence the different chiral components. The renormalised fermion self energy is obtained after performing the renormalisation transformations (4.6),

$$\hat{\Sigma}_f(k) = \not{k} P_L (\Sigma_L(s) + \delta Z_L) + \not{k} P_R (\Sigma_R(s) + \delta Z_R^f) + m_f \left( \Sigma_S(s) - \frac{\delta Z_L}{2} - \frac{\delta Z_R^f}{2} - \frac{\delta m_f}{m_f} \right). \quad (4.25)$$

The mass renormalisation counter-term is related to the Yukawa and Higgs vev renormalisation constants. From the definition of the bare mass of the fermion in terms of the Higgs vev and Yukawa couplings,  $m_{f_0} = v y_{f_0} / \sqrt{2}$ , performing the renormalisation expansion (4.5) gives

$$\frac{\delta m_f}{m_f} = \delta Z_1^f - \frac{\delta v}{v}, \quad (4.26)$$

where  $f$  identifies the fermion. Due to this relation, the renormalisation of the Yukawa couplings is fixed by the renormalisation the fermion masses.

The renormalised neutral vertices are obtained by performing the renormalisation transformations (4.6) in the  $\gamma f^+ f^-$  and  $Z f^+ f^-$  vertices. This is the same as summing to one loop order all contributing diagrams - the tree-level diagram, the vertex correction, the  $\gamma Z$  mixing diagrams and the self-energies of

the external legs. For the electromagnetic vertex, this gives [133]

$$\hat{\Gamma}_\mu^{\gamma ff} = -ieQ_f\gamma_\mu + ie\Lambda_\mu^{\gamma ff} - ieQ_f\gamma_\mu(\delta Z_1^\gamma - \delta Z_2^\gamma) - ieQ_f\gamma_\mu(\delta Z_L P_L + \delta Z_R P_R) - i\frac{e}{s_W c_W}\gamma_\mu(g_L P_L + g_R P_R)(\delta Z_1^{\gamma Z} - \delta Z_2^{\gamma Z}), \quad (4.27)$$

where  $\Lambda_\mu^{\gamma ff}$  are the one loop vertex corrections. Proceeding in a similar fashion, one obtains the renormalised neutral weak vertex

$$\hat{\Gamma}_\mu^{Z ff} = i\frac{e}{s_W c_W}\gamma_\mu(g_L P_L + g_R P_R) + ie\Lambda_\mu^{Z ff} + i\frac{e}{s_W c_W}\gamma_\mu(g_L P_L + g_R P_R)(\delta Z_1^Z - \delta Z_2^Z) + ieQ_f\gamma_\mu(\delta Z_1^{\gamma Z} - \delta Z_2^{\gamma Z}) + i\frac{e}{s_W c_W}\gamma_\mu(g_L \delta Z_L P_L + g_R \delta Z_R^f P_R), \quad (4.28)$$

with  $\Lambda_\mu^{Z ff}$  the one loop vertex contribution.

The structure of the first order vertex contributions  $\Lambda_\mu^{\gamma ff}$  and  $\Lambda_\mu^{Z ff}$  is addressed in Section 4.2.2.1.

#### 4.1.5 On-shell conditions

Once the renormalisation transformation from bare quantities is complete, a set of conditions must be chosen to define the renormalised quantities and counter-terms and relate them to some experimental observable. This set of rules are collectively called the renormalisation conditions. In the on-shell scheme, the counter-terms are defined in such a way that the renormalised parameters are equal to their physical values. This is the same as saying, for example, that the renormalised masses must correspond to their on-shell values, respecting the well known relativistic relations. This is an important advantage of this scheme, where the parameters have an obvious physical meaning and are experimentally well known.

The on-shell conditions for the masses and fields can be summarised as

1. The masses are the real parts of the poles of the propagators.
2. Mixing between fields must vanish on mass shell.
3. The fields are normalised by fixing the residue of the propagator at the pole to be equal to 1.

These conditions ensure the proper pole structure and lead to the renormalised propagator coinciding with the tree-level propagator when  $p^2 \approx m^2$ .

The on-shell conditions for the electroweak sector of the SM are written as

$$\begin{aligned} \text{Re} \left\{ \text{---} \text{W} \text{---} \text{---} \right\} \Big|_{s=M_W^2} &= 0 \Leftrightarrow \text{Re} \{ \hat{\Sigma}_W(M_W^2) \} = 0, \\ \text{Re} \left\{ \text{---} \text{Z} \text{---} \text{---} \right\} \Big|_{s=M_Z^2} &= 0 \Leftrightarrow \text{Re} \{ \hat{\Sigma}_Z(M_Z^2) \} = 0, \\ \text{Re} \left\{ \text{---} \text{f} \text{---} \text{---} \right\} \Big|_{s=m_f^2} &= 0 \Leftrightarrow \text{Re} \{ \hat{\Sigma}_f(m_f^2) \} = 0, \end{aligned} \quad (4.29)$$

$$\left( \text{diagram: } \gamma \text{ (wavy line)} \text{ --- } \text{blob} \text{ --- } Z \text{ (wavy line)} \right) \Big|_{s=0} = 0 \Leftrightarrow \hat{\Sigma}_{\gamma Z}(0) = 0, \quad (4.30)$$

where the (4.29) corresponds to the first on-shell condition and (4.30) to the second. There are more renormalisation constants than there are free parameters. As such, following [133], the remaining counter-terms can be fixed by applying the third condition to the photon and charged lepton propagators,

$$\begin{aligned} \frac{\partial}{\partial s} \left( \text{diagram: } \gamma \text{ (wavy line)} \text{ --- } \text{blob} \text{ --- } \gamma \text{ (wavy line)} \right) \Big|_{s=0} &= 0 \Leftrightarrow \frac{\partial \hat{\Sigma}_{\gamma}}{\partial s} \Big|_{s=0} = 0, \\ \frac{1}{\not{k} - m_-^2} \left( \text{diagram: } f \text{ (solid line)} \text{ --- } \text{blob} \text{ --- } f \text{ (solid line)} \right) \Big|_{\not{k}=m_-^2} &= 0 \Leftrightarrow \lim_{\not{k} \rightarrow m_-} \frac{1}{\not{k} - m_-^2} \hat{\Sigma}_f(\not{k}) u_-(k) = 0. \end{aligned} \quad (4.31)$$

$u_-(k)$  is the spinor for the external fermion with  $I_3 = -\frac{1}{2}$ . This condition is valid for both charged leptons and quarks and defines  $Z_L$  and  $Z_R^-$ .  $Z_L$  determines the neutrino field renormalisation as well. For the  $I_3 = +\frac{1}{2}$  quarks, the condition for renormalisation is that the residues of the left- and right-handed propagators become equal at  $s = m_+^2$ , but different from one. This fixes  $Z_R^+$ .

The on-shell condition for the renormalisation of the electric charge is

$$\left( \text{diagram: } Z \text{ (wavy line)} \text{ --- } \text{blob} \text{ --- } f^- \text{ (solid line)} \text{ and } f^+ \text{ (solid line)} \right) \Big|_{s=0, q_1=q_2=m_e} = ie\gamma_\mu \Leftrightarrow \hat{\Gamma}_\mu^{\gamma ee}(s=0, q_1=q_2=m_e) = ie\gamma_\mu, \quad (4.32)$$

which means all corrections to the vertex must disappear in the Thomson limit of zero momentum transfer and on-shell particles.

Solving the equations (4.29), (4.30), (4.31) and (4.32) using the renormalised self-energies for the gauge bosons (4.20) and the fermions (4.25) and the renormalised electromagnetic vertex (4.27), gives the explicit expressions for the various counter-terms.

The mass renormalisation counter-terms for the bosons and the fermions in the on-shell scheme at one loop order are

$$\begin{aligned} \delta M_W^2 &= \text{Re} \{ \Sigma_W(M_W^2) \}, \\ \delta M_Z^2 &= \text{Re} \{ \Sigma_Z(M_Z^2) \}, \\ \frac{\delta m_f}{m_f} &= \frac{1}{2} \left[ \Sigma_L(m_f^2) + \Sigma_R(m_f^2) \right] + \Sigma_S(m_f^2). \end{aligned} \quad (4.33)$$



The field renormalisation counter-terms for the gauge bosons are

$$\begin{aligned}
\delta Z_2^\gamma &= -\frac{\partial \Sigma^\gamma}{\partial s}(0), \\
\delta Z_1^\gamma &= -\frac{\partial \Sigma^\gamma}{\partial s}(0) - \frac{s_W}{c_W} \frac{\Sigma^{\gamma Z}}{M_Z^2}(0), \\
\delta Z_2^Z &= -\frac{\partial \Sigma^\gamma}{\partial s}(0) - 2 \frac{c_W^2 - s_W^2}{s_W c_W} \frac{\Sigma^{\gamma Z}(0)}{M_Z^2} + \frac{c_W^2 - s_W^2}{s_W^2} \left( \frac{\delta M_Z^2}{M_Z^2} - \frac{\delta M_W^2}{M_W^2} \right), \\
\delta Z_1^Z &= -\frac{\partial \Sigma^\gamma}{\partial s}(0) - \frac{3c_W^2 - 2s_W^2}{s_W c_W} \frac{\Sigma^{\gamma Z}(0)}{M_Z^2} + \frac{c_W^2 - s_W^2}{s_W^2} \left( \frac{\delta M_Z^2}{M_Z^2} - \frac{\delta M_W^2}{M_W^2} \right), \\
\delta Z_2^W &= -\frac{\partial \Sigma^\gamma}{\partial s}(0) - 2 \frac{c_W}{s_W} \frac{\Sigma^{\gamma Z}(0)}{M_Z^2} + \frac{c_W^2}{s_W^2} \left( \frac{\delta M_Z^2}{M_Z^2} - \frac{\delta M_W^2}{M_W^2} \right), \\
\delta Z_1^W &= -\frac{\partial \Sigma^\gamma}{\partial s}(0) - \frac{3 - 2s_W^2}{s_W c_W} \frac{\Sigma^{\gamma Z}(0)}{M_Z^2} + \frac{c_W^2}{s_W^2} \left( \frac{\delta M_Z^2}{M_Z^2} - \frac{\delta M_W^2}{M_W^2} \right).
\end{aligned} \tag{4.34}$$

The counter-terms  $\delta Z_i^W$  are combinations of  $\delta Z_i^\gamma$  and  $\delta Z_i^Z$  obtained from (4.9). For the left- and right-handed fermion fields,

$$\begin{aligned}
\delta Z_L &= -\Sigma_L(m_-^2) - m_-^2 \left[ \frac{\partial \Sigma_L}{\partial s}(m_-^2) + \frac{\partial \Sigma_R}{\partial s}(m_-^2) + 2 \frac{\partial \Sigma_S}{\partial s}(m_-^2) \right], \\
\delta Z_R &= -\Sigma_R(m_-^2) - m_-^2 \left[ \frac{\partial \Sigma_L}{\partial s}(m_-^2) + \frac{\partial \Sigma_R}{\partial s}(m_-^2) + 2 \frac{\partial \Sigma_S}{\partial s}(m_-^2) \right].
\end{aligned} \tag{4.35}$$

The renormalised electric charge can be written in terms of the counter-terms by applying the transformation (4.6) directly to (2.24),

$$e_0^2 \rightarrow e^2(1 + 2\delta Z_1^\gamma - 3\delta Z_2^\gamma) = e^2 \left( 1 + 2 \frac{\delta e}{e} \right) \tag{4.36}$$

with

$$\frac{\delta e}{e} = \delta Z_1^\gamma - \frac{3}{2} \delta Z_2^\gamma. \tag{4.37}$$

Equivalently, from multiplicative renormalisation one gets  $\delta Z_e = 2 \frac{\delta}{e} e$ . Solving (4.32) yields

$$\frac{\delta e}{e} = \frac{1}{2} \frac{\partial \Sigma^\gamma}{\partial s} \Big|_{s=0} - \frac{s_W}{c_W} \frac{\Sigma^{\gamma Z}(0)}{M_Z^2}, \tag{4.38}$$

where the first term in  $\frac{\delta e}{e}$  is formally identical to the renormalised charge in QED, although it here contains contributions from the weak bosons.

The electroweak couplings  $g$  and  $g'$  are changed by (4.34), getting higher order contributions from

the self-energies of the bosons. As a consequence, the Weinberg angle (2.18) is redefined as

$$s_{W0}^2 \rightarrow s_W^2 + c_W^2 \left( \frac{\delta M_Z^2}{M_Z^2} - \frac{\delta M_W^2}{M_W^2} \right) \quad (4.39)$$

## 4.2 Radiative corrections to $Z \rightarrow f^+ f^-$ and $e^+ e^- \rightarrow f^+ f^-$

One of the advantages of this on-shell scheme is that it allows the separation of the radiative corrections into gauge invariant classes that can be treated separately. This is because of the unbroken  $U(1)_{\text{EM}}$  symmetry, which allows to compute the purely photonic radiative corrections and QED renormalisation independently of the rest of the electroweak sector [128]. The QED corrections come from virtual photon exchange and real photon emission in the initial and final states. Summing these diagrams eliminates all IR divergences as per the Kinoshita-Sirlin-Lee-Nauenberg theorem [153–155], the electroweak extension of the Bloch-Nordsieck theorem of QED [156], and the result is UV finite by itself. Addressing the QED corrections individually is also convenient since they depend on the experimental setup [129]. The weak corrections consist of all other non-photonic one loop diagrams and depend only on the fundamental content of the theory. They correspond to the vertex, propagator and box corrections. These corrections include all particles in the model that are allowed to couple in the loops, whether be they from the SM or some extension of it. It is this fact that, allied to the great sensitivity of modern detectors, makes the weak corrections such a great probe into new physics.

The weak corrections are the main interest in this work. We look exclusively at quantities that have been deconvoluted from the QED effects. However, the QED corrections depend on experimental conditions and are large around the  $Z$  pole, hence in practice one would need to know how to deal with them in order to subtract its effects from the data and probe the weak effects in the first place. As such, a brief description of the QED corrections is given in section 4.2.1.

In the case of a hadronic final state there are also final state QCD corrections. Their treatment is formally identical to that of the final state QED corrections, but because we deal only with leptonic final states they will not be addressed here, but can be seen in [127].

### 4.2.1 QED corrections

The one loop diagrams for  $Z \rightarrow f^+ f^-$  and  $e^+ e^- \rightarrow f^+ f^-$  with virtual photon exchange in the vertex or in the self-energy of the external legs are IR divergent. In order to eliminate these divergences, it is necessary to include the diagrams with real photon emission in the form of *bremsstrahlung* from the external legs. We can then define the initial and final state QED corrections as coming from the diagrams with a single extra real or virtual photon added to the initial or final state fermion legs in the Born type diagrams. In other words, they include the photonic vertex diagram and self-energy contributions to the external legs as well as the diagrams with the emission of real photons. There are also QED corrections from the interference of the initial and final states. The diagrams that contribute to the QED corrections to  $Z \rightarrow f^+ f^-$  are represented in Figs. 4.4 and the  $e^+ e^- \rightarrow f^+ f^-$  diagrams are represented in Figs. 4.5, 4.6 and 4.3.

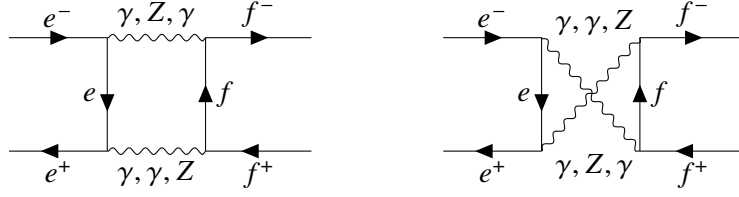


**Figure 4.3:** QED diagrams that contribute to the  $e^+ e^- \rightarrow f^+ f^-$  initial-final state interference corrections.

Because real photons are massless, there is no lower limit for their energy,  $E_\gamma$ , which can be smaller than the detector sensitivity [39]. The final state fermion can radiate any number of these photons. These diagrams are IR divergent in the limit of vanishing photon momentum and their divergences cancel to all orders if summed with the ones from virtual photon corrections [153–155]. Hence, one must sum over the diagrams that are consistent with the loop order in which the process is being dealt with.

When computing the cross section with the radiated photon, the integration can be performed over the whole kinematically allowed phase space or limited by a cut informed by the experimental setup. The case when the maximum energy of the emitted photon in the CM frame of the initial state electron-positron pair,  $\omega$ , is much smaller than the energy of the process  $E_\gamma \leq \omega \ll \sqrt{s}$ , is called the soft photon approximation. In this part of the phase space, the energy loss in the photon and Z boson propagators is very small. In the case of a near resonance Z propagator, the energy loss due to initial state photon emission is not necessarily small compared to the resonance width and must be taken into account in the propagator [129]. This approximation is usually not applicable in experiments because of the configuration of the detectors themselves. In these cases, the  $E_\gamma > \omega$  region is important and this hard photon part of the phase space is bounded by experimental cuts. The hard photon part is IR and UV finite and can be treated separately from the other corrections [157]. Typically this is done with Monte Carlo simulations [158].

The final state corrections are small in comparison to the corresponding decay rate or cross section. The QED  $O(\alpha)$  initial state corrections are large around the Z resonance, of the order of 25% [47], and as such require a comprehensive second order calculation in order to identify their effects for an electroweak precision study. The size of the contribution to the cross section coming from the interference of the initial and final states from the diagrams in Fig. 4.3 is negligibly small [129] and there is nothing particularly relevant to be gained from its discussion in this work.

#### 4.2.1.1 Final state corrections

First consider  $Z \rightarrow f^+ f^-$ , which only has final state corrections. Following [116], integrating over the full phase space and summing to order  $O(\alpha)$  all QED diagrams with virtual and real photons shown in Fig. 4.4 and the tree-level diagram for the process, one gets

$$\Gamma_f = \Gamma_f^0 \left[ 1 + \frac{3}{4} Q_f^2 \frac{\alpha (M_Z^2)}{\pi} + O(\alpha^2) \right]. \quad (4.40)$$

To first order in  $\alpha$ , the result is independent of the lepton species, which justifies our definition of  $R_{e\mu}$  in (3.6). Summing these diagrams is sufficient to guarantee an IR finite result [153–155]. We define

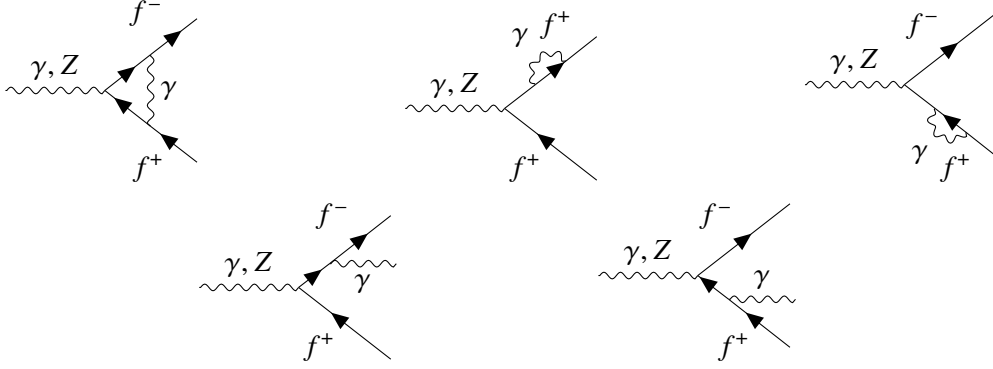


**Figure 4.4:** QED diagrams that contribute to the  $Z \rightarrow f^+ f^-$  final state corrections.

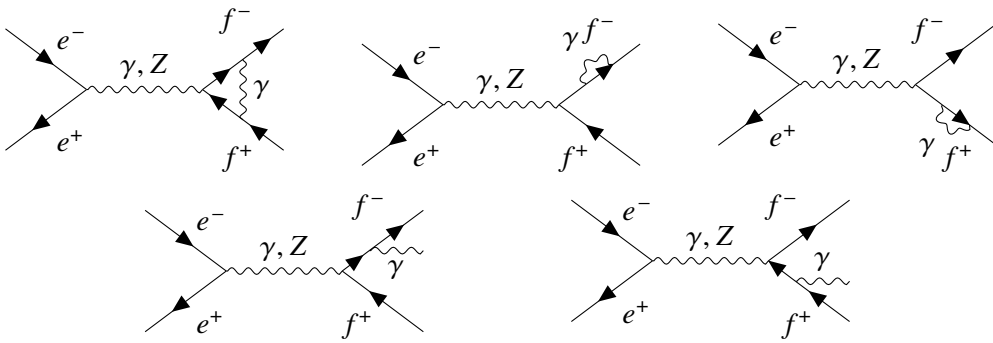


**Figure 4.5:** QED diagrams that contribute to the  $e^+ e^- \rightarrow f^+ f^-$  final state corrections.

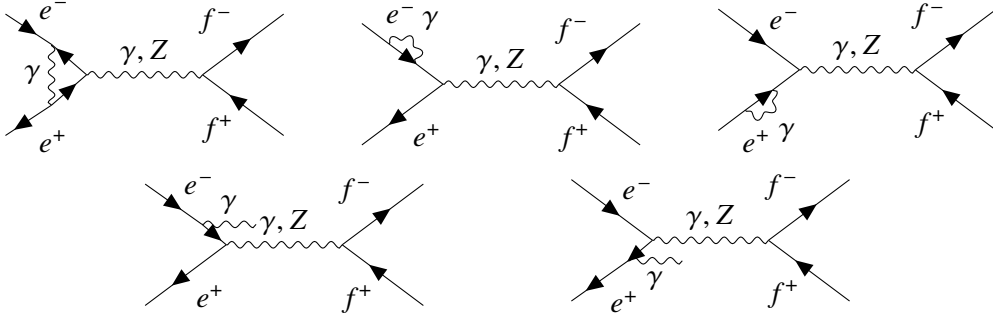


**Figure 4.6:** QED diagrams that contribute to the  $e^+ e^- \rightarrow f^+ f^-$  initial state corrections.

$\delta_{QED} = \frac{3}{4} Q_f^2 \frac{\alpha(M_Z^2)}{\pi}$ , which gives a correction smaller than 0.17% in relation to  $\Gamma_f^0$  [129, 159]. The final state QCD corrections are formally identical and the total multiplicative factor that accounts for both QED and QCD effects is sometimes called "radiator function".

The correction to the  $e^+ e^- \rightarrow f^+ f^-$  is similar. If no cuts are applied, to first order in  $\alpha$  the denominator in (3.3) gets a correction

$$(\sigma_F + \sigma_B) (1 + \delta_{QED}), \quad (4.41)$$

which results in a correction to  $A_{FB}^{0,f}$

$$A_{FB}^f \approx A_{FB}^{0,f} (1 - \delta_{QED}). \quad (4.42)$$

Like in the previous case, this translates into a sub-percent change in the value of the observable. If the energies are in the soft photon region, the correction to the cross section can be large and negative, but it multiplies both the numerator and denominator of  $A_{FB}^f$

$$(\sigma_F \pm \sigma_B) \left\{ 1 + \frac{\alpha}{\pi} Q_f^2 \left[ 2 \log \frac{2\omega}{\sqrt{s}} \left( \log \frac{s}{m_l^2} - 1 \right) + \frac{3}{2} \left( \log \frac{s}{m_l^2} - 1 \right) + \frac{\pi^2}{3} - \frac{1}{2} \right] \right\}, \quad (4.43)$$

and hence the observable is not affected.

#### 4.2.1.2 Initial state corrections

The diagrams that contribute to the initial state QED corrections of  $e^+ e^- \rightarrow f^+ f^-$  are shown in Fig. 4.6. One way to include them is to obtain the corrected cross section from the convolution of the weakly corrected cross section,  $\sigma^0$ , with a distribution function,  $G(z, s)$  [129],

$$\sigma(s) = \int_{z_0}^1 \sigma^0(zs) G(z, s) dz, \quad (4.44)$$

where  $zs$  is the invariant mass of the produced fermion pair with

$$4 \frac{m_f^2}{s} \leq z_0 \leq z \leq 1. \quad (4.45)$$

The kernel  $G(z, s)$  contains the higher order QED effects. For  $A_{FB}^f$ , an analogous procedure allows the inclusion of the QED corrections as [129]

$$A_{FB}^f(s) = \frac{1}{\sigma(s)} \int_{z_0}^1 \left( \sigma_F^0(s) - \sigma_B^0(s) \right) H(z, s) dz, \quad (4.46)$$

where  $\sigma(s)$  is the QED corrected total cross section for the process (4.44).

There are exact analytical results for the  $\mathcal{O}(\alpha)$  corrections [157]. For the higher order corrections, there are several distinct approaches, like performing soft photon resummation in the first order result [160], explicitly computing the two loop result [161] or applying QCD structure functions to obtain the equivalent QED result [162]. These methods have the advantage of giving formally identical expressions where only the function  $H(z, s)$  in (4.46) varies according to the different approach. As an alternative to the procedure outlined in the previous section for the final state radiation, those corrections can also be included in the convolution method here described.

As mentioned before, the initial state corrections are the most relevant of the QED corrections. They lead to a shift in the position of the peak of about +100 MeV [121]. Beyond that, the corrected cross section is also higher for smaller energies and lower for higher energies than the deconvoluted cross section [122]. The asymmetry is also significantly affected by the initial state QED corrections. Close to the peak they lead to a deviation of about  $\delta A_{FB}^f = -0.025$ , which is of the order of the asymmetry itself [129].

### 4.2.2 Weak corrections

The weak corrections include corrections to the vertices, corrections to the photon and  $Z$  propagators and box diagrams with massive boson exchange. The diagrams that contribute to the weak corrections to  $e^+ e^- \rightarrow f^+ f^-$  are represented in Figs. 4.8, 4.9 and 4.11. The contributions to  $Z \rightarrow f^+ f^-$  represented in Figs. 4.7 and 4.10 are similar, but the propagator corrections lack the purely photonic component.

One important aspect of the weak corrections is that they have a deep connection to the renormalisation procedure. The finite part of the counter-terms is included in the corrections and as such influences the final result. Moreover, the separate treatment of the QED corrections means that the diagrams which include the exchange of a photon in the loop are here excluded.

Comparatively to the QED corrections, the weak corrections are small, being typically only of the order of 1% [129].

#### 4.2.2.1 Vertex corrections

Vertex corrections are defined as the  $\gamma f^+ f^-$  and  $Z f^+ f^-$  3-point functions in one loop order after renormalisation [128], including the self-energy contributions to the external legs that comes from wave function renormalisation. These corrections depend on the fermion species.

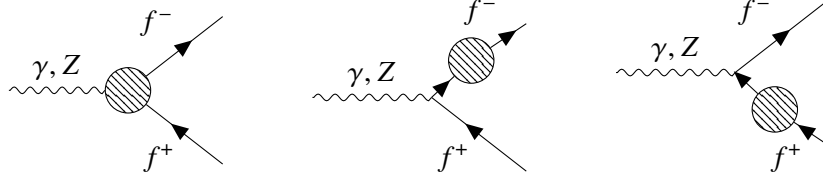


**Figure 4.7:** Weak diagrams that contribute to the  $Z \rightarrow f^+ f^-$  vertex corrections.

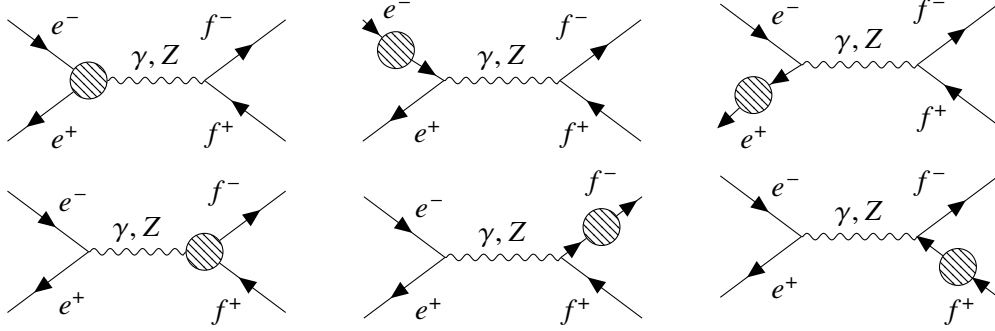


**Figure 4.8:** Weak diagrams that contribute to the  $e^+ e^- \rightarrow f^+ f^-$  vertex corrections.

The one loop vertex contributions  $\Lambda_{\mu}^{\gamma ff}$  and  $\Lambda_{\mu}^{\gamma Z ff}$  in (4.27) and (4.28), respectively, have the form

$$\Lambda_{\mu}^{\gamma, Z ff} = \gamma_{\mu} (\Lambda_L^{\gamma, Z ff} P_L + \Lambda_R^{\gamma, Z ff} P_R) + (q_2 - q_1)_{\mu} (\Lambda_M^{\gamma, Z ff} + \gamma_5 \Lambda_E^{\gamma, Z ff}) + (q_2 + q_1)_{\mu} (\Lambda_S^{\gamma, Z ff} + \gamma_5 \Lambda_P^{\gamma, Z ff}), \quad (4.47)$$

which is the most general covariant decomposition for on-shell fermions in the SM. The amplitudes  $\Lambda$  are functions of the scalar products  $q_1^2$ ,  $q_2^2$  and  $q_1 \cdot q_2$ , which means that for on-shell fermions,  $q_1^2 = q_2^2 = m_f^2$ , their only kinematical dependence is on  $s$ . By applying the Gordon identities [163], one recovers an expression similar to (2.44) which allows to interpret  $\Lambda_M$  and  $\Lambda_E$  as contributing to the magnetic moment and to the  $CP$  violating electric dipole moment, respectively.  $\Lambda_S$  and  $\Lambda_P$  come from scalar and pseudoscalar couplings, but are in fact redundant. Current conservation requires  $\Lambda_S = 0$  and leads to  $\Lambda_P$  being written in terms of  $\Lambda_L$  and  $\Lambda_R$  [92].

In the SM, when the fermion is on-shell and  $s \gg m_f^2$ , the terms that multiply the momenta are negligible and the vertex corrections can be written as additive form factors to the coupling constants to yield the "dressed vertices" [129]

$$\hat{\Gamma}_{\mu}^{\gamma ff} = -ieQ_f \gamma_{\mu} - ie\gamma_{\mu} \left( F_L^{\gamma f}(s) P_L + F_R^{\gamma f}(s) P_R \right), \quad (4.48)$$

$$\hat{\Gamma}_{\mu}^{Z ff} = \frac{ie}{s_W c_W} \gamma_{\mu} \left( g_{L_f} P_L + g_{R_f} P_R \right) + \frac{ie}{s_W c_W} \gamma_{\mu} \left( F_L^{Z f}(s) P_L + F_R^{Z f}(s) P_R \right). \quad (4.49)$$

The weak form factors  $F_{L,R}^{\gamma, Z ff}$  include the left- and right-handed components of (4.47) and the first order terms in the counter-terms coming from (4.27) or (4.28), respectively. These are functions of  $s$ , depending also on the masses. Because by definition they do not include the photon exchange contributions,



**Figure 4.9:** Weak diagrams that contribute to the  $e^+e^- \rightarrow f^+f^-$  propagator corrections.

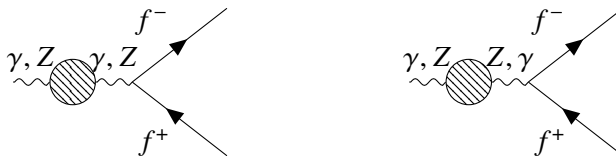


**Figure 4.10:** Weak diagrams that contribute to the  $Z \rightarrow f^+ f^-$  propagator corrections.

#### 4.2.2.2 Propagator corrections

There are three types of propagator corrections, photon exchange, Z exchange and  $\gamma Z$  mixing. The first one affects only the  $e^+e^- \rightarrow f^+f^-$  process, due to the photon mediated diagram in Fig. 3.2.

Making use of the propagators in (4.22), the photon exchange correction can be understood to come from the polarisation of the vacuum,

$$\text{wavy line } \gamma \text{ --- } \text{circle with diagonal lines} \text{ --- } \text{wavy line } \gamma = Q_e Q_f \frac{e^2}{s + \hat{\Sigma}_\nu(s)} = Q_e Q_f \frac{1}{s} \frac{e^2}{1 + \hat{\Pi}_\nu(s)}, \quad (4.50)$$

where the spinors and Dirac matrices are omitted. This effect can be accounted for by defining a running charge

$$e^2(s) = \frac{e^2}{1 + \Pi_\gamma(s)}, \quad (4.51)$$

with  $\hat{\Pi}_\gamma(s) = \hat{\Sigma}_\gamma(s)/s$ .

The situation is more complicated for the  $Z$  and  $\gamma Z$  mixing corrections, because the approximation in (4.22) is inadequate around the  $Z$  pole [128]. Defining  $M_Z \Gamma_Z^0 = \text{Im} \{ \hat{\Sigma}_Z(M_Z) \}$  as in (3.26) with  $\text{Re} \{ \hat{\Sigma}_Z(M_Z^2) \} = 0$  as per the renormalisation conditions (4.29) cancels the first order corrections to the cross section. To remedy this, the mixing terms in the complete renormalised  $Z$  propagator (4.19) have to be included, as well as second order corrections to the imaginary part of the denominator.

Omitting once again the spinors, with the higher order contributions from  $\gamma Z$  the  $Z$  propagator cor-



rection is given by

$$\begin{aligned} \text{Z} \text{ (wavy)} \text{---} \text{Z} \text{ (wavy)} &= \frac{e^2}{s_W^2 c_W^2} \frac{1}{s - M_Z^2 + \text{Re} \{ \tilde{\Sigma}_Z(s) \} + i \text{Im} \{ \tilde{\Sigma}_Z(s) \}} \\ &= \frac{e^2}{s_W^2 c_W^2} \frac{1}{1 + \hat{\Pi}_Z(M_Z^2)} \frac{1}{s - M_Z^2 + i \frac{\text{Im} \{ \tilde{\Sigma}_Z(s) \}}{1 + \hat{\Pi}_Z(M_Z^2)}}, \end{aligned} \quad (4.52)$$

with

$$\tilde{\Sigma}_Z(s) = \hat{\Sigma}_Z(s) - \frac{\left( \hat{\Sigma}_{\gamma Z}(s) \right)^2}{M_Z + \hat{\Sigma}_\gamma(s)^2}, \quad (4.53)$$

in the place of the  $Z$  self-energy in (4.22) as in (4.19) and

$$\text{Re} \{ \tilde{\Sigma}_Z(s) \} = (s - M_Z^2) \hat{\Pi}_Z(s). \quad (4.54)$$

Using the propagator with the mixing terms leads to a redefinition of the on-shell condition for the mass of the  $Z$  boson, which must now be  $\text{Re} \{ \tilde{\Sigma}_Z(M_Z^2) \} = 0$ . This changes the mass counter-term  $\delta M_Z^2$ , but all others remain unchanged, as do the vertex corrections [128].

$\tilde{\Sigma}_Z(s)$  is analytic close to  $s = M_Z^2$ , hence in the vicinity of the  $Z$  pole it can be Taylor expanded to first order as

$$\text{Re} \{ \tilde{\Sigma}_Z(s) \} \approx 0 + (s - M_Z^2) \frac{\partial}{\partial s} \text{Re} \{ \tilde{\Sigma}_Z(s) \} \Big|_{s=M_Z^2}, \quad (4.55)$$

where the first term is zero from the new on-shell condition. This gives the explicit definition  $\hat{\Pi}_Z(M_Z^2) = \frac{\partial}{\partial s} \text{Re} \{ \tilde{\Sigma}_Z(s) \} \Big|_{s=M_Z^2}$ .

The higher order corrections to the  $Z$  width are added as

$$\Gamma_Z = \frac{1}{M_Z} \frac{1}{1 + \hat{\Pi}_Z(M_Z^2)} \left[ \text{Im} \{ \tilde{\Sigma}_Z(M_Z^2) \} + \Delta\Gamma_Z \right]. \quad (4.56)$$

with  $\Delta\Gamma_Z$  containing the Weak, QED and QCD corrections to  $Z \rightarrow f^+ f^-$  that do not come from  $Z$  exchange.

The  $Z$  propagator correction at the  $Z$  pole is then given approximately by

$$\text{Z} \text{ (wavy)} \text{---} \text{Z} \text{ (wavy)} = \frac{e^2}{s_W^2 c_W^2} \frac{1}{1 + \hat{\Pi}_Z(M_Z^2)} \frac{1}{s - M_Z^2 + i \frac{s}{M_Z} \Gamma_Z}, \quad (4.57)$$

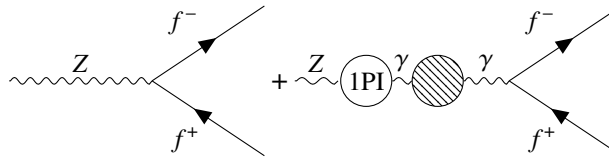
where it is now clear that the imaginary part of  $\tilde{\Sigma}_Z(s)$  contributes to the width and the real part amounts to a redefinition of the neutral current coupling.

The  $\gamma Z$  mixing corrections can be accounted for in the same manner as the vertex corrections, adding this contribution to the left- and right-handed coupling constants. The expression of the renormalised full

mixing propagator (4.19) can be rearranged as

$$\begin{aligned} \hat{D}_{\gamma Z} &= \frac{-\hat{\Sigma}_{\gamma Z}(s)}{[s + \hat{\Sigma}_\gamma(s)] [s - M_{Z_0}^2 + \hat{\Sigma}_Z(s)] - \hat{\Sigma}_{\gamma Z}^2(s)} = \frac{\frac{-\hat{\Sigma}_{\gamma Z}(s)}{[s + \hat{\Sigma}_\gamma(s)]}}{[s - M_{Z_0}^2 + \hat{\Sigma}_Z(s)] - \frac{\hat{\Sigma}_{\gamma Z}^2(s)}{[s + \hat{\Sigma}_\gamma(s)]}} \\ &= \frac{-\hat{\Sigma}_{\gamma Z}(s)}{[s + \hat{\Sigma}_\gamma(s)]} \hat{D}_Z, \end{aligned} \quad (4.58)$$

which shows that when writing the matrix elements for the processes the mixing contributions can be summed as



$$\begin{aligned} &= i \frac{e}{s_W c_W} \gamma_\mu (g_L P_L + g_R P_R) + i e Q_f \gamma_\mu \frac{\hat{\Sigma}_{\gamma Z}(s)}{s + \hat{\Sigma}_\gamma(s)} \\ &= i \frac{e}{s_W c_W} \gamma_\mu \left[ \left( g_L + s_W c_W Q_f \frac{\hat{\Pi}_{\gamma Z}(s)}{1 + \hat{\Pi}_\gamma(s)} \right) P_L + \left( g_R + s_W c_W Q_f \frac{\hat{\Pi}_{\gamma Z}(s)}{1 + \hat{\Pi}_\gamma(s)} \right) P_R \right], \end{aligned} \quad (4.59)$$

with the dimensionless quantities

$$\hat{\Pi}_\gamma(s) = \frac{\hat{\Sigma}_\gamma(s)}{s}, \quad \hat{\Pi}_{\gamma Z}(s) = \frac{\hat{\Sigma}_{\gamma Z}(s)}{s}. \quad (4.60)$$

Considering the definition of the couplings in (2.28), it can be seen that the  $\gamma Z$  mixing can also be included in an alternate manner, as redefinition of the mixing angle to an effective angle such that in the neutral current vertex

$$s_W^2 \rightarrow \bar{s}_W^2 = s_W^2 - s_W c_W \frac{\hat{\Pi}_{\gamma Z}(s)}{1 + \hat{\Pi}_\gamma(s)}. \quad (4.61)$$

Using the one loop expression in (4.22) without the mixing terms would amount to making the substitution

$$\frac{\hat{\Pi}_{\gamma Z}(s)}{1 + \hat{\Pi}_\gamma(s)} \rightarrow \frac{\hat{\Sigma}_{\gamma Z}(s)}{s}. \quad (4.62)$$

#### 4.2.2.3 Box corrections

The amplitudes corresponding to the box corrections of Fig. 4.11 can be written as the product of the initial and final currents,  $J_e$  and  $J_f$ , respectively, and a form factor  $\chi$  that is a function of the scattering angle through the Mandelstam variables,  $t = -\frac{s}{2}(1 - \cos \theta)$  and  $u = -\frac{s}{2}(1 + \cos \theta)$ , and of the mass of

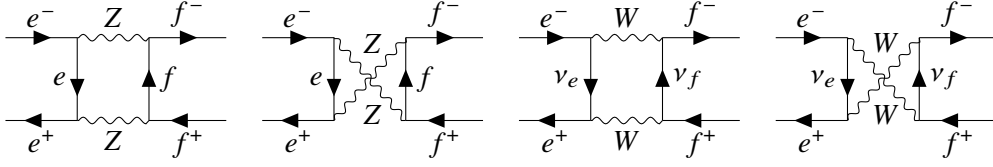


**Figure 4.11:** Weak diagrams that contribute to the  $e^+e^- \rightarrow f^+f^-$  box corrections.

the exchanged boson,  $M$ ,

$$J_e \cdot J_f \chi(s, \theta, M) \quad (4.63)$$

Considering the structure of the electroweak theory, when the fermions are on-shell and  $s \gg m_f^2$ ,  $J_e$  and  $J_f$  can only contain left- and right-handed contributions and the box corrections can be added to the left- and right-handed couplings. Once again, all diagrams with at least one photon in the loop are treated as part of the QED corrections to the process, making the weak box diagrams IR finite. They are also UV finite [129]. The contribution of the box diagrams to the cross section at the  $Z$  pole is less than 0.02% [129].

### 4.3 $A_\mu$ and $R_{e\mu}$ at one loop level and new physics

All one loop electroweak radiative corrections have now been identified and additional adjustments made to compensate the cancelling of first order corrections in the  $e^+e^- \rightarrow f^+f^-$  cross section. The results of the previous section show that the one loop corrections will not fundamentally alter the structure of the matrix elements (3.8) and (3.26) for the decay rate of  $Z \rightarrow f^+f^-$  and for the cross section of  $e^+e^- \rightarrow f^+f^-$ . The diagonal propagator corrections result in the redefinition of the QED and weak neutral couplings, while the  $\gamma Z$  mixing can be added to the vertex corrections and absorbed in an effective mixing angle. The box corrections can also be added to the vertex corrections. The reason as to why this is possible is because the theory for light fermions at one loop does not introduce Dirac terms that were not already present at tree-level. As such, one can get approximate Born-like expressions for the matrix elements at one loop.

Considering only the one loop weak corrections, the decay rate for  $Z \rightarrow f^+f^-$  (3.24) is affected by the vertex corrections (4.48) and the  $Z$  and  $\gamma Z$  mixing corrections, (4.52) and (4.59). The  $Z$  propagator corrections enter as a global normalisation constant due to the redefinition of the total width in (4.56). If  $\Gamma_Z = \sum_f \Gamma_f$ , then at the  $Z$  pole every partial decay rate must be multiplied by  $(1 + \hat{\Pi}(M_Z^2))^{-1}$ . The renormalised one loop expression for the decay rate is

$$\hat{\Gamma}_f = \frac{1}{1 + \hat{\Pi}_Z(M_Z^2)} \frac{3}{2} N_f^c \Gamma_0 \left[ g_L^2 + g_R^2 + 2g_{Lf} \left( F_L^{Zf}(M_Z^2) + s_W c_W \frac{\hat{\Pi}_{\gamma Z}(M_Z^2)}{1 + \hat{\Pi}_\gamma(M_Z^2)} \right) + 2g_{Rf} \left( F_R^{Zf}(M_Z^2) + s_W c_W \frac{\hat{\Pi}_{\gamma Z}(M_Z^2)}{1 + \hat{\Pi}_\gamma(M_Z^2)} \right) \right]. \quad (4.64)$$

At the vicinity of the  $Z$  pole, the one loop photon and  $Z$  boson exchange amplitudes for  $e^+e^- \rightarrow f^+f^-$  are given by

$$\mathcal{M}_\gamma \approx \frac{e^2(M_Z^2)}{s} \bar{v}_e(p_2) \gamma_\mu \left[ Q_e + F_L^{\gamma e}(M_Z^2) P_L + F_R^{\gamma e}(M_Z^2) P_R \right] u_e(p_1) \cdot \bar{u}_f(q_1) \gamma^\mu \left[ Q_f + F_L^{\gamma f}(M_Z^2) P_L + F_R^{\gamma f}(M_Z^2) P_R \right] v_f(q_2) \quad (4.65)$$

and

$$\mathcal{M}_Z \approx \left( \frac{e}{s_W c_W} \right)^2 \frac{1}{1 + \hat{\Pi}(M_Z^2)} \bar{v}_e(p_2) \gamma_\mu (\hat{g}_{L_e} P_L + \hat{g}_{R_e} P_R) u_e(p_1) \cdot \bar{u}_f(q_1) \gamma^\mu (\hat{g}_{L_f} P_L + \hat{g}_{R_f} P_R) v_f(q_2), \quad (4.66)$$

where the corrected left- and right-handed chiral couplings to the fermion are defined as

$$\mathcal{G}_{L,R} = \sqrt{\frac{1}{1 + \hat{\Pi}(M_Z^2)}} \left[ g_{L,R} - s_W c_W \frac{\hat{\Pi}_{\gamma Z}(M_Z^2)}{1 + \hat{\Pi}_\gamma(M_Z^2)} + F_{L,R}^{Zf}(M_Z^2) \right] = \sqrt{\frac{1}{1 + \hat{\Pi}(M_Z^2)}} \hat{g}_{L,R}, \quad (4.67)$$

defining an effective coupling,  $\mathcal{G}_{L,R}$ , [127].  $e(M_Z^2)$  is the running charge (4.51). The box contributions are neglected. Because the overall structure of the matrix elements does not change at one loop level, the expression for the squared matrix element (3.43) remains valid, with the functions  $G_1$ ,  $G_2$  and  $G_3$  getting new terms from the first order contributions. The complete expression for the one loop  $e^+e^- \rightarrow f^+f^-$  matrix element can be seen in [128].

Obtaining the explicit first order results for  $R_{e\mu}$  and  $\mathcal{A}_\mu$  is now straightforward. However, for the purposes of this work it is more relevant to see how the inclusion of the radiative corrections at the  $Z$  pole changes the mathematical form of the observable and how one can get a fairly general way of parameterising the effects of new physics on the observables.

By examining the definition of  $R_{el}$  (3.6) and the one loop result (4.64), it is simple to see that only the vertex and  $\gamma Z$  propagator corrections will influence the final result for this observable. The overall normalisation factor is independent of the fermion species and cancels. Consequently, the one loop expression for light leptons is similar the tree-level one (3.25) with all first order effects introduced through the modified couplings  $\hat{g}_{L,R}$  as in (4.67). For the second observable, because at the  $Z$  resonance the  $Z$  exchange diagram in  $e^+e^- \rightarrow f^+f^-$  is dominant, one can consider to a good approximation that the corrections to the  $Z f^+ f^-$  vertex and to the  $Z$  propagator will be the most important. Hence, for light fermions and in the narrow width approximation, (3.2) can be used with the tree-level couplings replaced by the effective coupling (4.67). The  $(1 + \hat{\Pi}(M_Z^2))^{-\frac{1}{2}}$  factor also cancels for this observable. For this reason we now drop this multiplicative constant and work with  $\hat{g}_{L,R}$ .

Rewriting the  $\hat{g}_{L,R}$  in (4.67) as  $\hat{g}_{L,R} = g_{L,R} + \delta g_{L,R}$ , where  $g_{L,R}$  is the tree-level coupling and  $\delta g_{L,R}$  is the small contribution from the weak radiative corrections to the  $Z f^+ f^-$  vertex, the observables (3.25)

and (3.2) can be expanded to first order in  $\delta g_{L,R}$ , giving

$$\hat{R}_{el} \approx R_{el} + \frac{2g_{Ll}}{\hat{g}_{Le}^2 + \hat{g}_{Le}^2} \delta g_{Ll} + \frac{2g_{Rl}}{\hat{g}_{Re}^2 + \hat{g}_{Re}^2} \delta g_{Rl}, \quad (4.68)$$

$$\hat{\mathcal{A}}_f \approx \mathcal{A}_f - \frac{4g_{Lf}g_{Rf}^2}{(g_{Lf}^2 + g_{Rf}^2)^2} \delta g_{Lf} - \frac{4g_{Lf}^2g_{Rf}}{(g_{Lf}^2 + g_{Rf}^2)^2} \delta g_{Rf}. \quad (4.69)$$

where the coupling for the electron is not expanded. This provides a simple formula to compute the shift to the observables caused by the radiative corrections of the coupling to the lepton to first order,  $\delta R_{el}$  and  $\delta \mathcal{A}_f$ . The question remains, however, as to how to include new physics in this scheme.

Physics from beyond the SM can be broadly classified into two types, depending on whether the tree-level SM relations have to be changed to account for the new particles [164]. This means, for example, changing the relations between the masses of the  $SU(2)$  bosons (2.20), inducing a mixing between SM and new fields or altering the structure of the couplings (2.28) in a way that changes the form of the tree-level matrix elements. This would further complicate the structure of the radiative corrections. On the other hand, if the lowest order relations are not modified, then the part of the Lagrangian that describes a process at tree-level is unchanged and the radiative corrections are formally identical to those from the SM. The new particles contribute only through virtual effects in the loops and the renormalisation constants, counter-terms and conditions can be used just as in the SM. In the context of this second case there is also a useful distinction that is often made between "oblique" and "direct" corrections, the first meaning the corrections to the bosonic propagators and the second to the couplings with the fermions. In the absence of the latter, the effect of new physics can be effectively quantified by the Peskin-Takeuchi  $S$ ,  $T$ , and  $U$  oblique parameters [165].

In the presence of new physics that respects the lowest-order structure, the deviations from the tree-level values of the observables can be parameterised in exactly the same way as in (4.68) and (4.69), with  $\delta g_{L,R}$  containing both the SM and new physics (NP) one loop contributions. To study the effect of new physics on the muon-related observables, we do a similar parameterisation as before, but now consider the effective coupling divided as  $\hat{g}_{L,R} = g_{L,R}^{\text{SM}} + \delta g_{L,R}^{\text{NP}}$ , with the first term containing the tree-level and one loop vertex contributions from the SM and the second term the one loop terms that contain the new fields.  $\delta g_{L,R}^{\text{NP}}$  is taken to be small in comparison to  $g_{L,R}^{\text{SM}}$ . This means that now  $\hat{R}_{el} \approx \hat{R}_{el}^{\text{SM}} + \delta R_{el}$  and  $\hat{\mathcal{A}}_f \approx \hat{\mathcal{A}}_f^{\text{SM}} + \delta \mathcal{A}_f$ , with the first terms corresponding to the SM tree-level plus one loop values.

This parametrisation requires we take a more careful look at (4.67). Because we consider only the corrections to the coupling with the muon,  $\delta R_{e\mu}$  depends on the weak current renormalisation factor  $(1 + \hat{\Pi}(M_Z^2))^{-\frac{1}{2}}$  which unlike in (4.68) does not cancel. Moreover, the corrections to the Weinberg angle (4.39) would also have to be taken into account in the expansion. Instead, we consider the following transformation [129]

$$\frac{e}{2s_W c_W} \sqrt{\frac{1}{1 + \hat{\Pi}(M_Z^2)}} \rightarrow \left( \sqrt{2} G_\mu M_Z^2 \right)^{\frac{1}{2}} \rho_f^{\frac{1}{2}}, \quad (4.70)$$

where  $G_\mu$  is the Fermi constant and  $\rho_f$  is the parameter that contains the terms that come from the

corrections to the Z propagator and to the Weinberg angle. At tree-level,  $\rho_f = 1$ . This parameter has been computed experimentally to be  $\rho_l = 1.0050 \pm 0.0010$  for leptons [122]. Hence, we use the transformation (4.70) and consider  $\rho_f \approx 1$ . As a consequence, we have  $\mathcal{G}_{L,R} \approx \hat{g}_{L,R}$  and the expansion is similar to (4.68) and (4.69).

Using the SM values in Table 3.2, for the muon we get

$$\begin{aligned}\delta R_{e\mu} &\approx -4.26189\delta g_{L_\mu}^{\text{NP}} + 3.67435\delta g_{R_\mu}^{\text{NP}}, \\ \delta \mathcal{A}_\mu &\approx -3.63429\delta g_{L_\mu}^{\text{NP}} - 4.21542\delta g_{R_\mu}^{\text{NP}}.\end{aligned}\tag{4.71}$$

It is now possible to compute the effect of new physics to  $\hat{R}_{e\mu}$  and  $\hat{\mathcal{A}}_\mu$  by calculating the deviations (4.71). Comparing the result with the experimental values in Table 3.1 serves as a constraint on the parameters in  $\delta g_{L,R}^{\text{NP}}$ , which must be such that when the new physics contributions are added to the SM values, the final result is compatible with the experimental value.

New physics contributions to the Weinberg angle are constrained by the oblique parameters. Separating this component from the rest of the vertex corrections introduces an extra term in (4.71) proportional to [166]

$$\delta s_W^2 = \frac{\alpha}{c_W^2 - s_W^2} \left( \frac{1}{4}S - s_W^2 c_W^2 T \right).\tag{4.72}$$

From the best experimental values for the two parameters [47],

$$\begin{aligned}S &= -0.02 \pm 0.10, \\ T &= 0.03 \pm 0.12,\end{aligned}\tag{4.73}$$

we see that at most the contribution to the observables is of the order of  $10^{-4}$ . As such, we neglect all new physics oblique corrections to the effective couplings and focus only on the vertex corrections.

## Chapter 5

# New model

In this chapter, we describe the model used to test the muon-related constraint defined in 4.3. After a general introduction on its origin and motivations, we present the field content of Model 5 and discuss some bounds on the masses of the new particles and the nature of the dark matter candidate. The new model leads to one loop diagrams for a number of flavour related processes which can be used to constrain the parameter space of the model. We introduce the new physics contributions to these processes as well as to the dark matter relic density, direct detection and Higgs invisible decays.

### 5.1 General description

The model studied in this work was first introduced in [33], being inspired by the model in [32]. It originally intended to address the anomalies in the decay rates of the  $B$  meson observed at the LHCb [167, 168] while simultaneously providing a viable dark matter candidate. For that end, the SM was expanded by adding two new scalar fields, one of them being  $SU(3)_c$  coloured, and an  $SU(2)_L$  singlet vector-like fermion. This is a spin- $\frac{1}{2}$  particle whose left- and right-handed components transform the same way under  $SU(2)_L$ . As such, this fermion couples to a vector current  $\psi_L \gamma_\mu \psi_L + \psi_R \gamma_\mu \psi_R = \psi \gamma_\mu \psi$  and hence the name. This particle was initially chosen to be the dark matter candidate, which is stable due to a  $\mathbb{Z}_2$  symmetry that prevents it from decaying to lighter SM particles. A listing of similar renormalisable models that introduce higher order contributions from new fields that couple to linear combinations of SM fermions via Yukawa like interactions that solve the  $B$  meson discrepancies can be seen in [169].

In [33], the authors also take into consideration the tension in the measurements of the anomalous magnetic moment of the muon and include constraints coming from contemporary experimental results [96]. The models there defined extend the SM by adding three new fields: a vector-like fermion  $\chi$  with an electric charge of 0 or  $\pm 1$ , an  $SU(3)_c$  coloured scalar  $\Phi_q$  and a colourless scalar  $\Phi_l$ . The electric charges of the scalar fields are determined by the following Yukawa Lagrangian

$$\mathcal{L}_Y^{\text{NP}} = y_{L_i} \bar{L}_{L_i} \Phi_l \chi_R + y_{Q_i} \bar{Q}_{L_i} \Phi_q \chi_R + \text{h.c.}, \quad (5.1)$$

where  $y_{L_i}$  and  $y_{Q_i}$  are constants,  $L_{L_i}$  and  $Q_{L_i}$  are the SM left-handed lepton and quark doublets and  $\chi_R$  is the right-handed component of the vector-like fermion. To write the Lagrangian in a form similar to

the SM Yukawa Lagrangian, only the right-handed component of the fermion appears. Together with the scalar potential, this Lagrangian connects the SM to the new sector. This is where the interaction terms relevant to solve the muon  $g - 2$  anomaly and  $B \rightarrow K^{(*)} \mu^+ \mu^-$  are written.

The lightest neutral particle will be the dark matter candidate. A  $\mathbb{Z}_2$  symmetry under which the SM fields are even,  $\phi^{SM} \rightarrow \phi^{SM}$ , and the new fields are odd,  $\phi^{NP} \rightarrow -\phi^{NP}$  is introduced to guarantee the stability of the dark matter candidate. Because the whole Lagrangian must be invariant under this symmetry, the interaction terms that include fields of the extended sector must always have an even number of the new fields. This effectively means that the lightest dark matter particle cannot decay, since the decay exclusively to SM particles is forbidden.

By making different combinations of the fields' representations under  $SU(2)_L$  and  $U(1)_Y$  charges, a class of eight models in total was created. The representation of a field under the symmetry group has a significant effect on the structure of the theory and consequently on the possible interactions of that field. The models are numbered from 1 to 8 and the charge assignments for the fields can be seen in the tables of [33]. In every model, the vector-like fermion  $\chi$  and  $\Phi_l$  are singlets and  $\Phi_q$  a triplet under  $SU(3)_c$ . Their representations under  $SU(2)_L$  vary from model to model, with  $\chi$  being in a singlet, doublet or triplet representation and the scalars either in a singlet or doublet representation. Model 2 has no electrically neutral particle and therefore cannot provide a dark matter candidate. In Models 1 and 6 the vector-like fermion is self-conjugate and can have a Majorana mass term, which means there is no need to introduce the left-handed component  $\chi_L$  to write a mass term. All models give similar results in terms of flavour and dark matter physics and the differences between them are reflected in their allowed parameter spaces. In this work, we use Model 5, which has already been thoroughly explored in [33].

## 5.2 Model 5

In Model 5, the scalars are singlets of  $SU(2)_L$  and the fermion is a doublet of the same group,  $\chi = (\chi^0, \chi^-)$ . The quantum numbers of the new fields can be seen in Table 5.1.

**Table 5.1:**  $SU(3)_c$ ,  $SU(2)_L$  and  $U(1)_Y$  charge assignments for the new fields of Model 5.

	$SU(3)_c$	$SU(2)_L$	$U(1)_Y$
$\chi_R$	<b>1</b>	<b>2</b>	-1/2
$\Phi_l$	<b>1</b>	<b>1</b>	0
$\Phi_q$	<b>3</b>	<b>1</b>	2/3

Having in mind the representations and charges in Table 5.1 and the SM expressions (2.6) and (2.7), the covariant derivatives for the new scalar fields are

$$D_\mu \Phi_l = \partial_\mu \Phi_l, \quad (5.2)$$

$$D_\mu \Phi_q = \partial_\mu \Phi_q + ie \frac{2}{3} A_\mu + ig \frac{2}{3} \frac{s_W^2}{c_W} Z_\mu \Phi_q. \quad (5.3)$$

Because  $\Phi_l$  is a neutral singlet it does not couple to any of the  $SU(2)_L \times U(1)_Y$  gauge bosons. The QCD couplings of  $\Phi_q$  are irrelevant for the following discussion, so they are not shown here explicitly.  $\chi$  is a



vector-like fermion, hence both its left- and right-handed components transform the same way under the gauge group. The covariant derivative is

$$D_\mu \chi_{L,R} = \begin{pmatrix} \partial_\mu - i \frac{g}{c_W} Z_\mu & -i \frac{g}{c_W} W_\mu^+ \\ -i \frac{g}{c_W} W_\mu^- & \partial_\mu - ie A_\mu - i \frac{g}{c_W} \left(-\frac{1}{2} + s_W^2\right) Z_\mu \end{pmatrix} \begin{pmatrix} \chi_{L,R}^0 \\ \chi_{L,R}^- \end{pmatrix}. \quad (5.4)$$

The gauge kinetic Lagrangian for the new fields is then given by

$$\mathcal{L}_K^{\text{NP}} = (D_\mu \Phi_l)^\dagger (D^\mu \Phi_l) + (D_\mu \Phi_q)^\dagger (D^\mu \Phi_q) + \bar{\chi} i \gamma^\mu D_\mu \chi, \quad (5.5)$$

with the derivatives defined above.

$\chi$  is charged under  $U(1)_Y$ , so it cannot have a Majorana mass term [41]. However, since the left- and right-handed components of  $\chi$  transform the same way under  $SU(2)$ , the vector-like fermion can have a Dirac mass term  $m_\chi (\bar{\chi}_L \chi_R + \bar{\chi}_R \chi_L)$ , which is invariant under the symmetry group. Both the neutral and charged component of the doublet will by definition have the same mass. Writing the Yukawa Lagrangian for Model 5 in the fermion mass basis by rotating the quarks and leptons to their mass eigenstates and including the mass term gives

$$\mathcal{L}_Y^{\text{NP}} = m_\chi \bar{\chi}_L \chi_R + y_{d_i} \left( \bar{u}_{L_j} V_{ji} \chi_R^0 + \bar{d}_{L_i} \chi_R^- \right) \Phi_q + \frac{y_{e_i}}{2} (S + iA) \left( \bar{\nu}_{L_j} U_{ji} \chi_R^0 + \bar{e}_{L_i} \chi_R^- \right) + \text{h.c.}, \quad (5.6)$$

with  $y_{d_i}$  and  $y_{e_i}$  obtained from  $y_{Q_i}$  and  $y_{L_i}$  using the CKM and PMNS matrices  $V$  and  $U$ , respectively. We assume that the flavour and mass basis are aligned for the charged leptons and down-type quarks. In order to suppress the strong flavour constraints on the first generation fermions and keep the number of interactions to a minimum, in [33] the authors only consider  $y_b$ ,  $y_s$  and  $y_\mu$  to be nonzero.

The most general scalar potential for Model 5,  $V_5 = V_5(H, \Phi_l, \Phi_q)$ , is given by

$$\begin{aligned} V_5 = & -\mu_H^2 |H|^2 + \mu_{\Phi_l}^2 |\Phi_l|^2 + \mu_{\Phi_q}^2 |\Phi_q|^2 + \lambda_H |H|^4 + \lambda_{\Phi_l} |\Phi_l|^4 + \lambda_{\Phi_q} |\Phi_q|^4 + \frac{\mu'_{\Phi_l}}{2} (\Phi_l^2 + \Phi_l^{*2}) \\ & + \lambda_{H\Phi_l} |H|^2 |\Phi_l|^2 + \lambda_{H\Phi_q} |H|^2 |\Phi_q|^2 + \lambda_{\Phi_l\Phi_q} |\Phi_l|^2 |\Phi_q|^2 \\ & + \frac{\lambda'_{\Phi_l}}{4} (\Phi_l^2 + \Phi_l^{*2})^2 + \frac{\lambda'_{H\Phi_l}}{2} |H|^2 (\Phi_l^2 + \Phi_l^{*2}) + \frac{\lambda'_{\Phi_l\Phi_q}}{2} |\Phi_q|^2 (\Phi_l^2 + \Phi_l^{*2}), \end{aligned} \quad (5.7)$$

which introduces thirteen free parameters. The scalar fields written in the unitary gauge as in (2.14).  $H$  is the SM Higgs doublet,

$$H = \begin{bmatrix} 0 \\ \frac{1}{\sqrt{2}} (v + h) \end{bmatrix}, \quad (5.8)$$

with a vacuum expectation value (vev)  $v = \sqrt{\mu_H^2 / \lambda_H} \approx 246$  GeV [47]. Only the Higgs acquires a non-zero vev.  $h$  is the Higgs boson field. The neutral scalar  $\Phi_l$  can be decomposed in its real and imaginary parts as  $\Phi_l = (S + iA) / \sqrt{2}$ . The potential must be bounded from below so that there is a minimum energy state. This condition leads to constraints on the parameters of the potential. However, these are of

no relevance to this work.

To obtain the masses of the scalars, one simply has to compute the minima of the potential in relation to the different fields. This gives the following mass spectrum

$$\begin{aligned} m_h^2 &= 2\lambda_H v^2, & M_{\Phi_q}^2 &= \mu_{\Phi_q}^2 + \frac{1}{2}\lambda_{H\Phi_q} v^2, \\ M_S^2 &= \mu_{\Phi_l}^2 + \mu_{\Phi_l'}^2 + \frac{1}{2}(\lambda_{H\Phi_l} + \lambda'_{H\Phi_l}) v^2, & M_A^2 &= \mu_{\Phi_l}^2 - \mu_{\Phi_l'}^2 + \frac{1}{2}(\lambda_{H\Phi_l} - \lambda'_{H\Phi_l}) v^2. \end{aligned} \quad (5.9)$$

Notice that  $S$  and  $A$  have the same mass if  $\mu_{\Phi_l'}^2 = -\frac{1}{2}\lambda'_{H\Phi_l} v^2$ .

The lightest neutral particle will be the dark matter candidate, so it will either be the neutral component of  $\chi$  or the real or imaginary part of  $\Phi_l$ . If  $\chi^0$  were to be considered the dark matter candidate, its mass would have to be of the order of TeV to avoid experimental constraints from direct dark matter searches, because it has a very large dark matter-nucleon scattering cross section due to tree-level  $Z$  mediation. The large mass is required to balance the strong gauge coupling to the  $Z$  in the cross section. But in that case, the other new particles would be required to have masses even greater, which would make the new loop contributions necessary to solve the muon-related problems too small. As such, and because the flavour phenomenology is the same for the real and imaginary parts of the neutral scalar,  $S$  is chosen as the dark matter particle. This means that a choice is made for  $M_S < M_A$ , or equivalently  $\mu_{\Phi_l'}^2 < -\frac{1}{2}\lambda'_{H\Phi_l} v^2$ .

Even before considering constraints related to flavour physics and to the couplings to the muon, it is possible to indicate some bounds on the masses. LEP searches for charged vector-like leptons [170] predict a lower mass of 101.2 GeV for  $\chi^\pm$ , meaning a similar limit for the neutral component in Model 5. More recent constraints from the LHC do not apply to this scenario, since they assume the fermion couples to the tau [171] or a small amount of missing transverse energy in the final state [172]. The colour charged scalar  $\Phi_q$  can be produced in pure QCD processes [33] and then decay through  $\Phi_q \rightarrow q\chi$ , with  $q$  a second or third generation quark. The dominant decay of the vector-like fermion is to  $S\nu_\mu$  or  $S\mu^\pm$ , depending on whether it is the neutral or charged component. The decay of  $\Phi_q$  can then generate the following signals in detectors:  $\Phi_q \rightarrow jj + \mu^+\mu^- + \cancel{E}_t$ ,  $jj + \mu^\pm + \cancel{E}_t$  or  $jj + \cancel{E}_T$ , where  $j$  represents a final state jet and  $\cancel{E}_T$  is a missing transverse energy associated with the dark matter particle  $S$ . According to [32], for a model where the colour charged scalar is a doublet of  $SU(2)_Y$  with  $Y = 1/6$ , LHC data [173] for the final signature suggests that  $M_{\Phi_q} \gtrsim 1000$  GeV. This result is valid for Model 5, because the production process for the coloured particle is the same [33]. Finally, if  $S$  is the dark matter candidate, then by definition all other  $\mathbb{Z}_2$ -odd particles must be heavier.

### 5.2.1 Flavour and dark matter constraints

As previously mentioned, Model 5 aims to introduce a dark matter candidate and present a possible solution to the discrepancies in the measurements of the magnetic moment of the muon. To fit the model to experimental data, in [33] a number of physically relevant processes to which this extension to the SM contributes were selected. Matching these processes with experimental results significantly restricts the parameter space. In this work, the same set of measurements is used, but with the results from  $B$  meson decays constituting just another constraint and no longer a source of tension with the SM to be resolved.

### 5.2.1.1 Muon $g - 2$

The new fields of Model 5 contribute to the magnetic moment of the muon through the diagrams in Fig. 5.1. The one loop new physics contribution for the anomalous moment (2.46) is given by [174]

$$\Delta a_\mu^{\text{NP}} = \frac{|y_\mu|^2 m_\mu^2}{16\pi^2 m_\chi^2} [\tilde{F}_7(x_S) + \tilde{F}_7(x_A)], \quad (5.10)$$

with  $x_{S,A} = M_{S,A}^2/m_\chi^2$  and

$$\tilde{F}_7(x) = \frac{1 - 6x + 3x^2 + 2x^3 - 6x^2 \ln x}{12(1-x)^4}. \quad (5.11)$$

$\Delta a_\mu^{\text{NP}}$  is constrained by the recent FermiLab results  $a_\mu^{\text{Exp}} = 116592059(22) \times 10^{-11}$  [31].

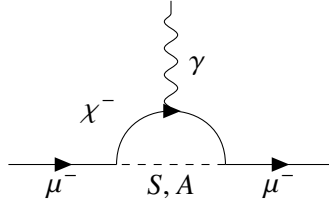


**Figure 5.1:** Feynman diagrams for the anomalous magnetic moment of the muon.

### 5.2.1.2 Dark matter

The first important dark matter measurement to be considered is the relic density. In Model 5, the standard freeze-out mechanism is assumed to be responsible for the generation of dark matter. The relic abundance of  $S$  is obtained by solving the Boltzmann equation [47],

$$\frac{dn_S}{dt} + 3H(t)n_S = -\langle\sigma v\rangle (n_S^2 - n_S^{02}), \quad (5.12)$$

where  $n_S$  is the number density of the dark matter particle  $S$ ,  $H(t)$  is the Hubble parameter,  $\langle\sigma v\rangle$  is the thermal average of the dark matter annihilation cross section times the relative velocity  $v$  and  $n_S^0$  is the equilibrium value of the number density.

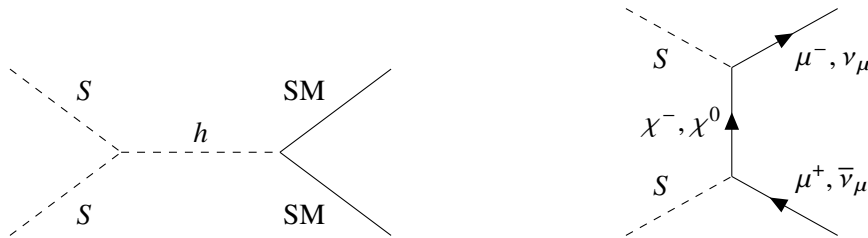


**Figure 5.2:** Feynman diagrams for the dark matter annihilation channels with Higgs mediation (left) and  $\chi$  mediation (right). "SM" represents all massive SM particles.

The main dark matter annihilation channels are represented in Fig. 5.2. In [33], the authors note that when  $M_A - M_S$  or  $m_\chi - M_S$  is smaller or comparable to the temperature of the universe, other co-annihilation processes become relevant in predicting the relic density. The current benchmark for the dark matter relic density is the result of the Planck Collaboration, which gives  $\Omega_{DM} h^2 = 0.1200 \pm 0.0012$  [69].

Another important restriction related to dark matter comes from direct detection experiments, which are concerned with dark matter-nucleon scattering processes. The main signal for Model 5 is due to the  $t$ -channel diagram in Fig. 5.3 (left), with tree-level Higgs mediation. The cross section is

$$\sigma(SN \rightarrow SN) = \frac{\left(\lambda_{H\Phi_l} + \lambda'_{\Phi_l}\right)^2}{4\pi} \frac{f_N^2 m_N^2 \mu_{SN}^2}{M_S^2 M_h^4}, \quad (5.13)$$

with  $m_N$  the mass of the nucleon  $N$  and  $\mu_N = M_S M_N / (M_S + M_N)$  the reduced mass of the  $S - N$  system.  $f_N \approx 0.3$  represents the effective Higgs-nucleon coupling [175–177]. Currently, the best upper bound on the dark matter direct detection cross section for masses above 6 GeV is from the LZ experiment [178].



**Figure 5.3:** Feynman diagrams for  $SN \rightarrow SN$  and  $h \rightarrow SS$ .

The final dark matter constraint arises from collider searches, in particular Higgs invisible decays. When the mass of the dark matter particle is small enough that the Higgs can decay to it, in this case  $M_S < M_h/2$ , one can resort to the experimental bounds on the invisible decay width. In Model 5, this is given by

$$\Gamma(h \rightarrow SS) = \frac{\left(\lambda_{H\Phi_l} + \lambda'_{\Phi_l}\right)^2 v^2}{32\pi M_h} \sqrt{1 - \frac{4M_S^2}{M_h^2}}. \quad (5.14)$$

for the process in Fig. 5.3 (right). The most recent bounds for the Higgs invisible decay are given by the LHC Collaboration [47].

### 5.2.1.3 $B \rightarrow K^{(*)} \mu^+ \mu^-$

Starting in 2014, results from the LHCb Collaboration [167, 168] for the exclusive branching fractions  $R(K^{(*)}) = \mathcal{B}(B \rightarrow K^{(*)} \mu^+ \mu^-) / \mathcal{B}(B \rightarrow K^{(*)} e^+ e^-)$ , were in disagreement with the SM [179, 180] in which  $R^{SM}(K^{(*)}) = 1$ . Other observables sensible to hadronic physics complemented this conclusion [181–185], with all these phenomena related to the transition  $b \rightarrow s \mu^+ \mu^-$ . This apparent suggestion of violation of lepton flavour universality served as motivation for constructing the class of models in [32]. The most recent results from the LHCb are now compatible with the SM [186, 187]. After the

implementation of stricter particle identification criteria and improved rejection of misidentified and partially reconstructed background, all measurements of  $R(K^{(*)})$  in  $B \rightarrow K^{(*)}\mu^+\mu^-$  coincide with the SM prediction,

$$R_K^{\text{Exp}} = 0.949_{-0.041-0.026}^{+0.042+0.022}, \quad R_K^{\text{SM}} = 1.0007 \pm 0.0003, \quad (5.15)$$

$$R_{K^*}^{\text{Exp}} = 1.027_{-0.068-0.026}^{+0.072+0.027}, \quad R_{K^*}^{\text{SM}} = 0.9832 \pm 0.0014, \quad (5.16)$$

with the first set of errors in the experimental results being statistical in nature and the second systematic. The fact that there is no longer tension between theory and experiment does not mean this observable should not be considered, since it still provides useful constraints. Moreover,  $b \rightarrow s\mu^+\mu^-$  related observables still exhibit large deviations from SM values. Hence, the new results for  $R(K^{(*)})$  can be said to suggest anomalous  $b \rightarrow s e^+ e^-$  transitions with possible implications for new physics [188, 189].

The flavour changing neutral current  $b \rightarrow s\mu^+\mu^-$  is described by the effective Hamiltonian [190, 191]

$$\mathcal{H}_{\text{eff}} = -\frac{4G_F}{\sqrt{2}} V_{tb} V_{ts}^* (C_9^{\text{NP}} \mathcal{O}_9 + C_{10}^{\text{NP}} \mathcal{O}_{10}) \quad (5.17)$$

where  $C_9^{\text{NP}}$  and  $C_{10}^{\text{NP}}$  are the new physics Wilson coefficients for the operators

$$\mathcal{O}_9 = \frac{\alpha}{4\pi} [\bar{s}\gamma^\nu P_L b] [\bar{\mu}\gamma_\nu \mu], \quad \mathcal{O}_{10} = \frac{\alpha}{4\pi} [\bar{s}\gamma^\nu P_L b] [\bar{\mu}\gamma_\nu \gamma^5 \mu], \quad (5.18)$$

in the operator product expansion [38]. The operators get contributions from three diagrams in Model 5, the box and penguin diagrams in Fig. 5.4. The Z penguin diagrams are neglected, being suppressed by a factor  $m_b^2/M_Z^2$ , and of the remaining two the box diagrams offer the dominant contribution.

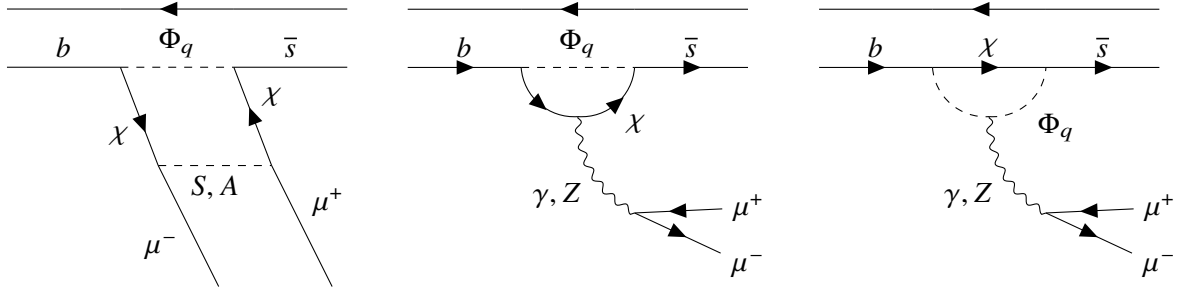


Figure 5.4: Feynman diagrams for  $B \rightarrow K^{(*)}\mu^+\mu^-$ .

The box diagrams contribute to the Wilson coefficients in (5.17) as [174]

$$C_9^{\text{box}} = -C_{10}^{\text{box}} = \frac{\sqrt{2}}{4G_F V_{tb} V_{ts}^*} \frac{y_s y_b^* |y_\mu|^2}{64\pi\alpha m_\chi^2} [F(x_{\Phi_q}, x_S) + F(x_{\Phi_q}, x_A)], \quad (5.19)$$

with

$$F(x_1, x_2) = \frac{1}{(1-x_1)(1-x_2)} + \frac{x_1^2 \ln x_1}{(1-x_1)^2(x_1-x_2)} + \frac{x_2^2 \ln x_2}{(1-x_2)^2(x_2-x_1)}, \quad (5.20)$$

and  $x_{\Phi_q, S, A}$  defined as before. From these results,  $C_9^{\text{NP}} \approx C_9^{\text{box}} = -C_{10}^{\text{box}} \approx C_{10}^{\text{NP}}$ .

The best value for the Wilson coefficient that takes into account the updated results from the LHCb is  $C_9^{\text{NP}} = -0.19 \pm 0.06$  [189].

#### 5.2.1.4 $B_s \rightarrow \mu^+ \mu^-$

The decay process  $B_s \rightarrow \mu^+ \mu^-$  can also be used to help constrain the model, since it depends on the  $O_{10}$  operator. In Model 5, the box diagrams in Fig. 5.5 contribute to this decay. The branching fraction for this channel is obtained from the SM one [192] replacing the SM Wilson coefficient with the new physics one [193],

$$\mathcal{B}^{\text{NP}}(B_s \rightarrow \mu^+ \mu^-) = f_{B_s}^2 m_{B_s} \tau_{B_s} \frac{\alpha^2 G_F^2 m_\mu^2}{16\pi^3} |V_{tb} V_{ts}^*| |C_{10}^{\text{NP}}|^2 \sqrt{1 - \frac{4m_\mu^2}{m_{B_s}^2}}, \quad (5.21)$$

where  $f_{B_s}^2$  is the meson decay constant and  $m_{B_s}$  and  $\tau_{B_s}$  are the meson's mass and lifetime.

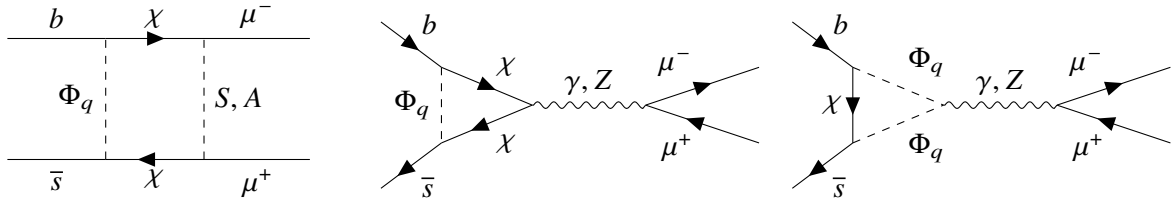


Figure 5.5: Feynman diagrams for  $B_s \rightarrow \mu^+ \mu^-$ .

The most recent SM prediction for this decay is [192]

$$\mathcal{B}^{\text{SM}}(B_s \rightarrow \mu^+ \mu^-) = (3.65 \pm 0.23) \times 10^{-9}, \quad (5.22)$$

and the best experimental value comes from the LHCb Collaboration [194],

$$\mathcal{B}^{\text{Exp}}(B_s \rightarrow \mu^+ \mu^-) = (2.7_{-0.5}^{+0.6}) \times 10^{-9}. \quad (5.23)$$

#### 5.2.1.5 $b \rightarrow s \gamma$

The process  $b \rightarrow s \gamma$  gets contributions at the one loop level in Model 5 and can be used to further constrain it. The diagrams are represented in Fig. 5.6. The effective Hamiltonian for this case is given by [174]

$$\mathcal{H}_{\text{eff}} = -\frac{4G_F}{\sqrt{2}} V_{tb} V_{ts}^* (C_7^{\text{NP}} O_7 + C_8^{\text{NP}} O_8), \quad (5.24)$$

with the operators

$$O_7 = \frac{e}{16\pi} m_b \bar{s} \sigma^{\mu\nu} P_R b F_{\mu\nu}, \quad O_8 = \frac{g_s}{16\pi} m_b \bar{s}_\alpha \sigma^{\mu\nu} P_R T_{\alpha\beta}^a b_\beta G_{\mu\nu}^a. \quad (5.25)$$

$F_{\mu\nu}$  and  $G_{\mu\nu}^a$  are the photon and gluon field strength tensors and  $g_s$  is the strong coupling constant.  $\alpha$  and  $\beta$  are colour indices. The operator  $O_8$  does not give a direct contribution to  $b \rightarrow s\gamma$ , but because of the renormalisation group running from QCD [195, 196] there is a mixing effect between  $O_7$  and  $O_8$ . The Wilson coefficients for the Model 5 contributions are [174]

$$C_7^{\text{NP}} = \frac{\sqrt{2}}{4G_F V_{tb} V_{ts}^*} \frac{y_s y_b^* |y_\mu|^2}{2m_\chi^2} [Q_{\Phi_q} F_7(x_{\Phi_q}) - Q_\chi \tilde{F}_7(x_{\Phi_q})], \quad (5.26)$$

$$C_8^{\text{NP}} = \frac{\sqrt{2}}{4G_F V_{tb} V_{ts}^*} \frac{y_s y_b^* |y_\mu|^2}{2m_\chi^2} Q_{\Phi_q} F_7(x_{\Phi_q}), \quad (5.27)$$

where  $F_7$  is given by

$$F_7(x) = \frac{2 + 3x - 6x^2 + x^3 + 6x \ln x}{12(1-x)^4}. \quad (5.28)$$



**Figure 5.6:** Feynman diagrams for  $b \rightarrow s\gamma$ .

The most recent SM prediction for this decay is [195, 196]

$$\mathcal{B}^{\text{SM}}(b \rightarrow s\gamma) = (3.36 \pm 0.23) \times 10^{-4}, \quad (5.29)$$

and the best experimental value comes from the HFLAV Collaboration [197],

$$\mathcal{B}^{\text{Exp}}(b \rightarrow s\gamma) = (3.32 \pm 0.15) \times 10^{-4}. \quad (5.30)$$

For  $b \rightarrow s\gamma$  and  $B_s - \bar{B}_s$  mixing the constraint on the model is defined through secondary quantities instead of using the cross sections or branching ratios directly. For the first process, following [174, 198], from the ratio

$$R_{b \rightarrow s\gamma} = \frac{\mathcal{B}(b \rightarrow s\gamma)}{\mathcal{B}^{\text{SM}}(b \rightarrow s\gamma)} - 1 = -2.7(C_7 + 0.19C_8^{\text{NP}}), \quad (5.31)$$

combined with (5.29) and (5.30) to obtain  $R_{b \rightarrow s\gamma} = (0.7 \pm 8.2 \times 10^{-2})$  at a  $2\sigma$  level, one gets

$$|C_7^{\text{NP}} + 0.19C_8^{\text{NP}}| \lesssim 0.06. \quad (5.32)$$

### 5.2.1.6 $B_s - \bar{B}_s$ mixing

The final flavour constraint is related to the  $B_s - \bar{B}_s$  mixing. The effective Hamiltonian that describes the contributions to this process is given by [33]

$$\mathcal{H}_{\text{eff}} = C_{B\bar{B}} [\bar{s}_\alpha \gamma^\mu P_L b_\alpha] [\bar{s}_\beta \gamma^\mu P_L b_\beta]. \quad (5.33)$$

the Wilson coefficient for the Model 5 contribution in Fig. 5.7 is

$$C_{B\bar{B}}^{\text{NP}} = \frac{(y_s y_b^*)^2}{128\pi^2 m_\chi^2} F(x_{\Phi_q}, x_{\Phi_q}), \quad (5.34)$$

with  $F$  defined as in (5.20).



**Figure 5.7:** Feynman diagrams for  $B_s - \bar{B}_s$  mixing.

The limit for  $C_{B\bar{B}}^{\text{NP}}$  is determined from the ratio [198]

$$R_{\Delta M_s} = \frac{\Delta M_s^{\text{Exp}}}{\Delta M_s^{\text{SM}}} - 1 = -0.09 \pm 0.08, \quad (5.35)$$

where  $\Delta M_s^{\text{Exp}}$  and  $\Delta M_s^{\text{SM}}$  are the experimental mass difference between  $B_s$  and  $\bar{B}_s$  and its SM value, which can be written in terms of the Wilson coefficient in the following way [199]

$$R_{\Delta M_s} = \left| 1 + \frac{0.8 C_{B\bar{B}}^{\text{NP}}(\mu_H)}{C_{B\bar{B}}^{\text{NP}}(\mu_b)} \right| - 1. \quad (5.36)$$

$C_{B\bar{B}}^{\text{NP}}(\mu_H)$  is the Model 5 coefficient computed at an energy scale  $\mu_H = 1 \text{ TeV}$  and  $C_{B\bar{B}}^{\text{NP}}(\mu_b) \approx 7.2 \times 10^{-11} \text{ GeV}^{-2}$  is the SM value at the energy scale  $\mu_b$  [200].



# Chapter 6

## Results

In this chapter, we present the new physics corrections  $\delta g_{\text{LR}}^{\text{NP}}$  to the muon-related observables  $\hat{R}_{e\mu}$  and  $\hat{\mathcal{A}}_\mu$ . We use the packages FeynRules [201, 202], FeynArts [203, 204] and FeynCalc [205, 206] to calculate the Model 5 diagrams that contribute to the vertex corrections and write an analytical expression for the loop integrals. With the package LoopTools [207], we investigate the impact of each component of the vertex corrections and see how  $\hat{R}_{e\mu}$  and  $\hat{\mathcal{A}}_\mu$  depend on the parameters. Finally, we show the results of a random scan over the parameter space of Model 5 where we apply the flavour and dark matter restrictions in 5.2.1 and a new constraint for the muon-related observables.

### 6.1 One loop radiative corrections in Model 5

Model 5 extends the SM by adding two new scalar fields and a vector-like fermion. However, the properties of the fields are such that the electroweak gauge group remains the SM  $SU(2)_L \times U(1)_Y$ , with only the SM  $W^\pm$ ,  $Z$  and  $\gamma$  bosons. The  $\mathbb{Z}_2$  symmetry forbids the mixing between the SM fields and any of the new ones as well as couplings with an odd number of the new particles. The tree-level structure of  $Z \rightarrow f^+ f^-$  and  $e^+ e^- \rightarrow f^+ f^-$  is the same as in the SM. All of the conditions set forth in 4.3 apply to Model 5, meaning that the method there described is valid.

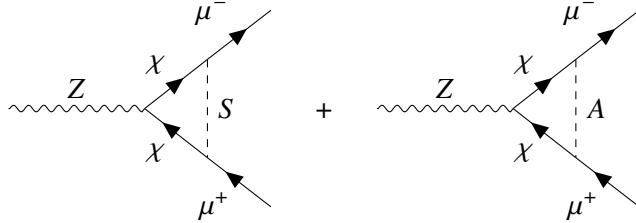
In order to determine the one loop new physics contributions to the processes and how they impact the observables, one must calculate all new diagrams that contribute to the vertex (4.48) and to the  $\gamma Z$  mixing self-energy (4.59), as well as any new box diagrams. Because the new fields only couple to the second generation fermions, no new box diagrams coming from Model 5 for  $e^+ e^- \rightarrow f^+ f^-$  are allowed. This characteristic of the model simplifies this approach even further, since the corrections to the couplings for both processes are precisely the same, which in general need not be the case.

#### 6.1.1 New diagrams

The model is written in the Mathematica [208] package FeynRules [201, 202], which identifies the allowed interactions, and then FeynArts [203, 204] is used to generate the diagrams. The amplitudes are calculated with FeynCalc [205, 206] and written in terms of the Passarino-Veltman functions [143, 209].

### 6.1.1.1 Vertex diagrams

There are two vertex diagrams from the extended sector contributing to the vertex corrections. At one loop, only the vector-like fermion couples to the Z boson, with the neutral scalar closing the loop in the vertex diagrams. One diagram has the real component and the other the imaginary component. The analytical expressions for these diagrams are formally identical,



$$= i \frac{e}{s_W c_W} \gamma_\mu \left( \Lambda_L^{NP}(s) P_L + \Lambda_R^{NP}(s) P_R \right) + (q_2 - q_1)_\mu \Lambda_M^{NP}(s) + (q_1 + q_2)_\mu \gamma_5 \Lambda_P^{NP}(s), \quad (6.1)$$

with the contributions to the left- and right-handed couplings at the Z pole

$$\begin{aligned} \Lambda_L^{NP}(M_Z^2) &= \frac{y_\mu^2}{64\pi^2} (c_W^2 - s_W^2) \left[ B_0(M_Z^2, m_\chi^2, m_\chi^2) + (M_S^2 - m_\chi^2) C_0(m_\mu^2, m_\mu^2, M_Z^2, m_\chi^2, M_S^2, m_\chi^2) \right. \\ &\quad \left. - 2C_{00}(m_\mu^2, M_Z^2, m_\mu^2, M_S^2, m_\chi^2, m_\chi^2) + 2m_\mu^2 C_1(m_\mu^2, M_Z^2, m_\mu^2, M_S^2, m_\chi^2, m_\chi^2) \right] \\ &\quad + M_S \leftrightarrow M_A, \end{aligned} \quad (6.2)$$

$$\begin{aligned} \Lambda_R^{NP}(M_Z^2) &= -\frac{y_\mu^2 m_\mu^2}{64\pi^2} (c_W^2 - s_W^2) \left[ C_0(m_\mu^2, m_\mu^2, M_Z^2, m_\chi^2, M_S^2, m_\chi^2) + 2C_1(m_\mu^2, M_Z^2, m_\mu^2, M_S^2, m_\chi^2, m_\chi^2) \right] \\ &\quad + M_S \leftrightarrow M_A. \end{aligned} \quad (6.3)$$

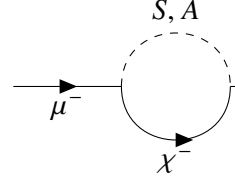
with  $M_S \leftrightarrow M_A$  representing the expression for the second diagram, which is similar to the first but with the masses changed. The final two terms correspond to the anomalous magnetic moment,  $\Lambda_M^{NP}$ , and to the pseudoscalar couplings,  $\Lambda_P^{NP}$ , in (4.47),

$$\begin{aligned} \Lambda_M^{NP}(M_Z^2) &= -\frac{y_\mu^2 m_\mu}{64\pi^2} (c_W^2 - s_W^2) \left[ C_1(m_\mu^2, M_Z^2, m_\mu^2, M_S^2, m_\chi^2, m_\chi^2) + C_{11}(m_\mu^2, M_Z^2, m_\mu^2, M_S^2, m_\chi^2, m_\chi^2) \right. \\ &\quad \left. + C_{12}(m_\mu^2, M_Z^2, m_\mu^2, M_S^2, m_\chi^2, m_\chi^2) + C_1(m_\mu^2, M_Z^2, m_\mu^2, M_A^2, m_\chi^2, m_\chi^2) \right. \\ &\quad \left. + C_{11}(m_\mu^2, M_Z^2, m_\mu^2, M_A^2, m_\chi^2, m_\chi^2) + C_{12}(m_\mu^2, M_Z^2, m_\mu^2, M_A^2, m_\chi^2, m_\chi^2) \right], \end{aligned} \quad (6.4)$$

$$\begin{aligned} \Lambda_P^{NP}(M_Z^2) &= \frac{y_\mu^2 m_\mu}{64\pi^2} (c_W^2 - s_W^2) \left[ C_1(m_\mu^2, M_Z^2, m_\mu^2, M_S^2, m_\chi^2, m_\chi^2) + C_{11}(m_\mu^2, M_Z^2, m_\mu^2, M_S^2, m_\chi^2, m_\chi^2) \right. \\ &\quad \left. - C_{12}(m_\mu^2, M_Z^2, m_\mu^2, M_S^2, m_\chi^2, m_\chi^2) + C_1(m_\mu^2, M_Z^2, m_\mu^2, M_A^2, m_\chi^2, m_\chi^2) \right. \\ &\quad \left. + C_{11}(m_\mu^2, M_Z^2, m_\mu^2, M_A^2, m_\chi^2, m_\chi^2) - C_{12}(m_\mu^2, M_Z^2, m_\mu^2, M_A^2, m_\chi^2, m_\chi^2) \right]. \end{aligned} \quad (6.5)$$

### 6.1.1.2 Muon self-energy diagrams

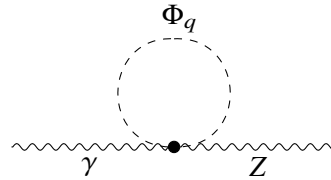
Like for the vertex contributions, there are only two new muon self-energy diagrams with the scalar  $\Phi_l$  and the fermion  $\chi$  in the loop. The two diagrams are also formally identical and for on-shell muons read



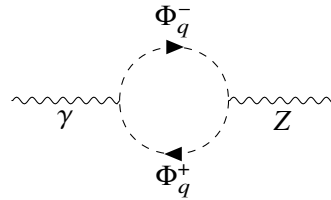
$$= -\frac{y_\mu^2}{32\pi^2} B_1(m_\mu^2, m_\chi^2, M_{S,A}^2) P_L. \quad (6.6)$$

### 6.1.1.3 $\gamma Z$ self-energy diagrams

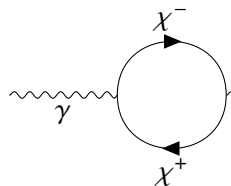
Three diagrams contribute to the  $\gamma Z$  mixing self-energy, which enters the corrected vertex through the renormalisation of the vertex itself in (4.28) and the  $\gamma Z$  propagator correction. Two of them, a self-energy diagram and a sunset diagram, have the scalar  $\Phi_q$  in the loop. The third includes the vector-like fermion. These diagrams lead to the following contributions to the transverse part of the propagator:



$$= \frac{e^2}{18\pi^2} \frac{s_W}{c_W} A_0(M_{\Phi_q}^2), \quad (6.7)$$



$$= -\frac{e^2}{9\pi^2} \frac{s_W}{c_W} B_{00}(s, M_{\Phi_q}^2, M_{\Phi_q}^2), \quad (6.8)$$



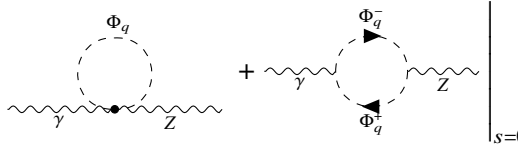
$$= -\frac{e^2}{16\pi^2} \frac{c_W^2 - s_W^2}{s_W c_W} s B_0(s, m_\chi^2, m_\chi^2) \quad (6.9)$$

$$+ \frac{e^2}{8\pi^2} \frac{c_W^2 - s_W^2}{s_W c_W} A_0(m_\chi^2) - \frac{e^2}{4\pi^2} \frac{c_W^2 - s_W^2}{s_W c_W} B_{00}(s, m_\chi^2, m_\chi^2).$$

Following the on-shell renormalisation prescription, the diagrams must be evaluated for zero exchanged momentum to calculate the counter-terms in (4.28). For  $d = 4$  [210],

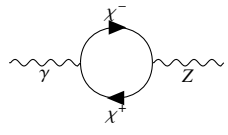
$$B_{00}(p^2, m_1^2, m_2^2) = \frac{1}{3} [A_0(m_1^2) + 2m_1^2 B_0(p^2, m_1^2, m_2^2) + (p^2 + m_1^2 - m_2^2) B_1(p^2, m_1^2, m_2^2) + m_1^2 + m_2^2 - \frac{p^2}{3}], \quad (6.10)$$

which for  $p^2 = 0$  and  $m_1 = m_2 = m$  simplifies to  $B_{00}(0, m^2, m^2) = \frac{1}{2} A_0(m^2)$ . Applying this result to the diagrams gives



$$\left. \begin{array}{c} \text{Diagram 1} + \text{Diagram 2} \end{array} \right|_{s=0} = \frac{e^2}{18\pi^2} \frac{s_W}{c_W} A_0(M_{\Phi_q}^2) - \frac{e^2}{9\pi^2} \frac{s_W}{c_W} \frac{1}{2} A_0(M_{\Phi_q}^2) = 0 \quad (6.11)$$

and



$$\left. \text{Diagram} \right|_{s=0} = \frac{e^2}{8\pi^2} \frac{c_W^2 - s_W^2}{s_W c_W} A_0(m_\chi^2) - \frac{e^2}{4\pi^2} \frac{c_W^2 - s_W^2}{s_W c_W} \frac{1}{2} A_0(m_\chi^2) = 0. \quad (6.12)$$

Hence, these diagrams do not contribute to the counter-terms.

At the Z pole these diagrams do not cancel and as such give a non-zero contribution to the  $\gamma Z$  mixing propagator corrections, but as explained in 4.3 these are left out of our calculations for the vertex.

### 6.1.2 Impact on $\hat{R}_{e\mu}$ and $\hat{\mathcal{A}}_\mu$

The deviation to the left- and right-handed couplings at the Z pole coming from new physics can be written as

$$\delta g_{L,R}^{\text{NP}} = -\frac{s_W c_W}{e} \Lambda_{L,R}^{\text{NP}}(M_Z^2) + g_{L,R} \delta Z_{L,R}^{\text{NP}} - g_{L,R} \frac{c_W}{s_W} \frac{\Sigma_{\gamma Z}^{\text{NP}}(0)}{M_Z^2} + s_W c_W \frac{\Sigma_{\gamma Z}^{\text{NP}}(0)}{M_Z^2}, \quad (6.13)$$

with  $\delta Z_{L,R}^{\text{NP}}$  defined as in (4.35) for the muon self-energy diagrams in (6.6).  $\Sigma_{\gamma Z}^{\text{NP}}$  is the sum of the new one loop  $\gamma Z$  mixing diagrams, which for this model calculated at  $s = 0$  gives zero. The terms proportional to the momenta are not included in this definition, since they do not contribute to  $g_{L,R}$ . They are discussed below.

By looking at the expressions for the diagrams alone one would assume that  $|\delta g_L^{\text{NP}}| \gg |\delta g_R^{\text{NP}}|$ , since  $\delta g_R^{\text{NP}} \propto m_\mu^2$ . In fact, that the left-handed coupling was larger than the right-handed was expected from the Lagrangian (5.1), where by definition  $\chi$  and  $\Phi_l$  couple to  $\mu_L$ . To get the right-handed coupling a mass insertion would be required, with a new term proportional to  $m_\mu$  and hence suppressed.  $\delta g_{L,R}^{\text{NP}}$  are functions of the masses  $m_\chi$ ,  $M_S$  and  $M_A$  and of the coupling  $y_\mu$ , as well as of SM parameters. By varying the relevant free parameters in those functions, one can get a more accurate assessment of the possible importance of the corrections. The input values for the Model 5 quantities are varied in the following

intervals

$$\begin{aligned}
M_S &\in [5, 1000] \text{ GeV}, \\
M_A &\in [M_S + 10, 1000] \text{ GeV}, \\
m_\chi &\in [\max\{M_S + 10, 101.2\}, 1000] \text{ GeV}, \\
y_\mu &\in [0, 4\pi],
\end{aligned} \tag{6.14}$$

and the rest fixed to their SM values [47]. Because  $S$  has to be the lightest particle, following [33] the lowest allowed masses for  $A$  and  $\chi$  have to be 10 GeV higher than  $M_S$ . This minimum difference of 10 GeV is an arbitrary definition related to the random scan. Values for the masses of the particles that were too close could lead to numerical instabilities. The maximum values of 1000 GeV were chosen to coincide with the search ranges of current dark matter experiments. The mass of the fermion has to respect the LEP limit of 101.2 GeV as well. The mass of the coloured scalar  $\Phi_q$  is fixed at 1500 GeV. We have chosen an upper limit of  $4\pi$  for  $y_\mu$  instead of the more conservative bound of  $\sqrt{4\pi}$  in [33]. This is to better gauge whether the muon-related constraints provide a limit for this quantity. A discussion about the limits on  $y_\mu$  can be seen in [34]. In Fig. 6.1 we show  $\delta g_{L,R}^{\text{NP}}$  as functions of  $M_S$ ,  $m_\chi$  and  $y_\mu$  for  $10^4$  random points where the parameters obey (6.14). The Passarino-Veltman functions are computed numerically using LoopTools [207].

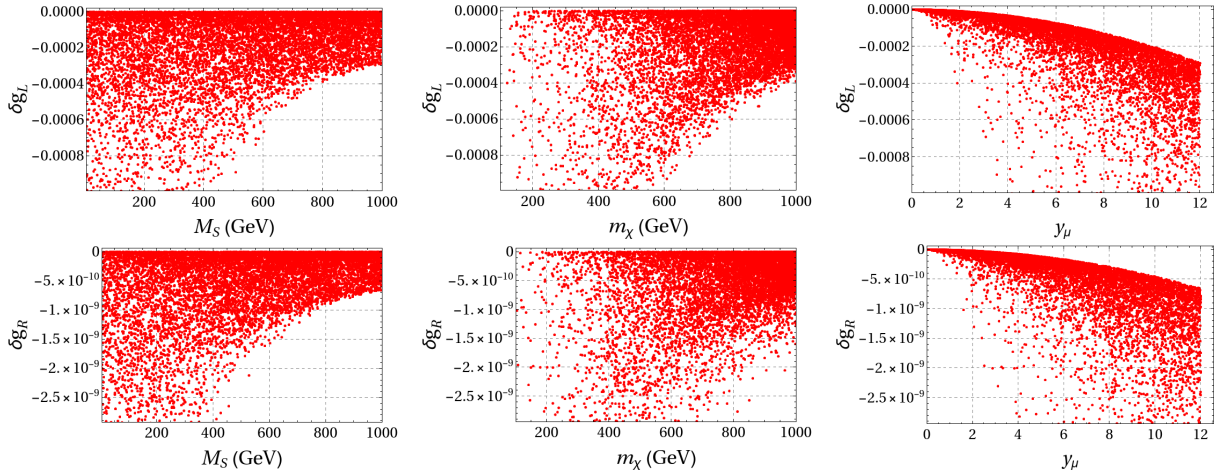


**Figure 6.1:** Scatter plot of  $\delta g_{L,R}^{\text{NP}}$  in terms of  $M_S$ ,  $m_\chi$  and  $y_\mu$  for  $10^4$  random points where the free parameters are varied in 6.14.  $|\delta g_L^{\text{NP}}|$  is always at least 100 times larger than  $|\delta g_R^{\text{NP}}|$ , with the largest deviations corresponding to  $\delta g_L^{\text{NP}} = -0.022$  and  $\delta g_L^{\text{NP}} = -8.043 \times 10^{-8}$ .

As shown in the plots, both  $\delta g_L^{\text{NP}}$  and  $\delta g_R^{\text{NP}}$  are negative, but differ by several orders of magnitude. At most,  $|\delta g_L^{\text{NP}}| \sim 10^{-2}$ , whereas  $|\delta g_R^{\text{NP}}| \sim 10^{-8}$ . This means that the left-handed correction can be of the same order of magnitude as the SM electroweak corrections [129]. For every point,  $|\delta g_L^{\text{NP}}|$  is always at least two orders of magnitude greater than  $|\delta g_R^{\text{NP}}|$ . Proceeding in a similar manner for  $\Lambda_P^{\text{NP}}$  and  $\Lambda_M^{\text{NP}}$  gives maximum values of  $|\Lambda_P^{\text{NP}}| \sim 10^{-7}$  and  $|\Lambda_M^{\text{NP}}| \sim 10^{-8}$ , with  $\Lambda_P^{\text{NP}} > 0$  and  $\Lambda_M^{\text{NP}} < 0$ . All contributions are orders of magnitude smaller than  $\delta g_L^{\text{NP}}$ , and are as a consequence neglected. This explains why it is safe to remove  $\Lambda_{M,P}^{\text{NP}}$  from (6.13).

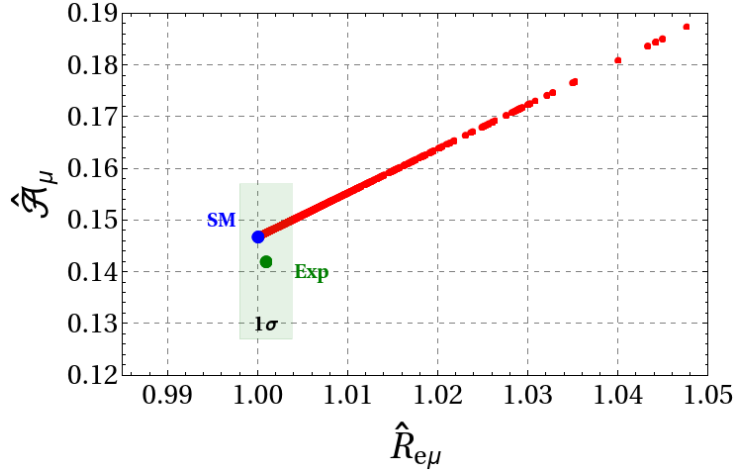


**Figure 6.2:** Plot of  $\hat{R}_{e\mu} - \hat{\mathcal{A}}_\mu$  for  $10^4$  random points shown in red. The central SM value is shown in blue and the experimental value in green. The green box represents the  $1\sigma$  uncertainty interval around the experimental point.  $\delta R_{e\mu}$  and  $\delta \mathcal{A}_\mu$  are always positive. Most of the points lie outside the experimental uncertainty range.

$\delta g_L^{\text{NP}}$  being negative means that according to (4.71), both  $\delta R_{e\mu}$  and  $\delta \mathcal{A}_\mu$  are positive. This would not necessarily be the case if  $\delta g_R^{\text{NP}}$  were not negligible in comparison to  $\delta g_L^{\text{NP}}$ . Fig. 6.2 shows how randomly varying the input parameters in the intervals in (6.14) affects the observables. The points shown in red are obtained by summing  $\delta R_{e\mu}$  and  $\delta \mathcal{A}_\mu$  calculated for the random points to the respective theoretical values. The blue and green points represent the best SM prediction and the central experimental value for the observables from Table 3.1. The green box encompasses the region defined by the  $1\sigma$  experimental uncertainty range. Fig. 6.2 shows that many points are excluded at  $1\sigma$ . This indicates that these observables can effectively be used to limit the allowed parameter space and get tighter bounds on (6.14).

Further information can be obtained by looking at the  $M_S - M_A$  plane for different values of  $m_\chi$  and of the coupling  $y_\mu$ . In Fig. 6.3, we plot the regions of parameter space that keep  $\hat{R}_{e\mu}$  and  $\hat{\mathcal{A}}_\mu$  within their  $1\sigma$  uncertainty range for  $m_\chi = 200, 500$  and  $600$  GeV. Each region corresponds to a fixed value of  $y_\mu$  and the higher the value of the coupling, the darker the shade of orange of the associated region. The different regions overlap. The grey shaded area marks the combinations of  $M_S$  and  $M_A$  that are out of the allowed ranges in (6.14). The first thing to note is that the  $M_S \leftrightarrow M_A$  exchange symmetry is visible in these plots, which are symmetric. Moreover, from these plots it is clear that the higher the value of  $y_\mu$ , the smaller the allowed region for a fixed mass of the fermion, particularly for lower values of  $M_S$  and  $M_A$ . On the other hand, if the coupling is kept fixed, then the constraints become weaker the higher  $m_\chi$  is.

## 6.2 Parameter space scans

To see how Model 5 fares against the constraints of 5.2.1, we perform a multiparameter scan to identify the common regions of allowed parameter space. Our procedure builds on the work in [33, 34], for beyond the dark matter and flavour related constraints, we consider also a new constraint coming from the muon-related observables.

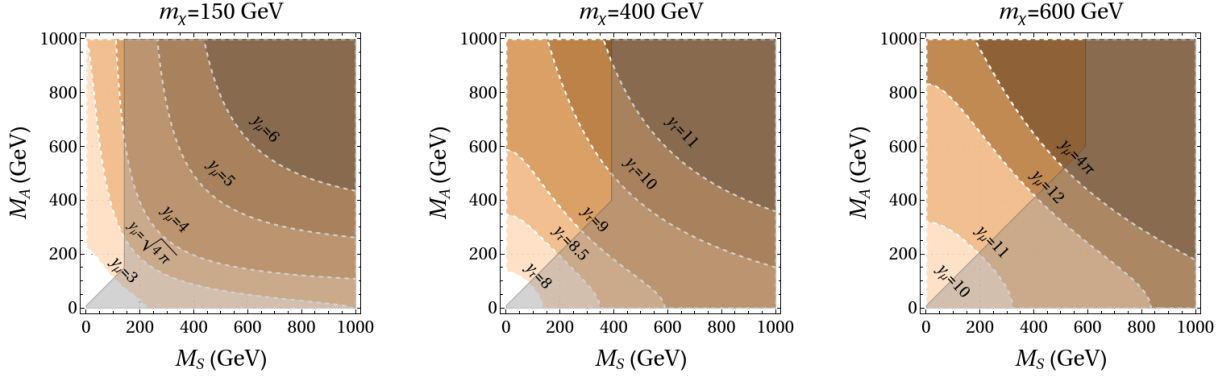


**Figure 6.3:**  $M_S - M_A$  parameter space regions for which  $\hat{R}_{e\mu}$  and  $\hat{\mathcal{A}}_\mu$  are within their  $1\sigma$  uncertainty range for fixed values of  $m_\chi$  and  $y_\mu$ . For fixed  $m_\chi$ , darker shades of orange correspond to higher values of the coupling. The grey zone is excluded because  $M_A > M_S + 10$  GeV and  $m_\chi > M_S + 10$  GeV. Higher values of  $y_\mu$  lead to more stringent constraints for fixed  $m_\chi$ . If  $y_\mu$  is fixed, the constraint becomes less stringent for larger  $m_\chi$ .

We perform a random scan of more than  $10^9$  points over the whole parameter space. The input parameters are the masses  $M_S$ ,  $M_A$ ,  $m_\chi$  and  $M_{\Phi_q}$ , the Yukawa couplings  $y_\mu$ ,  $y_b$  and  $y_s$  and the scalar couplings  $\lambda_{H\Phi_l}$  and  $\lambda'_{H\Phi_l}$ . Because the scalar couplings enter (5.13) and (5.14) exclusively as  $\lambda_{H\Phi_l} + \lambda'_{H\Phi_l}$ , we choose to take  $\lambda_{H\Phi_l} = \lambda'_{H\Phi_l}$ . Moreover, the new Yukawa couplings to the  $b$  and  $s$  quarks always appear combined as  $y_b y_s^*$ , which is required to be negative to agree with [189]. We then consider both  $y_b$  and  $y_s$  to be real and  $y_s = -y_b/4$ . Finally, after these simplifications, there are seven independent free parameters.  $M_\Phi$  is fixed at 1500 GeV and the remaining masses and  $y_\mu$  are varied in the same intervals as before (6.14).  $|y_b|$  and  $\lambda_{H\Phi_l} + \lambda'_{H\Phi_l}$  are both lesser than or equal to one.

The first set of tests applied to the data are the flavour constraints related to  $B \rightarrow K^{(*)}\mu^+\mu^-$ ,  $B_s \rightarrow \mu^+\mu^-$ ,  $b \rightarrow s\gamma$  and  $B_s - \bar{B}_s$ . A random point is accepted if it lies within the  $2\sigma$  experimental range. According to the discussion in 5.2.1, this means

$$\begin{aligned}
 C_9^{\text{NP}} &\in [-0.07, -0.031], \\
 \mathcal{B}^{\text{NP}}(B_s \rightarrow \mu^+\mu^-) &\in [1.7 \times 10^{-9}, 3.9 \times 10^{-9}], \\
 |C_7^{\text{NP}} + 0.19C_8^{\text{NP}}| &\in [0, 0.06], \\
 R_{\Delta M_s} &\in [-0.25, 0.07].
 \end{aligned} \tag{6.15}$$

The points that fail to verify these conditions are rejected. The second set of tests comes from the dark matter constraints. We use micrOMEGAS 5.3.41 [211, 212] to solve the Boltzmann equation (5.12) numerically. The code takes into account all annihilation and co-annihilation channels. The results must reproduce the current relic abundance to a  $2\sigma$  level,  $\Omega_{SM} h^2 \in [0.117, 0.122]$ . The points must also be within the direct detection limits and the  $2\sigma$  bound of the Higgs invisible decay,  $\Gamma(h \rightarrow SS) \in [0, 0.11]$ . The final flavour related condition comes from the anomalous moment of the muon. We consider that a point is valid if it agrees with the most recent results for  $g - 2$  to  $3\sigma$ ,  $\Delta a_\mu^{\text{NP}} \in [105 \times 10^{-11}, 393 \times 10^{-11}]$ .

On top of the previous conditions, we define a new constraint from the muon-related observables  $R_{e\mu}$  and  $\mathcal{A}_\mu$ . A point in the parameter space is accepted if  $\hat{R}_{e\mu}^{SM} + \delta R_{e\mu}$  and  $\hat{\mathcal{A}}_\mu^{SM} + \delta \mathcal{A}_\mu$  with the deviations defined as in (4.71) and the corrections to the couplings (6.13) are within the respective experimental



uncertainty intervals. Using the values of Table 3.1, this translates to

$$\begin{aligned} -0.002 &\leq \delta R_{e\mu} \leq 0.004, \\ -0.02 &\leq \delta \mathcal{A}_\mu \leq 0.01. \end{aligned} \quad (6.16)$$

In the following plots, the cyan points satisfy all flavour constraints and the blue points agree in addition with the dark matter relic density. Together with the previous constraints, the green points also verify the dark matter direct detection and Higgs invisible decay limits. The red points are the ones that satisfy the anomalous moment constraint as well as all flavour and dark matter constraints. Finally, the yellow points agree with all constraints, including the one coming from the muon-related observables (6.16). The results of the scans are shown in Figs. 6.4 and 6.5.

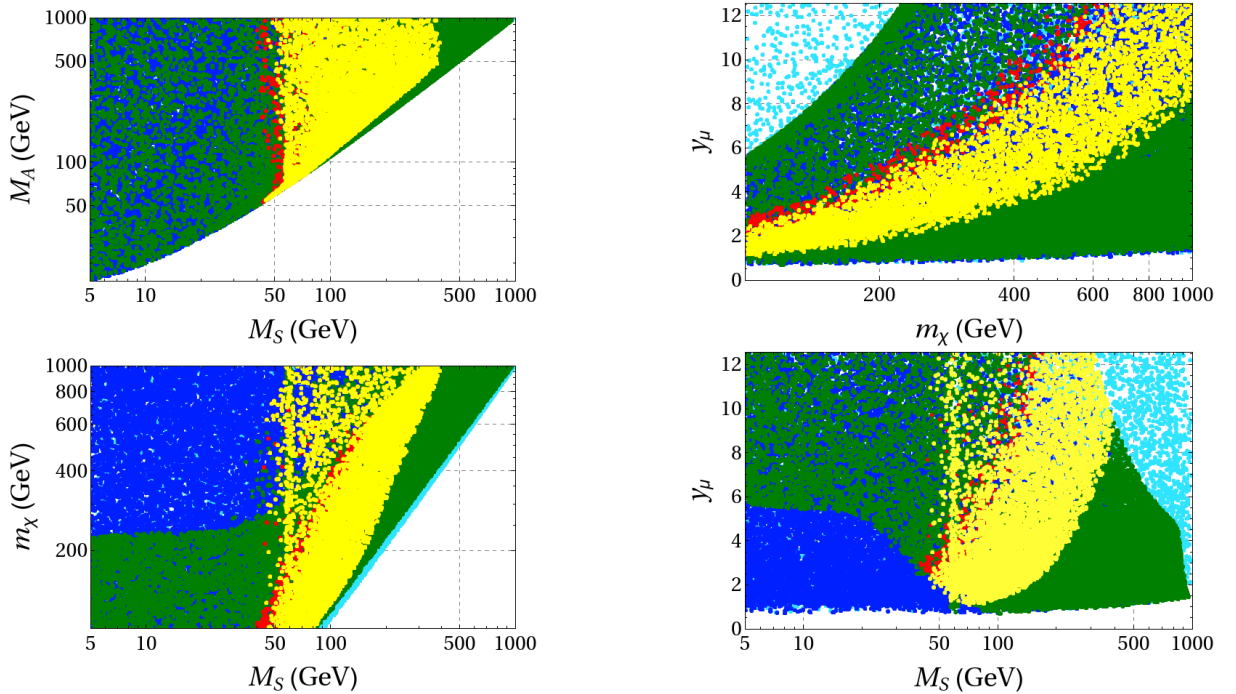


**Figure 6.4:** Allowed parameter space projected in the planes  $M_S - M_A$  (top left),  $m_\chi - y_\mu$  (top right),  $M_S - m_\chi$  (bottom left) and  $M_S - y_\mu$  (bottom right). The cyan points agree with the flavour constraints (6.15). In addition the blue points verify the dark matter relic density results and the green points also the direct detection and invisible decay results. The red points agree with all previous constraints as well as the muon  $g - 2$  limits. The yellow points satisfy all constraints including the one from the muon-related observables.

The results are consistent with [33], with the updated values for the flavour and dark matter results not changing the overall allowed regions. All points verify the  $B_s \rightarrow \mu^+ \mu^-$  and  $b \rightarrow s\gamma$  constraints, which do not limit the parameter space. Of the dark matter constraints, the relic density provides the weakest restrictions, with the direct detection constraints inducing some bounds for  $M_S$  for  $y_\mu \lesssim 5.5$  and  $m_\chi \lesssim 225$  GeV. Considering the  $3\sigma$  limit, the muon  $g - 2$  provides the strongest constraint, excluding many green points. The behaviour observed in the  $m_\chi - y_\mu$  plot on the top right of Fig 6.4 is consistent with (5.10). Higher values of  $m_\chi$  require higher coupling strengths in order to verify the  $g - 2$  constraint. This would still be the case had we considered  $y_\mu \leq \sqrt{4\pi}$ .



The new constraint coming from the muon-related observables excludes few of the red points that passed all the other tests.  $\hat{\mathcal{A}}_\mu$  proves much less restrictive than  $\hat{R}_{e\mu}$ , with all the red points being accepted to  $1\sigma$ .  $\hat{R}_{e\mu}$  still eliminates a small strip in the  $m_\chi - y_\mu$  plane. However, if this condition is relaxed to  $2\sigma$ , then all red points are accepted.

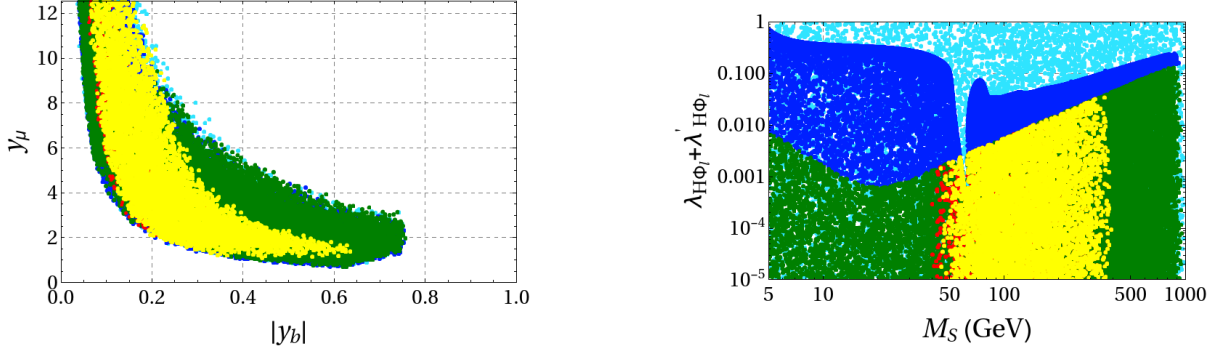


**Figure 6.5:** Allowed parameter space projected in the planes  $|y_b| - y_\mu$  (left) and  $\lambda_{H\Phi_l} + \lambda'_{H\Phi_l}$  (right). The cyan points agree with the flavour constraints (6.15). In addition the blue points verify the dark matter relic density results and the green points also the direct detection and invisible decay results. The red points agree with all previous constraints as well as the muon  $g - 2$  limits. The yellow points satisfy all constraints including the one from the muon-related observables. The clean separation of the green points is due to the experimental bound from [178].

Using the precision results at the  $Z$  pole for the muon observables is a means of obtaining a valid experimental upper limit for the coupling  $y_\mu$ , something which was missing in [33, 34]. For that reason, unlike in the previous analysis of this model,  $y_\mu$  was allowed to vary up to  $4\pi$ . Extending the range of the search ends up providing a new upper limit for  $M_S$ . Because of the positive correlation between  $M_S$  and  $m_\chi$  visible in the bottom left plot of Fig. 6.4, since the latter can now go up to 1000 GeV, the highest allowed value for  $M_S$  also increases slightly to 389 GeV from 350 GeV in [33]. The higher values for the coupling also lead to a different behaviour in the plot of  $M_S - \lambda_{H\Phi_l} + \lambda'_{H\Phi_l}$  in Fig. 6.5. The extended range for the coupling strength fills the region for  $M_S < 30$  GeV which was mostly inaccessible in [33]. Finally, raising the coupling strength to  $4\pi$  leads to a new lower bound for  $|y_b|$  of 0.07.

The bounds to the parameters that result from the application of the muon-related observables  $\hat{\mathcal{A}}_\mu$  and  $\hat{R}_{e\mu}$  are

$$\begin{aligned} M_S &\in [45, 389] \text{ GeV}, & y_\mu &\in [1.1, 4\pi], \\ M_A &\gtrsim 55 \text{ GeV}, & 0.07 &\lesssim |y_b| \lesssim 0.63. \\ m_\chi &\gtrsim 101.2 \text{ GeV}, \end{aligned}$$

For the mass ranges used in this work, the muon-related observables do not impose an upper bound on  $y_\mu$ ,  $M_A$  or  $m_\chi$ .

The method here discussed can be applied directly to the process  $Z \rightarrow \tau^+ \tau^-$  if one considers that the NP particles have a Yukawa coupling to the tau like that to the muon. The diagrams for this case are the same as for the muon, with only the mass and coupling needing to be replaced. Using the values in Table

3.1 to compute the limits to the tau related observables we get

$$\begin{aligned} -0.0009 &\leq \delta R_{e\tau} \leq 0.007, \\ -0.03 &\leq \delta \mathcal{A}_\tau \leq 0.004. \end{aligned} \quad (6.17)$$

With these limits, we reproduce the plot of Fig. 6.3 for the tau. Fig. 6.6 shows the regions of parameter space that keep  $\hat{R}_{e\tau}$  and  $\hat{\mathcal{A}}_\tau$  within their  $2\sigma$  uncertainty range for  $m_\chi = 200$  GeV in the  $M_S - M_A$  plane. As before, each region corresponds to a fixed value of  $y_\mu$  or  $y_\tau$  and the higher the value of the coupling, the darker the shade of orange of the associated region. The behaviour is similar to what was shown for the muon. A direct comparison between the two plots does not give much information on the relation between experimental precision and the constraints, since the SM prediction for  $R_{e\tau}$  lies outside the  $1\sigma$  experimental range.

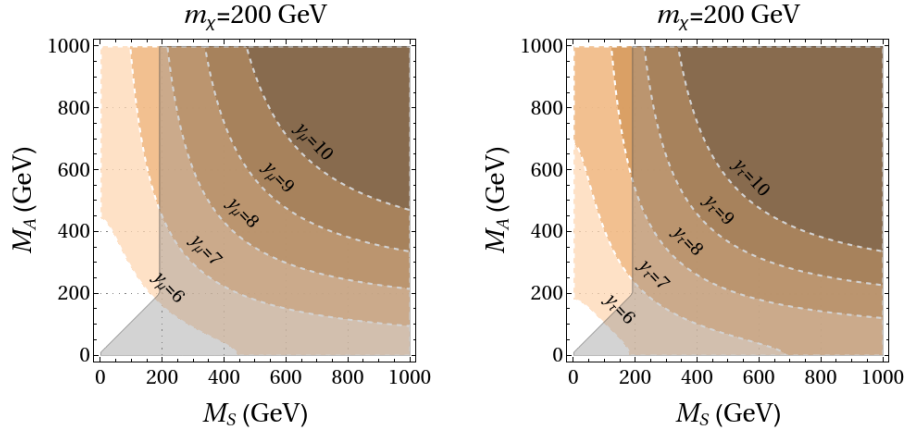


**Figure 6.6:**  $M_S - M_A$  parameter space regions for which  $\hat{R}_{e\mu}$ ,  $\hat{\mathcal{A}}_\mu$ ,  $\hat{R}_{e\tau}$  and  $\hat{\mathcal{A}}_\tau$  are within their  $2\sigma$  uncertainty range for  $m_\chi = 200$  GeV and fixed  $y_\mu$  or  $y_\tau$ . Darker shades of orange correspond to higher values of the coupling. The grey zone is excluded because  $M_A > M_S + 10$  GeV and  $m_\chi > M_S + 10$  GeV. Higher values of  $y_\mu$  or  $y_\tau$  lead to more stringent constraints for fixed  $m_\chi$ .

## Chapter 7

# Conclusion

With this work, we intended to present a method to use precision muon-related observables as a means to constrain BSM models. Our study was primarily motivated by recently proposed models that attempt to solve both the muon  $g - 2$  problem and present a viable dark matter candidate. These models require strong couplings between the new fields and the muon, which can be probed by studying the decay of the  $Z$  boson to muons. We select two  $Z$  pole observables, the muon asymmetry parameter  $\mathcal{A}_\mu$  and the ratio of the hadronic decay rates  $R_{e\mu} = R_e/R_\mu$ . This second quantity was chosen over the decay rates themselves to eliminate the final state QED corrections.

We followed Hollik's renormalisation scheme and successfully identified how the new physics corrections affect the matrix elements for  $Z \rightarrow f^+ f^-$  and  $e^+ e^- \rightarrow f^+ f^-$ , the latter used to get  $\mathcal{A}_\mu$ . We concluded that, under the specific conditions where new physics leaves the tree-level structure of the theory unchanged, the one loop matrix element has an approximate Born-like expression. The left- and right-handed couplings  $g_{L,R}$  get additive terms from the vertex corrections and the corrections to the propagators result in a redefinition of the QED and weak neutral current couplings and of the Weinberg angle.

We tested the impact of our new constraint on a model designated by Model 5, which introduces a vector-like fermion  $\chi$  and two scalar singlets of  $SU(2)_L$ ,  $\Phi_l = (S + iA)/\sqrt{2}$  and  $\Phi_q$ , the second with a colour charge. Through our review and analysis of the electroweak corrections to  $Z \rightarrow f^+ f^-$  and  $e^+ e^- \rightarrow f^+ f^-$ , we identified the new physics diagrams that contribute to the processes and calculated the corrections they induce to  $g_{L,R}$ . By varying the free parameters of the model that directly affect these corrections, we concluded that the left-handed contribution,  $\delta g_L^{\text{NP}}$ , is dominant. In fact,  $\delta g_R^{\text{NP}}$  and two other terms proportional to the momenta are negligible in comparison. Because of this, and since  $\delta g_L^{\text{NP}} < 0$ , the deviation to the observables caused by new physics,  $\delta \mathcal{A}_\mu$  and  $\delta R_{e\mu}$ , is always positive.  $\delta \mathcal{A}_\mu$  and  $\delta R_{e\mu}$  can increase the values of the observables beyond their  $1$  and  $2\sigma$  range. By plotting the  $1\sigma$  acceptance region in the  $M_S - M_A$  plane and by varying  $m_\chi$ , we see that the stronger the coupling to the muon,  $y_\mu$ , the more stringent the constraint. If the coupling is kept fixed instead, the higher the value of  $m_\chi$ , the weaker the constraint, which corresponds to a larger allowed region.

Model 5 can give contribute to several flavour-related processes at one loop order. We employed experimental limits on quantities related to these processes and to dark matter observables to establish a set of phenomenological conditions that Model 5 must verify. These limits together with the ones derived

from  $\mathcal{A}_\mu$  and  $R_{e\mu}$  were applied in the multiparameter scan we performed. Our results are consistent within the ranges explored in [33]. Having introduced a way to get an upper bound on  $y_\mu$ , we explored the region with  $\sqrt{4\pi} < y_\mu < 4\pi$  which was previously left out. The positive correlations between  $m_\chi$  and  $y_\mu$  and  $m_\chi$  and  $M_S$  combined with the higher values of the coupling in our scan result in new upper bound of 389 GeV for  $M_S$ , which compares to 350 GeV in [33].  $|y_b|$  also has its lowest value decreased to 0.007 from 0.25. In Model 5, the muon-related observables do not significantly further restrict the allowed space beyond what was constrained by the  $g - 2$  condition. It can be argued that in other models this will not be the case and that these constraints will provide tighter bounds. Finally, we considered an alternative decay channel,  $Z \rightarrow \tau^+\tau^-$ , and compared the results obtained using the equivalent observables,  $\mathcal{A}_\tau$  and  $R_{e\tau}$ , with the case of the muon in the  $M_S - M_A$  plane. The SM prediction for  $R_{e\tau}$  actually lies outside the  $1\sigma$  experimental uncertainty range, which makes a direct comparison between the plots a delicate subject. Nevertheless, the overall behaviour is similar to the case of the muon, which was expected because the only difference in the theoretical side is the mass of the lepton in question.

# Bibliography

- [1] J. J. Thomson. “Cathode rays”. In: *Phil. Mag. Ser. 5* 44 (1897), pp. 293–316. DOI: [10.1080/14786449708621070](https://doi.org/10.1080/14786449708621070).
- [2] E. Rutherford. “The scattering of alpha and beta particles by matter and the structure of the atom”. In: *Phil. Mag. Ser. 6* 21 (1911), pp. 669–688. DOI: [10.1080/14786440508637080](https://doi.org/10.1080/14786440508637080).
- [3] J. Chadwick. “Possible Existence of a Neutron”. In: *Nature* 129 (1932), p. 312. DOI: [10.1038/129312a0](https://doi.org/10.1038/129312a0).
- [4] Arthur H. Compton. “A Quantum Theory of the Scattering of X-rays by Light Elements”. In: *Phys. Rev.* 21 (1923), pp. 483–502. DOI: [10.1103/PhysRev.21.483](https://doi.org/10.1103/PhysRev.21.483).
- [5] Carl D. Anderson. “The Positive Electron”. In: *Phys. Rev.* 43 (6 Mar. 1933), pp. 491–494. DOI: [10.1103/PhysRev.43.491](https://doi.org/10.1103/PhysRev.43.491). URL: <https://link.aps.org/doi/10.1103/PhysRev.43.491>.
- [6] Carl D. Anderson and Seth H. Neddermeyer. “Cloud Chamber Observations of Cosmic Rays at 4300 Meters Elevation and Near Sea-Level”. In: *Phys. Rev.* 50 (1936), pp. 263–271. DOI: [10.1103/PhysRev.50.263](https://doi.org/10.1103/PhysRev.50.263).
- [7] Frederick Reines and Clyde L. Cowan. “The neutrino”. In: *Nature* 178 (1956), pp. 446–449. DOI: [10.1038/178446a0](https://doi.org/10.1038/178446a0).
- [8] J. R. Oppenheimer et al. “Theoretical interpretation of new particles”. In: *6th Annual Rochester Conference on High energy nuclear physics*. 1956, pp. VIII.1–36.
- [9] Murray Gell-Mann. “The Eightfold Way: A Theory of strong interaction symmetry”. In: (Mar. 1961). DOI: [10.2172/4008239](https://doi.org/10.2172/4008239).
- [10] Yuval Ne’eman. “Derivation of strong interactions from a gauge invariance”. In: *Nucl. Phys.* 26 (1961). Ed. by R. Ruffini and Y. Verbin, pp. 222–229. DOI: [10.1016/0029-5582\(61\)90134-1](https://doi.org/10.1016/0029-5582(61)90134-1).
- [11] Murray Gell-Mann. “A Schematic Model of Baryons and Mesons”. In: *Phys. Lett.* 8 (1964), pp. 214–215. DOI: [10.1016/S0031-9163\(64\)92001-3](https://doi.org/10.1016/S0031-9163(64)92001-3).
- [12] G. Zweig. “An SU(3) model for strong interaction symmetry and its breaking. Version 1”. In: (Jan. 1964).
- [13] Elliott D. Bloom et al. “High-Energy Inelastic e p Scattering at 6-Degrees and 10-Degrees”. In: *Phys. Rev. Lett.* 23 (1969), pp. 930–934. DOI: [10.1103/PhysRevLett.23.930](https://doi.org/10.1103/PhysRevLett.23.930).

- [14] Martin Breidenbach et al. “Observed behavior of highly inelastic electron-proton scattering”. In: *Phys. Rev. Lett.* 23 (1969), pp. 935–939. DOI: [10.1103/PhysRevLett.23.935](https://doi.org/10.1103/PhysRevLett.23.935).
- [15] S. Tomonaga. “On a relativistically invariant formulation of the quantum theory of wave fields”. In: *Prog. Theor. Phys.* 1 (1946), pp. 27–42. DOI: [10.1143/PTP.1.27](https://doi.org/10.1143/PTP.1.27).
- [16] Julian S. Schwinger. “On Quantum electrodynamics and the magnetic moment of the electron”. In: *Phys. Rev.* 73 (1948), pp. 416–417. DOI: [10.1103/PhysRev.73.416](https://doi.org/10.1103/PhysRev.73.416).
- [17] R. P. Feynman. “Space-time approach to nonrelativistic quantum mechanics”. In: *Rev. Mod. Phys.* 20 (1948), pp. 367–387. DOI: [10.1103/RevModPhys.20.367](https://doi.org/10.1103/RevModPhys.20.367).
- [18] Abdus Salam and John Clive Ward. “Weak and electromagnetic interactions”. In: *Nuovo Cim.* 11 (1959), pp. 568–577. DOI: [10.1007/BF02726525](https://doi.org/10.1007/BF02726525).
- [19] S. L. Glashow. “Partial Symmetries of Weak Interactions”. In: *Nucl. Phys.* 22 (1961), pp. 579–588. DOI: [10.1016/0029-5582\(61\)90469-2](https://doi.org/10.1016/0029-5582(61)90469-2).
- [20] Steven Weinberg. “A Model of Leptons”. In: *Phys. Rev. Lett.* 19 (1967), pp. 1264–1266. DOI: [10.1103/PhysRevLett.19.1264](https://doi.org/10.1103/PhysRevLett.19.1264).
- [21] F. Englert and R. Brout. “Broken Symmetry and the Mass of Gauge Vector Mesons”. In: *Phys. Rev. Lett.* 13 (1964). Ed. by J. C. Taylor, pp. 321–323. DOI: [10.1103/PhysRevLett.13.321](https://doi.org/10.1103/PhysRevLett.13.321).
- [22] Peter W. Higgs. “Broken Symmetries and the Masses of Gauge Bosons”. In: *Phys. Rev. Lett.* 13 (1964). Ed. by J. C. Taylor, pp. 508–509. DOI: [10.1103/PhysRevLett.13.508](https://doi.org/10.1103/PhysRevLett.13.508).
- [23] G. S. Guralnik, C. R. Hagen, and T. W. B. Kibble. “Global Conservation Laws and Massless Particles”. In: *Phys. Rev. Lett.* 13 (1964). Ed. by J. C. Taylor, pp. 585–587. DOI: [10.1103/PhysRevLett.13.585](https://doi.org/10.1103/PhysRevLett.13.585).
- [24] Gerard ’t Hooft. “Renormalizable Lagrangians for Massive Yang-Mills Fields”. In: *Nucl. Phys. B* 35 (1971). Ed. by J. C. Taylor, pp. 167–188. DOI: [10.1016/0550-3213\(71\)90139-8](https://doi.org/10.1016/0550-3213(71)90139-8).
- [25] Gerard ’t Hooft and M. J. G. Veltman. “Regularization and Renormalization of Gauge Fields”. In: *Nucl. Phys. B* 44 (1972), pp. 189–213. DOI: [10.1016/0550-3213\(72\)90279-9](https://doi.org/10.1016/0550-3213(72)90279-9).
- [26] K. Kodama et al. “Observation of tau neutrino interactions”. In: *Phys. Lett. B* 504 (2001), pp. 218–224. DOI: [10.1016/S0370-2693\(01\)00307-0](https://doi.org/10.1016/S0370-2693(01)00307-0). arXiv: [hep-ex/0012035](https://arxiv.org/abs/hep-ex/0012035).
- [27] Georges Aad et al. “Observation of a new particle in the search for the Standard Model Higgs boson with the ATLAS detector at the LHC”. In: *Phys. Lett. B* 716 (2012), pp. 1–29. DOI: [10.1016/j.physletb.2012.08.020](https://doi.org/10.1016/j.physletb.2012.08.020). arXiv: [1207.7214 \[hep-ex\]](https://arxiv.org/abs/1207.7214).
- [28] A. D. Sakharov. “Violation of CP Invariance, C asymmetry, and baryon asymmetry of the universe”. In: *Pisma Zh. Eksp. Teor. Fiz.* 5 (1967), pp. 32–35. DOI: [10.1070/PU1991v034n05ABEH002497](https://doi.org/10.1070/PU1991v034n05ABEH002497).
- [29] R. N. Mohapatra and A. Y. Smirnov. “Neutrino Mass and New Physics”. In: *Ann. Rev. Nucl. Part. Sci.* 56 (2006). Ed. by K. Anagnostopoulos et al., pp. 569–628. DOI: [10.1146/annurev.nucl.56.080805.140534](https://doi.org/10.1146/annurev.nucl.56.080805.140534). arXiv: [hep-ph/0603118](https://arxiv.org/abs/hep-ph/0603118).
- [30] Fred Jegerlehner. “The hierarchy problem and the cosmological constant problem in the Standard Model”. In: (Mar. 2015). arXiv: [1503.00809 \[hep-ph\]](https://arxiv.org/abs/1503.00809).

- [31] D. P. Aguillard et al. “Measurement of the Positive Muon Anomalous Magnetic Moment to 0.20 ppm”. In: (Aug. 2023). arXiv: [2308.06230 \[hep-ex\]](#).
- [32] D. G. Cerdeño et al. “B anomalies and dark matter: a complex connection”. In: *Eur. Phys. J. C* 79.6 (2019), p. 517. DOI: [10.1140/epjc/s10052-019-6979-x](#). arXiv: [1902.01789 \[hep-ph\]](#).
- [33] Da Huang, António P. Morais, and Rui Santos. “Anomalies in  $B$ -meson decays and the muon  $g - 2$  from dark loops”. In: *Phys. Rev. D* 102.7 (2020), p. 075009. DOI: [10.1103/PhysRevD.102.075009](#). arXiv: [2007.05082 \[hep-ph\]](#).
- [34] Rodrigo Capucha et al. “Impact of electroweak group representation in models for B and  $g - 2$  anomalies from dark loops”. In: *Phys. Rev. D* 106.9 (2022), p. 095032. DOI: [10.1103/PhysRevD.106.095032](#). arXiv: [2207.11556 \[hep-ph\]](#).
- [35] J. H. Field. “Indications for an anomalous right-handed coupling of the b quark from a model independent analysis of LEP and SLD data on Z decays”. In: *Mod. Phys. Lett. A* 13 (1998), pp. 1937–1954. DOI: [10.1142/S0217732398002059](#). arXiv: [hep-ph/9801355](#).
- [36] Howard E. Haber and Heather E. Logan. “Radiative corrections to the Z b anti-b vertex and constraints on extended Higgs sectors”. In: *Phys. Rev. D* 62 (2000), p. 015011. DOI: [10.1103/PhysRevD.62.015011](#). arXiv: [hep-ph/9909335](#).
- [37] Duarte Fontes et al. “One-loop corrections to the  $Zb\bar{b}$  vertex in models with scalar doublets and singlets”. In: *Nucl. Phys. B* 958 (2020), p. 115131. DOI: [10.1016/j.nuclphysb.2020.115131](#). arXiv: [1910.11886 \[hep-ph\]](#).
- [38] C. Itzykson and J. B. Zuber. *Quantum Field Theory*. International Series In Pure and Applied Physics. New York: McGraw-Hill, 1980. ISBN: 978-0-486-44568-7.
- [39] Michael E. Peskin and Daniel V. Schroeder. *An Introduction to quantum field theory*. Reading, USA: Addison-Wesley, 1995. ISBN: 978-0-201-50397-5.
- [40] Steven Weinberg. *The Quantum theory of fields. Vol. 1: Foundations*. Cambridge University Press, June 2005. ISBN: 978-0-521-67053-1. DOI: [10.1017/CB09781139644167](#).
- [41] Matthew D. Schwartz. *Quantum Field Theory and the Standard Model*. Cambridge University Press, Mar. 2014. ISBN: 978-1-107-03473-0.
- [42] Emmy Noether. “Invariant Variation Problems”. In: *Gott. Nachr.* 1918 (1918), pp. 235–257. DOI: [10.1080/00411457108231446](#). arXiv: [physics/0503066](#).
- [43] H. Fritzsch, Murray Gell-Mann, and H. Leutwyler. “Advantages of the Color Octet Gluon Picture”. In: *Phys. Lett. B* 47 (1973), pp. 365–368. DOI: [10.1016/0370-2693\(73\)90625-4](#).
- [44] H. David Politzer. “Reliable Perturbative Results for Strong Interactions?” In: *Phys. Rev. Lett.* 30 (1973). Ed. by J. C. Taylor, pp. 1346–1349. DOI: [10.1103/PhysRevLett.30.1346](#).
- [45] David J. Gross and Frank Wilczek. “Ultraviolet Behavior of Nonabelian Gauge Theories”. In: *Phys. Rev. Lett.* 30 (1973). Ed. by J. C. Taylor, pp. 1343–1346. DOI: [10.1103/PhysRevLett.30.1343](#).

- [46] Steven Weinberg. “Nonabelian Gauge Theories of the Strong Interactions”. In: *Phys. Rev. Lett.* 31 (1973), pp. 494–497. DOI: [10.1103/PhysRevLett.31.494](https://doi.org/10.1103/PhysRevLett.31.494).
- [47] R. L. Workman et al. “Review of Particle Physics”. In: *PTEP* 2022 (2022), p. 083C01. DOI: [10.1093/ptep/ptac097](https://doi.org/10.1093/ptep/ptac097).
- [48] F. Schwabl. *Advanced quantum mechanics (QM II)*. 1997.
- [49] T. Nakano and K. Nishijima. “Charge Independence for V-particles”. In: *Prog. Theor. Phys.* 10 (1953), pp. 581–582. DOI: [10.1143/PTP.10.581](https://doi.org/10.1143/PTP.10.581).
- [50] M. Gell-Mann. “The interpretation of the new particles as displaced charge multiplets”. In: *Nuovo Cim.* 4.S2 (1956), pp. 848–866. DOI: [10.1007/BF02748000](https://doi.org/10.1007/BF02748000).
- [51] Chen-Ning Yang and Robert L. Mills. “Conservation of Isotopic Spin and Isotopic Gauge Invariance”. In: *Phys. Rev.* 96 (1954). Ed. by Jong-Ping Hsu and D. Fine, pp. 191–195. DOI: [10.1103/PhysRev.96.191](https://doi.org/10.1103/PhysRev.96.191).
- [52] Yoichiro Nambu. “Quasiparticles and Gauge Invariance in the Theory of Superconductivity”. In: *Phys. Rev.* 117 (1960). Ed. by J. C. Taylor, pp. 648–663. DOI: [10.1103/PhysRev.117.648](https://doi.org/10.1103/PhysRev.117.648).
- [53] J. Goldstone. “Field Theories with Superconductor Solutions”. In: *Nuovo Cim.* 19 (1961), pp. 154–164. DOI: [10.1007/BF02812722](https://doi.org/10.1007/BF02812722).
- [54] Ta-Pei Cheng and Ling-Fong Li. *Gauge Theory of Elementary Particle Physics*. Oxford, UK: Oxford University Press, 1984. ISBN: 978-0-19-851961-4.
- [55] Nicola Cabibbo. “Unitary Symmetry and Leptonic Decays”. In: *Phys. Rev. Lett.* 10 (1963), pp. 531–533. DOI: [10.1103/PhysRevLett.10.531](https://doi.org/10.1103/PhysRevLett.10.531).
- [56] Makoto Kobayashi and Toshihide Maskawa. “CP Violation in the Renormalizable Theory of Weak Interaction”. In: *Prog. Theor. Phys.* 49 (1973), pp. 652–657. DOI: [10.1143/PTP.49.652](https://doi.org/10.1143/PTP.49.652).
- [57] Ziro Maki, Masami Nakagawa, and Shoichi Sakata. “Remarks on the unified model of elementary particles”. In: *Prog. Theor. Phys.* 28 (1962), pp. 870–880. DOI: [10.1143/PTP.28.870](https://doi.org/10.1143/PTP.28.870).
- [58] Y. Katayama et al. “Possible unified models of elementary particles with two neutrinos”. In: *Prog. Theor. Phys.* 28 (1962), p. 675. DOI: [10.1143/PTP.28.675](https://doi.org/10.1143/PTP.28.675).
- [59] B. Pontecorvo. “Neutrino Experiments and the Problem of Conservation of Leptonic Charge”. In: *Zh. Eksp. Teor. Fiz.* 53 (1967), pp. 1717–1725.
- [60] J. C. Kapteyn. “First Attempt at a Theory of the Arrangement and Motion of the Sidereal System”. In: *Astrophys. J.* 55 (1922), pp. 302–328. DOI: [10.1086/142670](https://doi.org/10.1086/142670).
- [61] J. H. Jeans. “The Motions of Stars in a Kapteyn-Universe”. In: *Monthly Notices of the Royal Astronomical Society* 82.3 (Jan. 1922), pp. 122–132. DOI: [10.1093/mnras/82.3.122](https://doi.org/10.1093/mnras/82.3.122).
- [62] J.H. Oort. “Observational evidence confirming Lindblad’s hypothesis of a rotation of the galactic system”. In: *BAIN* 3 (Apr. 1927), p. 275.
- [63] F. Zwicky. “Die Rotverschiebung von extragalaktischen Nebeln”. In: *Helv. Phys. Acta* 6 (1933), pp. 110–127. DOI: [10.1007/s10714-008-0707-4](https://doi.org/10.1007/s10714-008-0707-4).



- [64] Vera C. Rubin and W. Kent Ford Jr. “Rotation of the Andromeda Nebula from a Spectroscopic Survey of Emission Regions”. In: *Astrophys. J.* 159 (1970), pp. 379–403. doi: [10.1086/150317](https://doi.org/10.1086/150317).
- [65] Vera C. Rubin, W. Kent Ford Jr., and Norbert Thonnard. “Extended rotation curves of high-luminosity spiral galaxies. IV. Systematic dynamical properties, Sa through Sc”. In: *Astrophys. J. Lett.* 225 (1978), pp. L107–L111. doi: [10.1086/182804](https://doi.org/10.1086/182804).
- [66] Steven W. Allen, August E. Evrard, and Adam B. Mantz. “Cosmological Parameters from Observations of Galaxy Clusters”. In: *Ann. Rev. Astron. Astrophys.* 49 (2011), pp. 409–470. doi: [10.1146/annurev-astro-081710-102514](https://doi.org/10.1146/annurev-astro-081710-102514). arXiv: [1103.4829](https://arxiv.org/abs/1103.4829) [astro-ph.CO].
- [67] Douglas Clowe, Anthony Gonzalez, and Maxim Markevitch. “Weak lensing mass reconstruction of the interacting cluster 1E0657-558: Direct evidence for the existence of dark matter”. In: *Astrophys. J.* 604 (2004), pp. 596–603. doi: [10.1086/381970](https://doi.org/10.1086/381970). arXiv: [astro-ph/0312273](https://arxiv.org/abs/astro-ph/0312273).
- [68] Maxim Markevitch et al. “Direct constraints on the dark matter self-interaction cross-section from the merging galaxy cluster 1E0657-56”. In: *Astrophys. J.* 606 (2004), pp. 819–824. doi: [10.1086/383178](https://doi.org/10.1086/383178). arXiv: [astro-ph/0309303](https://arxiv.org/abs/astro-ph/0309303).
- [69] N. Aghanim et al. “Planck 2018 results. VI. Cosmological parameters”. In: *Astron. Astrophys.* 641 (2020). [Erratum: *Astron. Astrophys.* 652, C4 (2021)], A6. doi: [10.1051/0004-6361/201833910](https://doi.org/10.1051/0004-6361/201833910). arXiv: [1807.06209](https://arxiv.org/abs/1807.06209) [astro-ph.CO].
- [70] Patrick Peter and Jean-Philippe Uzan. *Primordial Cosmology*. Oxford Graduate Texts. Oxford University Press, Feb. 2013. ISBN: 978-0-19-966515-0.
- [71] Joshua D. Simon. “The Faintest Dwarf Galaxies”. In: *Ann. Rev. Astron. Astrophys.* 57.1 (2019), pp. 375–415. doi: [10.1146/annurev-astro-091918-104453](https://doi.org/10.1146/annurev-astro-091918-104453). arXiv: [1901.05465](https://arxiv.org/abs/1901.05465) [astro-ph.GA].
- [72] Paolo Salucci. “The distribution of dark matter in galaxies”. In: *Astron. Astrophys. Rev.* 27.1 (2019), p. 2. doi: [10.1007/s00159-018-0113-1](https://doi.org/10.1007/s00159-018-0113-1). arXiv: [1811.08843](https://arxiv.org/abs/1811.08843) [astro-ph.GA].
- [73] Benoit Famaey and Stacy McGaugh. “Modified Newtonian Dynamics (MOND): Observational Phenomenology and Relativistic Extensions”. In: *Living Rev. Rel.* 15 (2012), p. 10. doi: [10.12942/lrr-2012-10](https://doi.org/10.12942/lrr-2012-10). arXiv: [1112.3960](https://arxiv.org/abs/1112.3960) [astro-ph.CO].
- [74] Scott W. Randall et al. “Constraints on the Self-Interaction Cross-Section of Dark Matter from Numerical Simulations of the Merging Galaxy Cluster 1E 0657-56”. In: *Astrophys. J.* 679 (2008), pp. 1173–1180. doi: [10.1086/587859](https://doi.org/10.1086/587859). arXiv: [0704.0261](https://arxiv.org/abs/0704.0261) [astro-ph].
- [75] Douglas Clowe et al. “A direct empirical proof of the existence of dark matter”. In: *Astrophys. J. Lett.* 648 (2006), pp. L109–L113. doi: [10.1086/508162](https://doi.org/10.1086/508162). arXiv: [astro-ph/0608407](https://arxiv.org/abs/astro-ph/0608407).
- [76] R. D. Peccei and Helen R. Quinn. “Constraints Imposed by CP Conservation in the Presence of Instantons”. In: *Phys. Rev. D* 16 (1977), pp. 1791–1797. doi: [10.1103/PhysRevD.16.1791](https://doi.org/10.1103/PhysRevD.16.1791).
- [77] Frank Wilczek. “Problem of Strong  $P$  and  $T$  Invariance in the Presence of Instantons”. In: *Phys. Rev. Lett.* 40 (1978), pp. 279–282. doi: [10.1103/PhysRevLett.40.279](https://doi.org/10.1103/PhysRevLett.40.279).

- [78] C. Alcock et al. “The MACHO project: Microlensing results from 5.7 years of LMC observations”. In: *Astrophys. J.* 542 (2000), pp. 281–307. DOI: [10.1086/309512](https://doi.org/10.1086/309512). arXiv: [astro-ph/0001272](https://arxiv.org/abs/astro-ph/0001272).
- [79] Gianfranco Bertone, Dan Hooper, and Joseph Silk. “Particle dark matter: Evidence, candidates and constraints”. In: *Phys. Rept.* 405 (2005), pp. 279–390. DOI: [10.1016/j.physrep.2004.08.031](https://doi.org/10.1016/j.physrep.2004.08.031). arXiv: [hep-ph/0404175](https://arxiv.org/abs/hep-ph/0404175).
- [80] W. B. Lin et al. “Nonthermal production of WIMPs and the subgalactic structure of the universe”. In: *Phys. Rev. Lett.* 86 (2001), p. 954. DOI: [10.1103/PhysRevLett.86.954](https://doi.org/10.1103/PhysRevLett.86.954). arXiv: [astro-ph/0009003](https://arxiv.org/abs/astro-ph/0009003).
- [81] Graciela B. Gelmini and Paolo Gondolo. “Neutralino with the right cold dark matter abundance in (almost) any supersymmetric model”. In: *Phys. Rev. D* 74 (2006), p. 023510. DOI: [10.1103/PhysRevD.74.023510](https://doi.org/10.1103/PhysRevD.74.023510). arXiv: [hep-ph/0602230](https://arxiv.org/abs/hep-ph/0602230).
- [82] Lisa Randall, Jakub Scholtz, and James Unwin. “Cores in Dwarf Galaxies from Fermi Repulsion”. In: *Mon. Not. Roy. Astron. Soc.* 467.2 (2017), pp. 1515–1525. DOI: [10.1093/mnras/stx161](https://doi.org/10.1093/mnras/stx161). arXiv: [1611.04590](https://arxiv.org/abs/1611.04590) [[astro-ph.GA](https://arxiv.org/abs/astro-ph.GA)].
- [83] Renée Hlozek et al. “A search for ultralight axions using precision cosmological data”. In: *Phys. Rev. D* 91.10 (2015), p. 103512. DOI: [10.1103/PhysRevD.91.103512](https://doi.org/10.1103/PhysRevD.91.103512). arXiv: [1410.2896](https://arxiv.org/abs/1410.2896) [[astro-ph.CO](https://arxiv.org/abs/astro-ph.CO)].
- [84] Matteo Nori et al. “Lyman  $\alpha$  forest and non-linear structure characterization in Fuzzy Dark Matter cosmologies”. In: *Mon. Not. Roy. Astron. Soc.* 482.3 (2019), pp. 3227–3243. DOI: [10.1093/mnras/sty2888](https://doi.org/10.1093/mnras/sty2888). arXiv: [1809.09619](https://arxiv.org/abs/1809.09619) [[astro-ph.CO](https://arxiv.org/abs/astro-ph.CO)].
- [85] Ethan O. Nadler et al. “Constraints on Dark Matter Microphysics from the Milky Way Satellite Population”. In: *Astrophys. J. Lett.* 878.2 (2019). [Erratum: *Astrophys.J.Lett.* 897, L46 (2020), Erratum: *Astrophys.J.* 897, L46 (2020)], p. 32. DOI: [10.3847/2041-8213/ab1eb2](https://doi.org/10.3847/2041-8213/ab1eb2). arXiv: [1904.10000](https://arxiv.org/abs/1904.10000) [[astro-ph.CO](https://arxiv.org/abs/astro-ph.CO)].
- [86] Miguel A. Monroy-Rodríguez and Christine Allen. “The end of the MACHO era- revisited: new limits on MACHO masses from halo wide binaries”. In: *Astrophys. J.* 790.2 (2014), p. 159. DOI: [10.1088/0004-637X/790/2/159](https://doi.org/10.1088/0004-637X/790/2/159). arXiv: [1406.5169](https://arxiv.org/abs/1406.5169) [[astro-ph.GA](https://arxiv.org/abs/astro-ph.GA)].
- [87] Samuel D. McDermott, Hai-Bo Yu, and Kathryn M. Zurek. “Turning off the Lights: How Dark is Dark Matter?” In: *Phys. Rev. D* 83 (2011), p. 063509. DOI: [10.1103/PhysRevD.83.063509](https://doi.org/10.1103/PhysRevD.83.063509). arXiv: [1011.2907](https://arxiv.org/abs/1011.2907) [[hep-ph](https://arxiv.org/abs/hep-ph)].
- [88] David Harvey et al. “The non-gravitational interactions of dark matter in colliding galaxy clusters”. In: *Science* 347 (2015), pp. 1462–1465. DOI: [10.1126/science.1261381](https://doi.org/10.1126/science.1261381). arXiv: [1503.07675](https://arxiv.org/abs/1503.07675) [[astro-ph.CO](https://arxiv.org/abs/astro-ph.CO)].
- [89] Benjamin Audren et al. “Strongest model-independent bound on the lifetime of Dark Matter”. In: *JCAP* 12 (2014), p. 028. DOI: [10.1088/1475-7516/2014/12/028](https://doi.org/10.1088/1475-7516/2014/12/028). arXiv: [1407.2418](https://arxiv.org/abs/1407.2418) [[astro-ph.CO](https://arxiv.org/abs/astro-ph.CO)].

- [90] James D. Bjorken and Sidney D. Drell. *Relativistic Quantum Mechanics*. International Series In Pure and Applied Physics. New York: McGraw-Hill, 1965. ISBN: 978-0-07-005493-6.
- [91] John David Jackson. *Classical Electrodynamics*. Wiley, 1998. ISBN: 978-0-471-30932-1.
- [92] Friedrich Jegerlehner. *The Anomalous Magnetic Moment of the Muon*. Vol. 274. Cham: Springer, 2017. DOI: [10.1007/978-3-319-63577-4](https://doi.org/10.1007/978-3-319-63577-4).
- [93] T. Aoyama et al. “The anomalous magnetic moment of the muon in the Standard Model”. In: *Phys. Rept.* 887 (2020), pp. 1–166. DOI: [10.1016/j.physrep.2020.07.006](https://doi.org/10.1016/j.physrep.2020.07.006). arXiv: [2006.04822 \[hep-ph\]](https://arxiv.org/abs/2006.04822).
- [94] J. Bailey et al. “Final Report on the CERN Muon Storage Ring Including the Anomalous Magnetic Moment and the Electric Dipole Moment of the Muon, and a Direct Test of Relativistic Time Dilation”. In: *Nucl. Phys. B* 150 (1979), pp. 1–75. DOI: [10.1016/0550-3213\(79\)90292-X](https://doi.org/10.1016/0550-3213(79)90292-X).
- [95] G. W. Bennett et al. “Final Report of the Muon E821 Anomalous Magnetic Moment Measurement at BNL”. In: *Phys. Rev. D* 73 (2006), p. 072003. DOI: [10.1103/PhysRevD.73.072003](https://doi.org/10.1103/PhysRevD.73.072003). arXiv: [hep-ex/0602035](https://arxiv.org/abs/hep-ex/0602035).
- [96] B. Abi et al. “Measurement of the Positive Muon Anomalous Magnetic Moment to 0.46 ppm”. In: *Phys. Rev. Lett.* 126.14 (2021), p. 141801. DOI: [10.1103/PhysRevLett.126.141801](https://doi.org/10.1103/PhysRevLett.126.141801). arXiv: [2104.03281 \[hep-ex\]](https://arxiv.org/abs/2104.03281).
- [97] Sz. Borsanyi et al. “Leading hadronic contribution to the muon magnetic moment from lattice QCD”. In: *Nature* 593.7857 (2021), pp. 51–55. DOI: [10.1038/s41586-021-03418-1](https://doi.org/10.1038/s41586-021-03418-1). arXiv: [2002.12347 \[hep-lat\]](https://arxiv.org/abs/2002.12347).
- [98] F. V. Ignatov et al. “Measurement of the  $e^+e^- \rightarrow \pi^+\pi^-$  cross section from threshold to 1.2 GeV with the CMD-3 detector”. In: (Feb. 2023). arXiv: [2302.08834 \[hep-ex\]](https://arxiv.org/abs/2302.08834).
- [99] “LEP Design Report Vol.1: The LEP Injector Chain”. In: (June 1983).
- [100] “LEP Design Report: Vol.2. The LEP Main Ring”. In: (June 1984).
- [101] “SLAC Linear Collider Conceptual Design Report”. In: (June 1980).
- [102] D. Decamp et al. “ALEPH: A detector for electron-positron annihilations at LEP”. In: *Nucl. Instrum. Meth. A* 294 (1990). [Erratum: *Nucl.Instrum.Meth.A* 303, 393 (1991)], pp. 121–178. DOI: [10.1016/0168-9002\(90\)91831-U](https://doi.org/10.1016/0168-9002(90)91831-U).
- [103] D. Buskulic et al. “Performance of the ALEPH detector at LEP”. In: *Nucl. Instrum. Meth. A* 360 (1995), pp. 481–506. DOI: [10.1016/0168-9002\(95\)00138-7](https://doi.org/10.1016/0168-9002(95)00138-7).
- [104] P. A. Aarnio et al. “The DELPHI detector at LEP”. In: *Nucl. Instrum. Meth. A* 303 (1991), pp. 233–276. DOI: [10.1016/0168-9002\(91\)90793-P](https://doi.org/10.1016/0168-9002(91)90793-P).
- [105] P. Abreu et al. “Performance of the DELPHI detector”. In: *Nucl. Instrum. Meth. A* 378 (1996), pp. 57–100. DOI: [10.1016/0168-9002\(96\)00463-9](https://doi.org/10.1016/0168-9002(96)00463-9).
- [106] B. Adeva et al. “The Construction of the L3 Experiment”. In: *Nucl. Instrum. Meth. A* 289 (1990), pp. 35–102. DOI: [10.1016/0168-9002\(90\)90250-A](https://doi.org/10.1016/0168-9002(90)90250-A).

- [107] M. Acciarri et al. “The L3 silicon microvertex detector”. In: *Nucl. Instrum. Meth. A* 351 (1994), pp. 300–312. DOI: [10.1016/0168-9002\(94\)91357-9](https://doi.org/10.1016/0168-9002(94)91357-9).
- [108] M. Chemarin et al. “Test beam results for an upgraded forward tagger of the L3 Experiment at LEP-2”. In: *Nucl. Instrum. Meth. A* 349 (1994), pp. 345–355. DOI: [10.1016/0168-9002\(94\)91198-3](https://doi.org/10.1016/0168-9002(94)91198-3).
- [109] A. Adam et al. “The Forward muon detector of L3”. In: *Nucl. Instrum. Meth. A* 383 (1996), pp. 342–366. DOI: [10.1016/S0168-9002\(96\)00777-2](https://doi.org/10.1016/S0168-9002(96)00777-2).
- [110] K. Ahmet et al. “The OPAL detector at LEP”. In: *Nucl. Instrum. Meth. A* 305 (1991), pp. 275–319. DOI: [10.1016/0168-9002\(91\)90547-4](https://doi.org/10.1016/0168-9002(91)90547-4).
- [111] P. P. Allport et al. “The OPAL silicon microvertex detector”. In: *Nucl. Instrum. Meth. A* 324 (1993), pp. 34–52. DOI: [10.1016/0168-9002\(93\)90964-J](https://doi.org/10.1016/0168-9002(93)90964-J).
- [112] P. P. Allport et al. “The OPAL silicon strip microvertex detector with two coordinate readout”. In: *Nucl. Instrum. Meth. A* 346 (1994), pp. 476–495. DOI: [10.1016/0168-9002\(94\)90583-5](https://doi.org/10.1016/0168-9002(94)90583-5).
- [113] B. E. Anderson et al. “The OPAL silicon - tungsten calorimeter front end electronics”. In: *IEEE Trans. Nucl. Sci.* 41 (1994), pp. 845–852. DOI: [10.1109/23.322818](https://doi.org/10.1109/23.322818).
- [114] M. J. Fero et al. “Performance of the SLD central drift chamber”. In: *Nucl. Instrum. Meth. A* 367 (1995). Ed. by W. Bartl et al., pp. 111–114. DOI: [10.1016/0168-9002\(95\)00732-6](https://doi.org/10.1016/0168-9002(95)00732-6).
- [115] D. Axen et al. “The Lead liquid argon sampling calorimeter of the SLD detector”. In: *Nucl. Instrum. Meth. A* 328 (1993), pp. 472–494. DOI: [10.1016/0168-9002\(93\)90664-4](https://doi.org/10.1016/0168-9002(93)90664-4).
- [116] K. Abe et al. “Performance of the CRID at SLD”. In: *Nucl. Instrum. Meth. A* 343 (1994). Ed. by E. Nappi and T. Ypsilantis, pp. 74–86. DOI: [10.1016/0168-9002\(94\)90536-3](https://doi.org/10.1016/0168-9002(94)90536-3).
- [117] S. C. Berridge et al. “First results from the SLD silicon calorimeters”. In: *IEEE Trans. Nucl. Sci.* 39 (1992). Ed. by G. T. Baldwin, pp. 1242–1248. DOI: [10.1109/23.173184](https://doi.org/10.1109/23.173184).
- [118] K. Abe et al. “Design and performance of the SLD vertex detector, a 307 Mpixel tracking system”. In: *Nucl. Instrum. Meth. A* 400 (1997), pp. 287–343. DOI: [10.1016/S0168-9002\(97\)01011-5](https://doi.org/10.1016/S0168-9002(97)01011-5).
- [119] A. C. Benvenuti et al. “The Iron Calorimeter and Muon Identifier for Sld”. In: *Nucl. Instrum. Meth. A* 276 (1989), p. 94. DOI: [10.1016/0168-9002\(89\)90620-7](https://doi.org/10.1016/0168-9002(89)90620-7).
- [120] P. Langacker, ed. *Precision tests of the standard electroweak model*. Singapore: WSP, 1996. DOI: [10.1142/1927](https://doi.org/10.1142/1927).
- [121] Sabine Riemann. “Precision electroweak physics at high energies”. In: *Rept. Prog. Phys.* 73 (2010), p. 126201. DOI: [10.1088/0034-4885/73/12/126201](https://doi.org/10.1088/0034-4885/73/12/126201).
- [122] S. Schael et al. “Precision electroweak measurements on the Z resonance”. In: *Phys. Rept.* 427 (2006), pp. 257–454. DOI: [10.1016/j.physrep.2005.12.006](https://doi.org/10.1016/j.physrep.2005.12.006). arXiv: [hep-ex/0509008](https://arxiv.org/abs/hep-ex/0509008).
- [123] Kenji Abe et al. “A High precision measurement of the left-right Z boson cross-section asymmetry”. In: *Phys. Rev. Lett.* 84 (2000), pp. 5945–5949. DOI: [10.1103/PhysRevLett.84.5945](https://doi.org/10.1103/PhysRevLett.84.5945). arXiv: [hep-ex/0004026](https://arxiv.org/abs/hep-ex/0004026).

- [124] Koya Abe et al. “An Improved direct measurement of leptonic coupling asymmetries with polarized Z bosons”. In: *Phys. Rev. Lett.* 86 (2001), pp. 1162–1166. DOI: [10.1103/PhysRevLett.86.1162](https://doi.org/10.1103/PhysRevLett.86.1162). arXiv: [hep-ex/0010015](https://arxiv.org/abs/hep-ex/0010015).
- [125] Koya Abe et al. “First direct measurement of the parity violating coupling of the Z0 to the s quark”. In: *Phys. Rev. Lett.* 85 (2000), pp. 5059–5063. DOI: [10.1103/PhysRevLett.85.5059](https://doi.org/10.1103/PhysRevLett.85.5059). arXiv: [hep-ex/0006019](https://arxiv.org/abs/hep-ex/0006019).
- [126] K. Abe et al. “First measurement of the left-right charge asymmetry in hadronic Z boson decays and a new determination of  $\sin^2 \theta(W)(\text{eff})$ ”. In: *Phys. Rev. Lett.* 78 (1997), pp. 17–21. DOI: [10.1103/PhysRevLett.78.17](https://doi.org/10.1103/PhysRevLett.78.17). arXiv: [hep-ex/9609019](https://arxiv.org/abs/hep-ex/9609019).
- [127] “Reports of the working group on precision calculations for the Z resonance”. In: *Workshop Group on Precision Calculations for the Z Resonance (2nd meeting held Mar 31, 3rd meeting held Jun 13)*. CERN Yellow Reports: Monographs. Mar. 1995. DOI: [10.5170/CERN-1995-003](https://doi.org/10.5170/CERN-1995-003).
- [128] W. F. L. Hollik. “Radiative Corrections in the Standard Model and their Role for Precision Tests of the Electroweak Theory”. In: *Fortsch. Phys.* 38 (1990), pp. 165–260. DOI: [10.1002/prop.2190380302](https://doi.org/10.1002/prop.2190380302).
- [129] G. Altarelli, R. Kleiss, and C. Verzegnassi, eds. *Z PHYSICS AT LEP-1. PROCEEDINGS, WORKSHOP, GENEVA, SWITZERLAND, SEPTEMBER 4-5, 1989. VOL. 1: STANDARD PHYSICS*. CERN Yellow Reports: Conference Proceedings. Sept. 1989. DOI: [10.5170/CERN-1989-008-V-1](https://doi.org/10.5170/CERN-1989-008-V-1).
- [130] Mark Thomson. *Modern particle physics*. New York: Cambridge University Press, 2013. ISBN: 978-1-107-03426-6. DOI: [10.1017/CB09781139525367](https://doi.org/10.1017/CB09781139525367).
- [131] Wilhelmus Johannes Petrus Beenakker. “Electroweak corrections: Techniques and applications”. PhD thesis. Leiden, NL: University of Leiden, Oct. 1989.
- [132] G. Breit and E. Wigner. “Capture of Slow Neutrons”. In: *Phys. Rev.* 49 (1936), pp. 519–531. DOI: [10.1103/PhysRev.49.519](https://doi.org/10.1103/PhysRev.49.519).
- [133] Wolfgang Hollik. “Renormalization of the Standard Model”. In: *Adv. Ser. Direct. High Energy Phys.* 14 (1995), pp. 37–116. DOI: [10.1142/9789814503662\\_0003](https://doi.org/10.1142/9789814503662_0003).
- [134] M. Bohm, H. Spiesberger, and W. Hollik. “On the One Loop Renormalization of the Electroweak Standard Model and Its Application to Leptonic Processes”. In: *Fortsch. Phys.* 34 (1986), pp. 687–751. DOI: [10.1002/prop.19860341102](https://doi.org/10.1002/prop.19860341102).
- [135] John C. Collins. *Renormalization: An Introduction to Renormalization, The Renormalization Group, and the Operator Product Expansion*. Vol. 26. Cambridge Monographs on Mathematical Physics. Cambridge: Cambridge University Press, 1986. ISBN: 978-0-521-31177-9. DOI: [10.1017/CB09780511622656](https://doi.org/10.1017/CB09780511622656).
- [136] Kenneth G. Wilson. “Confinement of Quarks”. In: *Phys. Rev. D* 10 (1974). Ed. by J. C. Taylor, pp. 2445–2459. DOI: [10.1103/PhysRevD.10.2445](https://doi.org/10.1103/PhysRevD.10.2445).

- [137] W. Pauli and F. Villars. “On the Invariant regularization in relativistic quantum theory”. In: *Rev. Mod. Phys.* 21 (1949), pp. 434–444. DOI: [10.1103/RevModPhys.21.434](https://doi.org/10.1103/RevModPhys.21.434).
- [138] C. G. Bollini, J. J. Giambiagi, and A. González Domínguez. “Analytic regularization and the divergences of quantum field theories”. In: *Il Nuovo Cimento (1955-1965)* 31.3 (Feb. 1964), pp. 550–561. ISSN: 1827-6121. DOI: [10.1007/BF02733756](https://doi.org/10.1007/BF02733756). URL: <https://doi.org/10.1007/BF02733756>.
- [139] C. G. Bollini and J. J. Giambiagi. “Dimensional Renormalization: The Number of Dimensions as a Regularizing Parameter”. In: *Nuovo Cim. B* 12 (1972), pp. 20–26. DOI: [10.1007/BF02895558](https://doi.org/10.1007/BF02895558).
- [140] P. Breitenlohner and D. Maison. “Dimensionally Renormalized Green’s Functions for Theories with Massless Particles. 2.” In: *Commun. Math. Phys.* 52 (1977), p. 55. DOI: [10.1007/BF01609071](https://doi.org/10.1007/BF01609071).
- [141] Dirk Kreimer. “The Role of  $\gamma(5)$  in dimensional regularization”. In: (Dec. 1993). arXiv: [hep-ph/9401354](https://arxiv.org/abs/hep-ph/9401354).
- [142] S. A. Larin. “The Renormalization of the axial anomaly in dimensional regularization”. In: *Phys. Lett. B* 303 (1993), pp. 113–118. DOI: [10.1016/0370-2693\(93\)90053-K](https://doi.org/10.1016/0370-2693(93)90053-K). arXiv: [hep-ph/9302240](https://arxiv.org/abs/hep-ph/9302240).
- [143] G. Passarino and M. J. G. Veltman. “One Loop Corrections for  $e^+e^-$  Annihilation Into  $\mu^+\mu^-$  in the Weinberg Model”. In: *Nucl. Phys. B* 160 (1979), pp. 151–207. DOI: [10.1016/0550-3213\(79\)90234-7](https://doi.org/10.1016/0550-3213(79)90234-7).
- [144] Gerard ’t Hooft. “Dimensional regularization and the renormalization group”. In: *Nucl. Phys. B* 61 (1973), pp. 455–468. DOI: [10.1016/0550-3213\(73\)90376-3](https://doi.org/10.1016/0550-3213(73)90376-3).
- [145] Steven Weinberg. “New approach to the renormalization group”. In: *Phys. Rev. D* 8 (1973), pp. 3497–3509. DOI: [10.1103/PhysRevD.8.3497](https://doi.org/10.1103/PhysRevD.8.3497).
- [146] William J. Marciano. “The Weak Mixing Angle and Grand Unified Gauge Theories”. In: *Phys. Rev. D* 20 (1979), p. 274. DOI: [10.1103/PhysRevD.20.274](https://doi.org/10.1103/PhysRevD.20.274).
- [147] G. Passarino and M. J. G. Veltman. “On the Definition of the Weak Mixing Angle”. In: *Phys. Lett. B* 237 (1990), pp. 537–544. DOI: [10.1016/0370-2693\(90\)91221-V](https://doi.org/10.1016/0370-2693(90)91221-V).
- [148] Francesco Antonelli, Maurizio Consoli, and Guido Corbo. “One Loop Correction to Vector Boson Masses in the Glashow-Weinberg-Salam Model of Electromagnetic and Weak Interactions”. In: *Phys. Lett. B* 91 (1980), pp. 90–94. DOI: [10.1016/0370-2693\(80\)90668-1](https://doi.org/10.1016/0370-2693(80)90668-1).
- [149] J. Fleischer and F. Jegerlehner. “Radiative Corrections to Higgs Decays in the Extended Weinberg-Salam Model”. In: *Phys. Rev. D* 23 (1981), pp. 2001–2026. DOI: [10.1103/PhysRevD.23.2001](https://doi.org/10.1103/PhysRevD.23.2001).
- [150] K. I. Aoki et al. “Electroweak Theory. Framework of On-Shell Renormalization and Study of Higher Order Effects”. In: *Prog. Theor. Phys. Suppl.* 73 (1982), pp. 1–225. DOI: [10.1143/PTPS.73.1](https://doi.org/10.1143/PTPS.73.1).



- [151] A. A. Slavnov. “Ward Identities in Gauge Theories”. In: *Theor. Math. Phys.* 10 (1972), pp. 99–107. DOI: [10.1007/BF01090719](https://doi.org/10.1007/BF01090719).
- [152] J. C. Taylor. “Ward Identities and Charge Renormalization of the Yang-Mills Field”. In: *Nucl. Phys. B* 33 (1971), pp. 436–444. DOI: [10.1016/0550-3213\(71\)90297-5](https://doi.org/10.1016/0550-3213(71)90297-5).
- [153] Toichiro Kinoshita and Alberto Sirlin. “Radiative corrections to Fermi interactions”. In: *Phys. Rev.* 113 (1959), pp. 1652–1660. DOI: [10.1103/PhysRev.113.1652](https://doi.org/10.1103/PhysRev.113.1652).
- [154] T. Kinoshita. “Mass singularities of Feynman amplitudes”. In: *J. Math. Phys.* 3 (1962), pp. 650–677. DOI: [10.1063/1.1724268](https://doi.org/10.1063/1.1724268).
- [155] T. D. Lee and M. Nauenberg. “Degenerate Systems and Mass Singularities”. In: *Phys. Rev.* 133 (1964). Ed. by G. Feinberg, B1549–B1562. DOI: [10.1103/PhysRev.133.B1549](https://doi.org/10.1103/PhysRev.133.B1549).
- [156] F. Bloch and A. Nordsieck. “Note on the Radiation Field of the electron”. In: *Phys. Rev.* 52 (1937), pp. 54–59. DOI: [10.1103/PhysRev.52.54](https://doi.org/10.1103/PhysRev.52.54).
- [157] O. M. Fedorenko and T. Riemann. “Analytic Bremsstrahlung Integraton for the Process  $e^+e^- \rightarrow \mu^+\mu^-\gamma$  in QED”. In: *Acta Phys. Polon. B* 18 (1987), p. 761.
- [158] D. C. Kennedy et al. “Electroweak Cross-Sections and Asymmetries at the  $Z^0$ ”. In: *Nucl. Phys. B* 321 (1989), pp. 83–107. DOI: [10.1016/0550-3213\(89\)90243-5](https://doi.org/10.1016/0550-3213(89)90243-5).
- [159] David Albert et al. “Decays of Intermediate Vector Bosons, Radiative Corrections and QCD Jets”. In: *Nucl. Phys. B* 166 (1980), pp. 460–492. DOI: [10.1016/0550-3213\(80\)90208-4](https://doi.org/10.1016/0550-3213(80)90208-4).
- [160] Dmitri Yu. Bardin et al. “The Convolution Integral for the Forward - Backward Asymmetry in  $e^+e^-$  Annihilation”. In: *Phys. Lett. B* 229 (1989), pp. 405–408. DOI: [10.1016/0370-2693\(89\)90428-0](https://doi.org/10.1016/0370-2693(89)90428-0).
- [161] Frits A. Berends, G. J. H. Burgers, and W. L. van Neerven. “On Second Order QED Corrections to the  $Z$  Resonance Shape”. In: *Phys. Lett. B* 185 (1987), p. 395. DOI: [10.1016/0370-2693\(87\)91022-7](https://doi.org/10.1016/0370-2693(87)91022-7).
- [162] O. Nicrosini and L. Trentadue. “SECOND ORDER ELECTROMAGNETIC RADIATIVE CORRECTIONS TO  $e^+e^- \rightarrow \gamma^*, Z^0 \rightarrow \mu^+\mu^-$ ”. In: *Z. Phys. C* 39 (1988), p. 479. DOI: [10.1007/BF01555976](https://doi.org/10.1007/BF01555976).
- [163] Walter Gordon. “Der Comptoneffekt nach der Schrödingerschen Theorie”. In: *Zeitschrift für Physik* 40 (), pp. 117–133. URL: <https://api.semanticscholar.org/CorpusID:122254400>.
- [164] W. Hollik. “NEW PHYSICS FROM PRECISION MEASUREMENTS”. In: *Workshop on Polarization at LEP*. Aug. 1988.
- [165] Michael E. Peskin and Tatsu Takeuchi. “Estimation of oblique electroweak corrections”. In: *Phys. Rev. D* 46 (1992), pp. 381–409. DOI: [10.1103/PhysRevD.46.381](https://doi.org/10.1103/PhysRevD.46.381).
- [166] Aaron K. Grant and Tatsu Takeuchi. “An Analysis of precision electroweak measurements: Summer 1998 update”. In: (July 1998). arXiv: [hep-ph/9807413](https://arxiv.org/abs/hep-ph/9807413).

- [167] Roel Aaij et al. “Test of lepton universality using  $B^+ \rightarrow K^+ \ell^+ \ell^-$  decays”. In: *Phys. Rev. Lett.* 113 (2014), p. 151601. doi: [10.1103/PhysRevLett.113.151601](https://doi.org/10.1103/PhysRevLett.113.151601). arXiv: [1406.6482](https://arxiv.org/abs/1406.6482) [hep-ex].
- [168] Roel Aaij et al. “Search for lepton-universality violation in  $B^+ \rightarrow K^+ \ell^+ \ell^-$  decays”. In: *Phys. Rev. Lett.* 122.19 (2019), p. 191801. doi: [10.1103/PhysRevLett.122.191801](https://doi.org/10.1103/PhysRevLett.122.191801). arXiv: [1903.09252](https://arxiv.org/abs/1903.09252) [hep-ex].
- [169] Ben Gripaios, M. Nardecchia, and S. A. Renner. “Linear flavour violation and anomalies in B physics”. In: *JHEP* 06 (2016), p. 083. doi: [10.1007/JHEP06\(2016\)083](https://doi.org/10.1007/JHEP06(2016)083). arXiv: [1509.05020](https://arxiv.org/abs/1509.05020) [hep-ph].
- [170] P. Achard et al. “Search for heavy neutral and charged leptons in  $e^+e^-$  annihilation at LEP”. In: *Phys. Lett. B* 517 (2001), pp. 75–85. doi: [10.1016/S0370-2693\(01\)01005-X](https://doi.org/10.1016/S0370-2693(01)01005-X). arXiv: [hep-ex/0107015](https://arxiv.org/abs/hep-ex/0107015).
- [171] Albert M Sirunyan et al. “Search for low mass vector resonances decaying into quark-antiquark pairs in proton-proton collisions at  $\sqrt{s} = 13$  TeV”. In: *Phys. Rev. D* 100.11 (2019), p. 112007. doi: [10.1103/PhysRevD.100.112007](https://doi.org/10.1103/PhysRevD.100.112007). arXiv: [1909.04114](https://arxiv.org/abs/1909.04114) [hep-ex].
- [172] Stefan Bißmann et al. “Multi-lepton signatures of vector-like leptons with flavor”. In: *Eur. Phys. J. C* 81.2 (2021), p. 101. doi: [10.1140/epjc/s10052-021-08886-3](https://doi.org/10.1140/epjc/s10052-021-08886-3). arXiv: [2011.12964](https://arxiv.org/abs/2011.12964) [hep-ph].
- [173] Morad Aaboud et al. “Search for dark matter produced in association with bottom or top quarks in  $\sqrt{s} = 13$  TeV pp collisions with the ATLAS detector”. In: *Eur. Phys. J. C* 78.1 (2018), p. 18. doi: [10.1140/epjc/s10052-017-5486-1](https://doi.org/10.1140/epjc/s10052-017-5486-1). arXiv: [1710.11412](https://arxiv.org/abs/1710.11412) [hep-ex].
- [174] Pere Arnau et al. “Loop effects of heavy new scalars and fermions in  $b \rightarrow s \mu^+ \mu^-$ ”. In: *JHEP* 04 (2017), p. 043. doi: [10.1007/JHEP04\(2017\)043](https://doi.org/10.1007/JHEP04(2017)043). arXiv: [1608.07832](https://arxiv.org/abs/1608.07832) [hep-ph].
- [175] James M. Cline et al. “Update on scalar singlet dark matter”. In: *Phys. Rev. D* 88 (2013). [Erratum: *Phys.Rev.D* 92, 039906 (2015)], p. 055025. doi: [10.1103/PhysRevD.88.055025](https://doi.org/10.1103/PhysRevD.88.055025). arXiv: [1306.4710](https://arxiv.org/abs/1306.4710) [hep-ph].
- [176] J. M. Alarcon, J. Martin Camalich, and J. A. Oller. “The chiral representation of the  $\pi N$  scattering amplitude and the pion-nucleon sigma term”. In: *Phys. Rev. D* 85 (2012), p. 051503. doi: [10.1103/PhysRevD.85.051503](https://doi.org/10.1103/PhysRevD.85.051503). arXiv: [1110.3797](https://arxiv.org/abs/1110.3797) [hep-ph].
- [177] Xiu-Lei Ren, Xi-Zhe Ling, and Li-Sheng Geng. “Pion–nucleon sigma term revisited in covariant baryon chiral perturbation theory”. In: *Phys. Lett. B* 783 (2018), pp. 7–12. doi: [10.1016/j.physletb.2018.05.063](https://doi.org/10.1016/j.physletb.2018.05.063). arXiv: [1710.07164](https://arxiv.org/abs/1710.07164) [hep-ph].
- [178] J. Aalbers et al. “First Dark Matter Search Results from the LUX-ZEPLIN (LZ) Experiment”. In: *Phys. Rev. Lett.* 131.4 (2023), p. 041002. doi: [10.1103/PhysRevLett.131.041002](https://doi.org/10.1103/PhysRevLett.131.041002). arXiv: [2207.03764](https://arxiv.org/abs/2207.03764) [hep-ex].
- [179] Gudrun Hiller and Frank Kruger. “More model-independent analysis of  $b \rightarrow s$  processes”. In: *Phys. Rev. D* 69 (2004), p. 074020. doi: [10.1103/PhysRevD.69.074020](https://doi.org/10.1103/PhysRevD.69.074020). arXiv: [hep-ph/0310219](https://arxiv.org/abs/hep-ph/0310219).



- [180] Marzia Bordone, Gino Isidori, and Andrea Pattori. “On the Standard Model predictions for  $R_K$  and  $R_{K^*}$ ”. In: *Eur. Phys. J. C* 76.8 (2016), p. 440. DOI: [10.1140/epjc/s10052-016-4274-7](https://doi.org/10.1140/epjc/s10052-016-4274-7). arXiv: [1605.07633](https://arxiv.org/abs/1605.07633) [hep-ph].
- [181] R. Aaij et al. “First observation of the decay  $B_s^0 \rightarrow K^- \mu^+ \nu_\mu$  and Measurement of  $|V_{ub}|/|V_{cb}|$ ”. In: *Phys. Rev. Lett.* 126.8 (2021), p. 081804. DOI: [10.1103/PhysRevLett.126.081804](https://doi.org/10.1103/PhysRevLett.126.081804). arXiv: [2012.05143](https://arxiv.org/abs/2012.05143) [hep-ex].
- [182] T. Aaltonen et al. “Measurements of the Angular Distributions in the Decays  $B \rightarrow K^{(*)} \mu^+ \mu^-$  at CDF”. In: *Phys. Rev. Lett.* 108 (2012), p. 081807. DOI: [10.1103/PhysRevLett.108.081807](https://doi.org/10.1103/PhysRevLett.108.081807). arXiv: [1108.0695](https://arxiv.org/abs/1108.0695) [hep-ex].
- [183] Vardan Khachatryan et al. “Angular analysis of the decay  $B^0 \rightarrow K^{*0} \mu^+ \mu^-$  from pp collisions at  $\sqrt{s} = 8$  TeV”. In: *Phys. Lett. B* 753 (2016), pp. 424–448. DOI: [10.1016/j.physletb.2015.12.020](https://doi.org/10.1016/j.physletb.2015.12.020). arXiv: [1507.08126](https://arxiv.org/abs/1507.08126) [hep-ex].
- [184] Albert M Sirunyan et al. “Measurement of angular parameters from the decay  $B^0 \rightarrow K^{*0} \mu^+ \mu^-$  in proton-proton collisions at  $\sqrt{s} = 8$  TeV”. In: *Phys. Lett. B* 781 (2018), pp. 517–541. DOI: [10.1016/j.physletb.2018.04.030](https://doi.org/10.1016/j.physletb.2018.04.030). arXiv: [1710.02846](https://arxiv.org/abs/1710.02846) [hep-ex].
- [185] Morad Aaboud et al. “Angular analysis of  $B_d^0 \rightarrow K^{*0} \mu^+ \mu^-$  decays in  $pp$  collisions at  $\sqrt{s} = 8$  TeV with the ATLAS detector”. In: *JHEP* 10 (2018), p. 047. DOI: [10.1007/JHEP10\(2018\)047](https://doi.org/10.1007/JHEP10(2018)047). arXiv: [1805.04000](https://arxiv.org/abs/1805.04000) [hep-ex].
- [186] +.  $\rightarrow K + + -$  et al. “Measurement of lepton universality parameters in  $B^+ \rightarrow K^+ \ell^+ \ell^-$  and  $B^0 \rightarrow K^{*0} \ell^+ \ell^-$  decays”. In: *Phys. Rev. D* 108.3 (2023), p. 032002. DOI: [10.1103/PhysRevD.108.032002](https://doi.org/10.1103/PhysRevD.108.032002). arXiv: [2212.09153](https://arxiv.org/abs/2212.09153) [hep-ex].
- [187] R. Aaij et al. “Test of lepton universality in  $b \rightarrow s \ell^+ \ell^-$  decays”. In: *Phys. Rev. Lett.* 131.5 (2023), p. 051803. DOI: [10.1103/PhysRevLett.131.051803](https://doi.org/10.1103/PhysRevLett.131.051803). arXiv: [2212.09152](https://arxiv.org/abs/2212.09152) [hep-ex].
- [188] Ben Allanach and Anna Mullin. “Plan B: new  $Z'$  models for  $b \rightarrow s \ell^+ \ell^-$  anomalies”. In: *JHEP* 09 (2023), p. 173. DOI: [10.1007/JHEP09\(2023\)173](https://doi.org/10.1007/JHEP09(2023)173). arXiv: [2306.08669](https://arxiv.org/abs/2306.08669) [hep-ph].
- [189] Marcel Algueró et al. “To (b)e or not to (b)e: no electrons at LHCb”. In: *Eur. Phys. J. C* 83.7 (2023), p. 648. DOI: [10.1140/epjc/s10052-023-11824-0](https://doi.org/10.1140/epjc/s10052-023-11824-0). arXiv: [2304.07330](https://arxiv.org/abs/2304.07330) [hep-ph].
- [190] Wolfgang Altmannshofer et al. “Symmetries and Asymmetries of  $B \rightarrow K^{*0} \mu^+ \mu^-$  Decays in the Standard Model and Beyond”. In: *JHEP* 01 (2009), p. 019. DOI: [10.1088/1126-6708/2009/01/019](https://doi.org/10.1088/1126-6708/2009/01/019). arXiv: [0811.1214](https://arxiv.org/abs/0811.1214) [hep-ph].
- [191] Damir Becirevic et al. “Complementarity of the constraints on New Physics from  $B_s \rightarrow \mu^+ \mu^-$  and from  $B \rightarrow K l^+ l^-$  decays”. In: *Phys. Rev. D* 86 (2012), p. 034034. DOI: [10.1103/PhysRevD.86.034034](https://doi.org/10.1103/PhysRevD.86.034034). arXiv: [1205.5811](https://arxiv.org/abs/1205.5811) [hep-ph].
- [192] Christoph Bobeth et al. “ $B_{s,d} \rightarrow l^+ l^-$  in the Standard Model with Reduced Theoretical Uncertainty”. In: *Phys. Rev. Lett.* 112 (2014), p. 101801. DOI: [10.1103/PhysRevLett.112.101801](https://doi.org/10.1103/PhysRevLett.112.101801). arXiv: [1311.0903](https://arxiv.org/abs/1311.0903) [hep-ph].

- [193] Basabendu Barman et al. “Correlating the anomalous results in  $b \rightarrow s$  decays with inert Higgs doublet dark matter and muon  $(g - 2)$ ”. In: *Phys. Rev. D* 100.11 (2019), p. 115010. doi: [10.1103/PhysRevD.100.115010](https://doi.org/10.1103/PhysRevD.100.115010). arXiv: [1808.06639](https://arxiv.org/abs/1808.06639) [hep-ph].
- [194] Roel Aaij et al. “Measurement of the  $B_s^0 \rightarrow \mu^+ \mu^-$  branching fraction and effective lifetime and search for  $B^0 \rightarrow \mu^+ \mu^-$  decays”. In: *Phys. Rev. Lett.* 118.19 (2017), p. 191801. doi: [10.1103/PhysRevLett.118.191801](https://doi.org/10.1103/PhysRevLett.118.191801). arXiv: [1703.05747](https://arxiv.org/abs/1703.05747) [hep-ex].
- [195] M. Misiak et al. “Updated NNLO QCD predictions for the weak radiative B-meson decays”. In: *Phys. Rev. Lett.* 114.22 (2015), p. 221801. doi: [10.1103/PhysRevLett.114.221801](https://doi.org/10.1103/PhysRevLett.114.221801). arXiv: [1503.01789](https://arxiv.org/abs/1503.01789) [hep-ph].
- [196] Mikolaj Misiak, Abdur Rehman, and Matthias Steinhauser. “NNLO QCD counterterm contributions to  $\bar{B} \rightarrow X_{s\gamma}$  for the physical value of  $m_c$ ”. In: *Phys. Lett. B* 770 (2017), pp. 431–439. doi: [10.1016/j.physletb.2017.05.008](https://doi.org/10.1016/j.physletb.2017.05.008). arXiv: [1702.07674](https://arxiv.org/abs/1702.07674) [hep-ph].
- [197] Y. Amhis et al. “Averages of  $b$ -hadron,  $c$ -hadron, and  $\tau$ -lepton properties as of summer 2016”. In: *Eur. Phys. J. C* 77.12 (2017), p. 895. doi: [10.1140/epjc/s10052-017-5058-4](https://doi.org/10.1140/epjc/s10052-017-5058-4). arXiv: [1612.07233](https://arxiv.org/abs/1612.07233) [hep-ex].
- [198] Pere Arnau et al. “Generic Loop Effects of New Scalars and Fermions in  $b \rightarrow s \ell^+ \ell^-$ ,  $(g - 2)_\mu$  and a Vector-like 4<sup>th</sup> Generation”. In: *JHEP* 06 (2019), p. 118. doi: [10.1007/JHEP06\(2019\)118](https://doi.org/10.1007/JHEP06(2019)118). arXiv: [1904.05890](https://arxiv.org/abs/1904.05890) [hep-ph].
- [199] F. Gabbiani et al. “A complete analysis of FCNC and CP constraints in general SUSY extensions of the standard model”. In: *Nuclear Physics B* 477.2 (1996), pp. 321–352. issn: 0550-3213. doi: [https://doi.org/10.1016/0550-3213\(96\)00390-2](https://doi.org/10.1016/0550-3213(96)00390-2). URL: <https://www.sciencedirect.com/science/article/pii/0550321396003902>.
- [200] A. Bazavov et al. “ $B_{(s)}^0$ -mixing matrix elements from lattice QCD for the Standard Model and beyond”. In: *Phys. Rev. D* 93.11 (2016), p. 113016. doi: [10.1103/PhysRevD.93.113016](https://doi.org/10.1103/PhysRevD.93.113016). arXiv: [1602.03560](https://arxiv.org/abs/1602.03560) [hep-lat].
- [201] Neil D. Christensen and Claude Duhr. “FeynRules - Feynman rules made easy”. In: *Comput. Phys. Commun.* 180 (2009), pp. 1614–1641. doi: [10.1016/j.cpc.2009.02.018](https://doi.org/10.1016/j.cpc.2009.02.018). arXiv: [0806.4194](https://arxiv.org/abs/0806.4194) [hep-ph].
- [202] Adam Alloul et al. “FeynRules 2.0 - A complete toolbox for tree-level phenomenology”. In: *Comput. Phys. Commun.* 185 (2014), pp. 2250–2300. doi: [10.1016/j.cpc.2014.04.012](https://doi.org/10.1016/j.cpc.2014.04.012). arXiv: [1310.1921](https://arxiv.org/abs/1310.1921) [hep-ph].
- [203] J. Kublbeck, M. Bohm, and Ansgar Denner. “Feyn Arts: Computer Algebraic Generation of Feynman Graphs and Amplitudes”. In: *Comput. Phys. Commun.* 60 (1990), pp. 165–180. doi: [10.1016/0010-4655\(90\)90001-H](https://doi.org/10.1016/0010-4655(90)90001-H).
- [204] Thomas Hahn. “Generating Feynman diagrams and amplitudes with FeynArts 3”. In: *Comput. Phys. Commun.* 140 (2001), pp. 418–431. doi: [10.1016/S0010-4655\(01\)00290-9](https://doi.org/10.1016/S0010-4655(01)00290-9). arXiv: [hep-ph/0012260](https://arxiv.org/abs/hep-ph/0012260).

- [205] R. Mertig, M. Bohm, and Ansgar Denner. “FEYN CALC: Computer algebraic calculation of Feynman amplitudes”. In: *Comput. Phys. Commun.* 64 (1991), pp. 345–359. doi: [10.1016/0010-4655\(91\)90130-D](https://doi.org/10.1016/0010-4655(91)90130-D).
- [206] Vladyslav Shtabovenko, Rolf Mertig, and Frederik Orellana. “FeynCalc 9.3: New features and improvements”. In: *Comput. Phys. Commun.* 256 (2020), p. 107478. doi: [10.1016/j.cpc.2020.107478](https://doi.org/10.1016/j.cpc.2020.107478). arXiv: [2001.04407](https://arxiv.org/abs/2001.04407) [hep-ph].
- [207] T. Hahn and M. Perez-Victoria. “Automatized one loop calculations in four-dimensions and D-dimensions”. In: *Comput. Phys. Commun.* 118 (1999), pp. 153–165. doi: [10.1016/S0010-4655\(98\)00173-8](https://doi.org/10.1016/S0010-4655(98)00173-8). arXiv: [hep-ph/9807565](https://arxiv.org/abs/hep-ph/9807565).
- [208] Wolfram Research Inc. *Mathematica, Version 13.3*. Champaign, IL, 2023. URL: <https://www.wolfram.com/mathematica>.
- [209] Gerard 't Hooft and M. J. G. Veltman. “Scalar One Loop Integrals”. In: *Nucl. Phys. B* 153 (1979), pp. 365–401. doi: [10.1016/0550-3213\(79\)90605-9](https://doi.org/10.1016/0550-3213(79)90605-9).
- [210] Matthias Steinhauser. *Übungen zu Strahlungskorrekturen in Eichtheorien*. 2003.
- [211] G. Belanger et al. “MicrOMEGAs: A Program for calculating the relic density in the MSSM”. In: *Comput. Phys. Commun.* 149 (2002), pp. 103–120. doi: [10.1016/S0010-4655\(02\)00596-9](https://doi.org/10.1016/S0010-4655(02)00596-9). arXiv: [hep-ph/0112278](https://arxiv.org/abs/hep-ph/0112278).
- [212] Gael Alguero et al. “Co-scattering in micrOMEGAs: A case study for the singlet-triplet dark matter model”. In: *SciPost Phys.* 13 (2022), p. 124. doi: [10.21468/SciPostPhys.13.6.124](https://doi.org/10.21468/SciPostPhys.13.6.124). arXiv: [2207.10536](https://arxiv.org/abs/2207.10536) [hep-ph].